

Advancing active hydroacoustic methods with broadband echosounders for ecological surveys

by

© *Muriel Dunn*

A thesis submitted to the
School of Graduate Studies
in partial fulfilment of the
requirements for the degree of
Doctor of Philosophy

Fisheries and Marine Institute
Memorial University of Newfoundland

January 2024

St. John's

Newfoundland

Abstract

Marine ecosystems are undergoing increasing environmental pressure from climate change and industry developments. These environmental pressures are particularly impacting in the Arctic. Increased monitoring of Arctic marine ecosystems with active acoustic surveys could improve our understanding of the ecological impacts from climate change stressors. However, traditional research vessel-based surveys are very expensive, have limited availability and measure a disrupted pelagic environment by introducing light and noise. We propose that broadband echosounders mounted on uncrewed vehicles, moorings or lowered probes would provide complementary measurements to address these shortcomings. In the case of uncrewed vehicles, they could complement traditional vessel-based surveys by extending the temporal and spatial extent. Because broadband echosounders are relatively new technologies, methods and standard processing procedures need to be modified and tested. The present thesis studies three methods for broadband echosounders to increase the independence of acoustic data from research vessels for monitoring marine ecosystems, with the Arctic as a case study. The three methods are the inverse method, model-informed classification and mesocosm-informed classification. These methods aim to increase the information retrieved from acoustic data by maximizing the use of the broadband target spectra measurements. The methods are applied to sound scattering layers of zooplankton aggregations, individual zooplankton, shrimp, and fish to advance methods for analyzing broadband acoustic data from uncrewed vehicles or moorings where few or no direct sampling data are available. However, new challenges intrinsic to broadband echosounders and their signal processing arise, such as understanding the

sensitivity of broadband measurements of targets as individuals and as aggregations. To conclude, I discuss the applicability of these methods for ecosystem-based fisheries management and commercial fishing. I conclude on the progress towards fulfilling the promise of broadband acoustics for species identification.

General Summary

In the Arctic, climate change is affecting the environment at unprecedented rates. The warming is melting sea ice and increasing access to the Arctic; therefore, there is an increase in industrial developments (shipping, oil exploration, fishing). The combination of these factors is imposing new stressors on the ecosystems in the Arctic. Increased monitoring of Arctic marine ecosystems could prepare us for the effects of climate change and industrial development to ensure a sustainable future. Normally, the Arctic marine ecosystems are monitored with large research ships. Ship surveys are critical for validating the acoustic signal by collecting samples of fish and zooplankton with trawls and nets for information on size distributions and community composition. However, these ships are very expensive to use, have limited availability and disturb the fish and other species near the surface because of the ship's lights, noise and draft. We propose complementing ship surveys with acoustics mounted on uncrewed vehicles or moorings, where light, noise and vessel draft are reduced. Uncrewed vehicles are easier and cheaper to deploy and can monitor a region for extended periods of time (\sim months). Moorings can collect data for months at a single location. Furthermore, as with ships, these alternative monitoring methods can be equipped with the latest technology in active acoustics: broadband echosounders. These instruments record the presence of fish and zooplankton in the water column over a wide range of frequencies. The frequency range is considered an important component for remote species identification of fish and zooplankton because it can contain information on the size and material properties of the organisms. However, broadband echosounders are relatively new technologies; therefore, new or modified

methods are needed to maximize their potential. In this thesis I present three methods to increase the information retrieved from broadband echosounders to improve marine ecosystem monitoring. These methods are applied to the Arctic because of the strong need for complimentary monitoring methods in this region. I demonstrate that broadband echosounder data can be used to discriminate between coinciding species. However, I found challenges intrinsic to broadband echosounders, such as understanding the sensitivity of the measured signal. To conclude, I discuss the practical use of these methods for ecosystem-based fisheries management and commercial fishing and I discuss the progress towards fulfilling the promise of broadband echosounders for species identification.

Acknowledgements

Thank you to my supervisors Maxime Geoffroy and Geir Pedersen for sharing their knowledge, curiosity and passion for acoustics, the ocean and its inhabitants. They always carved out time in their busy schedules for our Super Meetings, to hear me out for a quick chat or for lively discussions.

A thesis is much more than just the science; thank you to Astrid Herendza, Eli Børve, Kristine Bondo Pedersen and Pierre Priou for being supportive and always ready for a coffee break on sunny days and rainy days. Thank you to Håvard Espenes for being patient, supportive and always having a well-timed joke, gif, or delicious dinner ready when I needed it the most.

Thank you to Malin Daase, Sünnje Basedow and Stig Falk-Petersen for being my very valuable in-person mentors, for being always willing to chat about copepods, euphausiids, and acoustics, for your help with fieldwork, and all-around support throughout these four years.

Thank you to Emily Venables, Marine Ilg, Erlend Havenstrøm and Havbruksstasjonen for turning ideas of AZKABAN into a functional reality.

Thank you to the Geoffroy Lab mates for the fun lab meetings, in particular, to Jenny Herbig for her sharing her amazing wisdom in stats, ecology and life.

Thank you to Marilena Geng and Kathy Dunlop for their advice and support, and to the friends that made my PhD and the pandemic easier; Ottawa Super Squad, Friendship Partytime, Vancouver roommates and APN Sporty.

Thank you to my family in Canada who support me, encourage me to take risks, even

when moving to the other side of the ocean, and even came to visit me in Norway. Finally, thank you to Chelsey McGowan-Yallop for being an incredible collaborator and friend. Without Chelsey the AZKABAN/AFKABAN experiments and their thesis chapters wouldn't exist.

The thesis was financially supported by Glider Phase II financed by ConocoPhillips Skandinavia AS. Fieldwork and research were also financed by Arctic Field Grant project AZKABAN-light (Norwegian Research Council project ES675268), PolarFront (Norwegian Research Council project 326635), Bioglider (EU Horizon 2020 research and innovation programme 202094), Deep Impact (Norwegian Research Council project 3300333) and Deeper Impact (Norwegian Research Council project 329305).

Publication permission for Chapter two

The screenshot shows the top navigation bar of the Canadian Science Publishing website. The logo is on the left, and navigation links include 'AUTHORS & REVIEWERS', 'LIBRARIANS & AGENTS', 'CART', 'REGISTER', and 'LOGIN'. Below the navigation bar, the main heading reads 'Permissions for reuse of published material'. A breadcrumb trail shows 'Home / About / Policies / Permissions for reuse'. The main content area is titled 'Journal content' and contains text about reuse permissions, contact information for customer support, and an important note about acknowledgment. A sidebar on the right is titled 'MORE ABOUT CSP' and lists various categories like Leadership, Policies, Diversity, etc.

Subscriber access provided by
UTI NORØGES ARKTISKE UNIVERSITET

AUTHORS & REVIEWERS LIBRARIANS & AGENTS CART REGISTER LOGIN

JOURNALS BOOKS OPEN SCIENCE ABOUT BLOG

Permissions for reuse of published material

Home / About / Policies / **Permissions for reuse**

Cette politique est également disponible [en français](#).

Journal content

Anyone may reuse figures, tables, and short excerpts from any article in Canadian Science Publishing (CSP) journals without permission and at no charge for any non-commercial use that respects the moral rights of authors. For for-profit purposes or if a license for permission is required by the user, users are referred to [Copyright Clearance Center](#). It can be accessed by selecting the appropriate [CSP journal](#) article, clicking on the Request Permissions button, and following the instructions.

For questions about using Copyright Clearance Center, please contact customer support:
Toll free: 1-855-239-3415 or 1-978-646-2600
Email: support@copyright.com

Important: For any reuse, the original publication must be acknowledged with a credit line that includes the author, article title, journal title, volume number, issue number, inclusive pages, and DOI. The credit line must also include the wording "© Canadian Science Publishing or its licensors", except when an author of an original article published in 2009 or later is reproducing his/her own work.

MORE ABOUT CSP

- Leadership
- Policies
- Diversity
- Advertising
- Community
- Partners
- Careers
- News
- Contact

Publication permission for Chapter three

Copyright

It is a condition of publication in the journal that authors grant an exclusive license to the International Council for the Exploration of the Sea. This ensures that requests from third parties to reproduce articles are handled efficiently and consistently and will also allow the article to be as widely disseminated as possible. As part of the license agreement, authors may use their own material in other publications provided that the journal is acknowledged as the original place of publication.

Upon receipt of accepted manuscripts at Oxford University Press authors will be invited to complete an online copyright licence to publish form.

Please note that by submitting an article for publication you confirm that you are the corresponding/submitting author and that Oxford University Press ("OUP") may retain your email address for the purpose of communicating with you about the article. You agree to notify OUP immediately if your details change. If your article is accepted for publication OUP will contact you using the email address you have used in the registration process. Please note that OUP does not retain copies of rejected articles.

Publications arising

The following publications were produced as part of this dissertation:

Chapter 2

Dunn, M., Pedersen, G., Basedow, S.L., Daase, M., Falk-Petersen, S., Bachelot, L., Camus, L. & Geoffroy, M. (2022). Inverse method applied to autonomous broadband hydroacoustic survey detects higher densities of zooplankton in near-surface aggregations than vessel-based net survey. *Canadian Journal of Fisheries and Aquatic Sciences* 80 (3), 451-467 <https://doi.org/10.1139/cjfas-2022-0105>.

Chapter 3

Dunn, M., McGowan-Yallop, C., Pedersen, G., Falk-Petersen, S., Daase, M., Last, L., Langbehn, T.J., Fielding, S., Brierly, A., Cotter, F., Basedow, S.L., Camus, L. & Geoffroy, M. (2023). Model-informed classification of broadband acoustic backscatter from zooplankton in an in situ mesocosm. *ICES Journal of Marine Sciences - Echosounder to the Cloud Symposium Issue*, <https://doi.org/10.1093/icesjms/fsad192>

Chapter 4

Dunn, M., Pedersen, G., Daase, M., Berge, J., Venables, E., Basedow, S.L., Falk-Petersen, S., Jensen, J., Langbehn T.J., Camus, L. & Geoffroy, M. Classification of three coinciding species (Atlantic cod, polar cod, and northern shrimp) using broadband hydroacoustics. *In Prep*.

The work from this thesis has been presented in multiple international conferences and workshops:

- **Dunn, M.**, Pedersen, G., Basedow, S.L., Daase, M., Camus, L., Falk-Petersen, S. & Geoffroy, M. (2021). Autonomous measurements of an undisturbed epipelagic sound scattering layer at high latitudes. *Arctic Science Summit Week (Online)*, Lisbon, Portugal.
- **Dunn, M.**, Pedersen, G., Basedow, S.L., Daase, M., Falk-Petersen, S., Bachelot, L., Camus, L. & Geoffroy, M. (2021). AZKABAN: An ex situ experiment for informing the inverse method *ICES Working Group on Fisheries Acoustics Science and Technology (WGFAST) Meeting (Online)*, Bergen, Norway.
- **Dunn, M.**, Pedersen, G., Basedow, S.L., Daase, M., Camus, L., Falk-Petersen, S. & Geoffroy, M. (2022). Comparison of sampling strategies for epipelagic sound scattering layers at high latitudes. *Ocean Sciences Meeting (Online)*, Hawaii, US.
- **Dunn, M.**, Pedersen, G., Basedow, S.L., Daase, M., Camus, L., Falk-Petersen, S. & Geoffroy, M. (2022). Using an autonomous surface vehicle and hydroacoustics to survey epipelagic organisms at high-latitudes. *Fourth ICES/PICES Early Career Scientist Conference*, St-John's, Canada.
- **Dunn, M.** (2022). Get more from EK80 data. *Kongsberg EK80 Workshop Tromsø*, Tromsø, Norway.
- **Dunn, M.**, McGowan-Yallop, C., Pedersen, G., Falk-Petersen, S., Daase, M., Last, L., Langbehn, T.J., Fielding, S., Brierly, A., Cotter, F., Basedow, S.L., Camus, L. & Geoffroy, M. (2023). Model-informed classification of broadband

acoustic backscattering from zooplankton in an *in situ* mesocosm. *ICES Symposium: From echosounders to the cloud*, Portland, ME.

- **Dunn, M.**, Pedersen, G., Daase, M., Berge, J., Venables, E., Basedow, S.L., Falk-Petersen, S., Jensen, J., Langbehn, T.J., Camus, L. & Geoffroy, M. (2023). Discrimination of target strength spectra from three coinciding Arctic species (*Boreogadus saida*, *Gadus morhua*, *Pandalus borealis*). *Canadian Meteorological and Oceanographic Society (CMOS) conference* St-John's, Canada. (Presented by Geoffroy, M.).

In addition to my thesis chapters I have published a peer-reviewed publication, contributed to one conference proceedings, one publication in preparation, two scientific reports and obtained one research grant:

- Ponçon, Y., et al., [including **Dunn, M.**] (2023) Bioglider: an integrated glider solution for enhancing environmental knowledge. In *OCEANS 2023 Gulf Coast conference*
- **Dunn, M.** & Zedel, L. (2022). Evaluation of discrete target detection with an acoustic Doppler current profiler. *Limnology and Oceanography: Methods*, 20(5), 249-259. <https://doi.org/10.1002/lom3.10484>
- Ramasco, V., **Dunn, M.** (2021). Sailbuoy in Antarctica: A survey for the Norwegian Polar Institute. *Akvaplan-niva Report*. 2021 62586.01.
- **Dunn, M.** (2021). Arrested Zooplankton Kept Alive for Broadband Acoustic Net experiment for light reactions (AZKABAN-light). Funded by the Research Council of Norway (NOK 60 000-).

- Niemi, A., et al. [including **Dunn, M.**] (2020). Data from the BREA-MFP and CBS-MEA research programs describing the Anguniaqvia niqiqyuam Marine Protected Area (ANMPA) ecosystem. *Can. Data Rep. Fish. Aquat. Sci.* 1316: ix + 90 p.
- Renaud, P.E., et al., [including **Dunn, M.**]. Extreme mismatch during Arctic spring blooms and consequences for the pelagic food-web. *In prep.*

Co-authorship statement

Co-authorship statements are described below for each chapter following the CRediT classification.

Chapter 1 **Muriel Dunn:** Writing – original draft. **Geir Pedersen:** Writing – review & editing. **Sünnje L. Basedow:** Writing – Review & editing. **Stig Falk-Petersen:** Writing – Review & editing. **Maxime Geoffroy:** Writing – review & editing.

Chapter 2 **Muriel Dunn:** Conceptualisation, Methodology, Software, Formal Analysis, Visualisation, Writing – original draft. **Geir Pedersen:** Conceptualisation, Supervision, Writing – review & editing. **Sünnje L. Basedow:** Investigation, Writing – review & editing. **Malin Daase:** Conceptualisation, Investigation, Writing – review & editing. **Stig Falk-Petersen:** Investigation, Writing – review & editing. **Loïc Bachelot:** Software, Visualisation. **Lionel Camus:** Funding Acquisition, Resources. **Maxime Geoffroy:** Conceptualisation, Supervision, Writing – review & editing.

Chapter 3 **Muriel Dunn:** Conceptualization, Investigation, Methodology, Software, Formal analysis, Visualisation, Funding Acquisition, Writing – original draft. **Chelsey McGowan-Yallop:** Conceptualization, Investigation, Methodology, Software, Formal analysis, Visualisation, Funding Acquisition, Writing – original draft. **Geir Pedersen:** Conceptualization, Methodology, Supervision, Writing – Review & editing. **Stig Falk-Petersen:** Investigation, Writing – Review & editing. **Malin**

Daase: Investigation, Funding Acquisition, Writing – Review & editing. **Kim Last:** Conceptualization, Supervision, Writing – Review & editing. **Tom J. Langbehn:** Investigation, Visualization, Writing – Review & editing. **Sophie Fielding:** Methodology, Resources, Supervision, Writing – Review & editing. **Andrew S. Brierley:** Supervision, Writing – Review & editing. **Finlo Cottier:** Supervision, Writing – Review & editing. **Sünnje L. Basedow:** Resources, Writing – Review & editing. **Lionel Camus:** Funding Acquisition, Resources. **Maxime Geoffroy:** Conceptualisation, Methodology, Resources, Supervision, Writing – Review & editing.

Chapter 4 Muriel Dunn: Conceptualization, Investigation, Methodology, Software, Formal analysis, Visualisation, Writing – original draft. **Geir Pedersen:** Conceptualization, Methodology, Supervision, Writing – Review & editing. **Malin Daase:** Investigation, Methodology, Funding Acquisition, Writing – Review & editing. **Jørgen Berge:** Investigation, Funding Acquisition, Resources, Writing – Review & editing. **Emily Venables:** Investigation, Methodology. **Sünnje L. Basedow:** Resources, Writing – Review & editing. **Stig Falk-Petersen:** Investigation, Methodology. **Jenny Jensen:** Methodology, Resources. **Tom J. Langbehn:** Visualisation, Writing – Review & editing. **Lionel Camus:** Funding Acquisition, Resources, Writing – Review & editing. **Maxime Geoffroy:** Conceptualisation, Investigation, Methodology, Resources, Supervision, Writing – Review & editing.

Chapter 5 Muriel Dunn: Writing – original draft. **Geir Pedersen:** Writing – review & editing. **Sünnje L. Basedow:** Writing – Review & editing. **Stig Falk-Petersen:** Writing – Review & editing. **Maxime Geoffroy:** Writing – review &

editing.

Contents

Abstract	ii
General Summary	iv
Acknowledgements	vi
Publications arising	ix
Authorship statement	xiii
List of Tables	xxii
List of Figures	xxiv
1 Introduction	1
1.1 Monitoring marine ecosystems	1
1.2 Acoustic monitoring	4
1.2.1 Active acoustics	4
1.2.2 Quantifying acoustic backscatter	7
1.2.3 Hydroacoustic surveys	9

1.2.4	Broadband echosounders	12
1.3	Uncrewed ocean monitoring vehicles	15
1.4	Scattering models	17
1.5	Machine learning in fisheries acoustics	20
1.6	Chapter outline and research objectives	23
2	Inverse method applied to autonomous broadband hydroacoustic survey detects higher densities of zooplankton in near-surface ag- gregations than vessel-based net survey	26
2.1	Abstract	27
2.2	Introduction	28
2.3	Materials and methods	31
2.3.1	Study area and survey design	31
2.3.2	Biological sampling	34
2.3.3	Acoustic sampling	37
2.3.3.1	Acoustic data processing	37
2.3.3.2	Sound scattering layer backscatter spectra	37
2.3.3.3	Sound scattering models	41
2.3.3.4	Density estimates	47
2.3.3.5	Comparison analysis	50
2.4	Results	50
2.4.1	Biological sampling	50
2.4.2	Acoustics	55
2.4.3	Density analysis across methods	60

2.5	Discussion	62
2.5.1	Comparison of sampling methods	62
2.5.2	Assessment of the autonomous acoustic survey and inverse method for density estimates	65
2.6	Conclusion	68
3	Model-informed classification of broadband acoustic backscattering from zooplankton in an <i>in situ</i> mesocosm	70
3.1	Abstract	71
3.2	Introduction	72
3.3	Material and methods	76
3.3.1	Study area and zooplankton collection	76
3.3.2	Mesocosm design and experiment	77
3.3.3	Acoustic data collection and calibration	80
3.3.4	Scattering models	81
3.3.5	Acoustic data processing	84
3.3.6	Noise level	85
3.3.7	Classifier training	86
3.3.7.1	Training on modelled target spectra	88
3.3.7.2	Classifier sensitivity	90
3.3.8	Classification	91
3.4	Results	91
3.4.1	Species composition	91
3.4.2	Scattering models	93

3.4.3	Noise level	94
3.4.4	Mesocosm target detections	96
3.4.5	Evaluation of classifier training	96
3.4.5.1	Classifier performance	96
3.4.5.2	Classifier sensitivity	97
3.4.6	Classification of <i>in situ</i> measurements	98
3.5	Discussion	102
3.5.1	AZKABAN: A mesocosm for <i>in situ</i> broadband acoustic backscatter measurements	102
3.5.2	Performance of classifiers trained by modelled target spectra .	103
3.5.3	Discrepancies between classifiers predictions and <i>in situ</i> measurements	105
3.5.4	Recommendations to improve model-informed classification of zooplankton	106
3.6	Summary and conclusions	108
4	Classification of three coinciding species (Atlantic cod, polar cod, and northern shrimp) using broadband hydroacoustics	110
4.1	Abstract	111
4.2	Introduction	112
4.3	Methods	114
4.3.1	Species collection	114
4.3.2	Mesocosm experiment	116
4.3.3	Acoustic data analysis	119

4.3.4	Classifier training	123
4.4	Results	124
4.4.1	Species composition	124
4.4.2	Single species target spectra	125
4.4.3	Classifier training	127
4.5	Discussion	128
4.5.1	Species-specific patterns	128
4.5.2	Intensity variability of broadband target spectra	130
4.5.3	Classification of <i>in situ</i> targets	132
4.6	Conclusion	134
5	General conclusions	136
5.1	Overview of research goal	136
5.2	The role of acoustic surveys with uncrewed vehicles in fisheries	138
5.2.1	Ecosystem-based fisheries management	138
5.2.2	Commercial fishing	140
5.3	The promise of broadband fisheries echosounders	141
5.3.1	The use of broadband echosounders	141
5.3.2	Broadband sensitivity	142
5.4	Limitations of study and recommendations for future research	144
	Bibliography	147
	A Supplementary Materials 1	192
	B Supplementary Materials 2	205

C Ethics approval for AFKABAN experiments	215
D Supplementary Materials 3	218

List of Tables

2.1	The location and time of sampling stations within the Tromsøflaket region during the SeaPatches research cruise with R/V Helmer Hanssen.	34
2.2	PC-DWBA model parameter distributions for each taxonomic group. The distribution used are gamma: $\Gamma(\text{shape}, \text{rate})$, log normal: $L(\text{meanlog}, \text{sigmalog})$ and normal: $N(\text{mean}, \text{sigma})$.	43
2.3	Viscous elastic model ensemble shape and material properties parameters for pteropods and fish larvae in Tromsøflaket.	45
2.4	The size distribution of the dominant species from each taxonomic group. MultiNet and Tucker trawl length measurements were taken from subsamples. The “acoustics” sampling method shows the mean length and standard deviation (SD) used in the scattering models for the forward and inverse methods.	54
3.1	Scattering model parameters distributions for each zooplankton group. The distributions are log-normal: $L(\text{meanlog}, \text{sdlog})$, normal: $N(\text{mean}, \text{sd})$ and gamma: $\Gamma(\text{shape}, \text{rate})$, where sd is the standard deviation.	82
3.2	Overview of the machine learning algorithms compared in this study. The strengths and limitations are detailed for use in fisheries acoustics.	86

3.3	Taxonomic group, species, count and proportion of the sample retrieved from the net after the experiment. Samples with <1000 individuals were counted for the entire recovered mesocosm sample. The species with a "Median length" value were modelled to create the labelled training dataset for the classification algorithms.	92
3.4	Classifier mean F1 scores estimated through nested cross-validation (mean \pm standard deviation) for the 185-255 kHz bandwidth. A score of 1.0 indicates that a classifier could correctly classify each sample (100% classification success).	97
4.1	Overview of the trawling when the catch was used for single species mesocosm experiments. The pelagic trawl was used unless otherwise noted. All dates are in 2023.	115
4.2	Single echo detection - wideband 1 detector settings, where TS is target strength.	120
4.3	Classifier F1 scores estimated by classifier training (mean \pm SD) of the normalized target spectra collected with the 120 kHz and 200 kHz transducer.	128

List of Figures

1.1	Image of a wideband autonomous transceiver (yellow cylinder; Kongsberg Discovery AS, Horten, Norway) with a 38 kHz split-beam transducer (orange). Photo taken by Stig Falk-Petersen.	6
1.2	Target strength of marine animals at a range of frequencies. Swimbladdered fish is representative of a 20 cm Atlantic cod (<i>Gadus morhua</i>), euphausiid is representative of a 25 mm <i>Thysanoessa inermis</i> , hydrozoan is representative of 15 mm <i>Aglantha digitale</i> , pteropod is representative of a 1.5 mm <i>Limacina retroversa</i> and copepod is representative of a 5 mm <i>Calanus</i> spp. The vertical grey dashed lines indicate commonly used frequencies in fisheries acoustics. The target strength spectra are calculated using the scattering models described in Section 1.4.	12

2.1	Map of the Norwegian Sea and Norway’s coasts. The red box in the inset indicates the area shown in the large bathymetric map of Tromsøflaket. The Tromsøflaket map indicates the vessel-based research cruise track in red as it travelled between sampling stations (black stars). Time and GPS location of stations are described in Table 1, and the Sailbuoy track in purple is the autonomous acoustic survey. Map produced with cartopy (ver. 0.18.0; scitools.org.uk/cartopy) in orthographic projection and the inset in plate carrée projection (UTM coordinate system).	32
2.2	Example of a) raw pulse-compressed volume backscattering strength (S_v) echogram data upper and lower boundaries of Cluster 0 in red; b) echogram after the mean filtering in time and depth (70 s and 0.09 m filter, respectively); c) projection of raw data by removing the time dimension; and d) projection of filtered data in the depth/ S_v dimensions classified into clusters (k=3 in this example) obtained by k-means clustering. In this example, the cluster corresponding to the SSL is Cluster 0.	39

2.3	<p>a-e) Density estimates in the logarithmic domain for each dominant taxonomic group in Tromsøflaket, in units of base 10 logarithm of individuals per m³. Each box summarises the density measurement from Net (MultiNet; n=11, blue), Trawl (Tucker trawl; n=11, orange), Forward (acoustic forward method; n=70, green) or Inverse (acoustic inverse method; n=70, red). Significant differences are denoted by the number of asterisks (*), with *** p < 0.001, ** p < 0.01 and * p < 0.05 from pairwise Dunn’s tests. f) is the total density estimate (sum of all species) for all stations (Net and Trawl) and all SSLs (sound scattering layers) (Forward and Inverse). Note the different y-axis scale in subplot f.</p>	52
2.4	<p>Relative density of each taxonomic group as calculated by each sampling method across the whole survey region of Tromsøflaket with standard deviation error bars representing variability between stations (Net and Trawl) or SSLs (Inverse). Taxonomic groups are ordered from smallest (left) to largest (right). Size details of each taxonomic group are described in Table 2.4.</p>	55
2.5	<p>Median target strength results of ensemble simulations from the scattering models for each dominant taxonomic group in Tromsøflaket, including the 90% bootstrap confidence intervals of the median as the shaded region. Vertical grey dashed line indicates the nominal frequency (333 kHz).</p>	57

2.6	<p>The sensitivity analysis results for predicted density estimates of each taxonomic group (a-e) for the inversion of acoustic data with scattering model results varying randomly between median, the 5th and 95th percentiles and the volume backscatter spectra varying randomly between median, and interquartile range for each SSL (x-axis). The blue line in each panel is the median of the sensitivity analysis, and the shaded region displays the extent of the 5th and 95th percentile. The red lines indicate the standard deviation of the density estimates for all the SSLs. Note the difference in scale of the y-axis.</p>	59
3.1	<p>Study area in Kongsfjorden with locations of the mesocosm experiment from the wharf in Ny-Ålesund (red square) and Tucker trawl deployments for the experiment (blue circles with some overlap; n=12). The yellow circle indicates the Tucker trawl deployment from which zooplankton was preserved for morphometric analyses (yellow circle; n=1). The red box in the inset shows the location of the study area within the Svalbard archipelago.</p>	77

3.2	A) Schematic of the AZKABAN mesocosm with the small zooplankton net (left) and large fish net (left). Only the configuration with a small net (left) was used for this study to limit the volume of insonified mesozooplankton. The acoustic transceiver (yellow cylinder) is attached to the frame and the transducer (orange cylinder). There is a hole at the top of the net for the transducer face to be unobstructed inside the net. B) The AZKABAN mesocosm was lifted with the crane at the end of the experiment.	78
3.3	a-d) All PC-DWBA model simulation results for each dominant zooplankton group. For copepods (a) the model results are shown for Arctic species (black; Kögeler et al., 1987) and the Antarctic species (blue; Chu & Wiebe, 2005). e-h) L^2 -normalised PC-DWBA model simulation results for each dominant zooplankton group.	94
3.4	Background noise profile inside AZKABAN across the available bandwidth (185-255 kHz; blue lines). The grey dots indicate the TS of each detected tracked target detection at 200 kHz. The detection zone is delimited by the horizontal black lines at 1 m and 2.25 m. The transducer face and top of the net are at 0 m range and the bottom of the net is at 3 m range.	95

3.5	a)	Composition of the zooplankton sample used in the mesocosm experiment as a proportion of the total sample for the four most abundant groups (n=26,435). b-d) the proportion of predicted targets of the total detections for tracked single targets (n=7,722) assigned to each group by k-nearest neighbours (kNN), LightGBM and support vector machine (SVM) classifiers.	99
3.6	<i>Modelled:</i>	PC-DWBA model simulations (theoretical) target spectra for each zooplankton group. <i>kNN</i> , <i>LightGBM</i> , and <i>SVM</i> : measured target spectra of tracked single targets from the mesocosm experiment as classified by k-Nearest Neighbours (kNN), LightGBM, and support vector machine (SVM). All panels include the number (n) of target spectra in each panel.	101
4.1	A) B) C)	Map of the Svalbard archipelago. Map of two species collection location (blue circles) and experiment location at the Ny-Ålesund wharf (red square) in Outer Krossfjorden and Outer Kongsfjorden. Map of a species collection location in Billefjorden in relation to Longyearbyen (red square).	116

- 4.2 A) Schematic of the frame with the small zooplankton net (left; northern shrimp experiment) and large fish net (right; Atlantic cod and polar cod experiments). The acoustic transceiver (yellow cylinder) is attached to the frame and the transducers (orange cylinder, two in this experiment). There is a hole at the top of the net for the transducer faces to be unobstructed inside the net. B) The AFKABAN mesocosm with the large fish net lifted with the crane at the end of the experiment. 119
- 4.3 Examples of the target spectra of each selected detection from an individual track of each species using multiplexing broadband echosounders. An image of the species from the experiment: A) Atlantic cod (*Gadus morhua*), B) polar cod (*Boreogardus saida*) C) northern shrimp (*Pandalus borealis*). D-F) Echogram of a selected isolated track from each species labelled above. Measured target spectra of the selected tracks; G) Atlantic cod with 19 detections in the 94-158 kHz bandwidth and 13 detections in the 189-249 kHz bandwidth (grey lines), H) polar cod track with 6 in the 94-158 kHz bandwidth and 4 target spectra in the 189-249 kHz bandwidth, I) northern shrimp track with 9 target spectra in the 94-158 kHz bandwidth and 10 target spectra in the 189-249 kHz bandwidth. Photo in Panel B was taken by Hauke Flores. 122
- 4.4 Target spectra of all single target detections from all single species experiments. Each target spectra was recorded as target strength (TS) over the 94-158 kHz or the 189-249 kHz bandwidth. *Panel A-D*: target spectra of single echo detections organized by species. *Panel E-H*: L^2 -normalized target spectra, each target spectra have a unit norm. 126

5.1 A) Echogram of a single fish track with clear processing sidelobes above and below the track. B) Echogram of a single fish track that is intercepted by another fish on the right end of the track, last two selected single echos. C) Target spectra of each selected single echo of the single fish. D) Target spectra of each selected single echo of the single fish with interference in two of the target spectra. 143

Chapter 1

Introduction

1.1 Monitoring marine ecosystems

Hydroacoustic surveying is a monitoring approach that is used in combination with traditional net and trawl sampling. Monitoring pelagic species with traditional methods introduces bias from the net and trawl avoidance biases (Skjoldal et al., 2013). In addition, the artificial light from the ship impacts the behaviour of pelagic species down to at least 200 m (Berge et al., 2020). Acoustic instruments are non-invasive and can be mounted on a vessel, mooring or buoy to study an undisturbed pelagic ecosystem (Trenkel et al., 2019). Furthermore, acoustics systems can collect long time series with minimal impact on the studied species. These data are particularly valuable for collecting data to increase our understanding of ecosystem processes. Globally, including in Canada, fisheries management has minimal consideration for ecosystem processes and is predominantly single-species focused (Pepin et al., 2020; Skern-Mauritzen et al., 2016). Nevertheless, there is a widespread agreement that,

to harvest the aquatic environment sustainably, there needs to be a shift towards an ecosystem-based approach to fisheries management (Brodziak & Link, 2002; FAO, 2003; Hilborn et al., 2004; Pepin et al., 2020). An ecosystem-based approach requires consideration of the impacts of the fishery on habitat, predator and prey interactions, as well as social impacts (Link et al., 2011). Ecosystem-based fisheries management also includes the increasing recognition of the effects of climate, weather, environmental conditions, and food web dynamics on the targeted stock (Fernandino et al., 2018; Tam et al., 2017). Comprehensive monitoring of living marine resources is fundamental to a successful ecosystem-based approach to fisheries management. In fact, Canada’s Oceans Act states that to perform its duties and function, Fisheries and Oceans Canada may “conduct marine scientific surveys relating to fisheries resources and their supporting habitat and ecosystems” and “participate in ocean technology development” (Branch, 1867). Ecosystem-based fisheries management requires baseline data on interspecific interactions and their connections with environmental factors, which will involve much more data inputs and technologies than traditional ship-based methods can provide (van Denderen et al., 2013). Efficient ecosystem-based fisheries management is urgently needed with the current state of declining fish stocks and increasing fishing efforts (Aronica et al., 2019).

It is imperative to consider the warming of the global ocean due to physical environmental variations driven by climate change in an ecosystem-based fisheries management approach. The rapid warming is affecting the ocean environment in many ways, in particular in the Arctic, e.g. early ice breakup and reduced coverage (Stroeve et al., 2012), increasing flow of warm Atlantic waters (Wang et al., 2020), and changing the sea temperatures (Steele et al., 2008). These effects are increasing both the indus-

trial development (commercial fishing, oil and gas exploration, and shipping) and the ecosystem changes (Doney et al., 2012; Fossheim et al., 2015; Frainer et al., 2017) in the Arctic.

Sustainable industrial development in the Arctic requires better ecosystem understanding and increased environmental monitoring. However, environmental monitoring in the Arctic can be challenging. The harsh and remote region presents logistical barriers to frequent ship-based surveys in the Arctic. Furthermore, the Arctic has a strong seasonal cycle which alternates between polar night in the winter and midnight sun, with constant sunlight in the summer. Until recently, the polar night, or winter, was not of interest to ecological studies because it was assumed to be a time of biological quiescence. However, recent studies have reported ecological processes, such as trophic interactions and vertical migrations, remain high during this dark period (Berge et al., 2015a; Geoffroy et al., 2011; Ludvigsen et al., 2018). We still have a lack of understanding of the extent of biological activity during the polar night, and therefore, the full seasonal cycle of the Arctic marine ecosystem should be monitored to understand the compounding impacts of climate change and industrial developments in the Arctic (Berge et al., 2015b).

In recent years, there has been significant technology and scientific development in three fields that are increasing the ecosystem monitoring potential, which are particularly valuable for addressing the challenges of ecosystem monitoring in the Arctic. These developments are: (1) the commercial availability of scientific broadband echosounders, (2) reliable uncrewed ocean monitoring vehicles, and (3) the development of accessible sound scattering models and machine learning algorithms. In this thesis, I use recent technological and scientific progress to advance methods for mon-

itoring and understanding Arctic marine ecosystems.

1.2 Acoustic monitoring

1.2.1 Active acoustics

Traditional large-scale scientific trawl surveys (Chadwick et al., 2007) are routinely used for stock assessments. Active acoustic monitoring, or hydroacoustics, is generally combined with these extractive surveys, i.e. acoustic-trawl surveys, where the targeted sampling is used to validate the species composition, relative abundance and their sound scattering properties to convert acoustic backscatter into biomass (Parker-Stetter et al., 2009). Active acoustics is the process of emitting a sound pulse through the water and recording the echo. The echo of the reflected sound pulse contains information about the fish or object that reflected the sound; therefore, it is used for remote sensing observations and monitoring of aquatic species (Simmonds & MacLennan, 2008). Active acoustics is a powerful tool for aquatic monitoring because sound travels much further underwater than light. It differs from passive acoustics, which records sounds emitted by other sources, such as whale songs.

Hydroacoustics surveys use echosounders (Figure 1.1), which consist of a transceiver and one or more transducers. The transducer converts the electrical energy sent from the transceiver into mechanical energy, an acoustic pulse (Simmonds & MacLennan, 2008; Urick, 1983). The transducer is typically mounted on a ship's hull, submerged in the water and pointing downwards. The acoustic pulse travels through the wa-

ter column and is reflected by surfaces and objects with an acoustic impedance that differs from that of the surrounding medium, e.g. seawater or fresh water. The impedance, z , is the product of the density (ρ) of the object and the speed of sound (c) ($z = \rho * c$) (Medwin & Clay, 1998). After transmission, the transducer takes on a listening role, and records the reflection of the emitted acoustic pulse (the echo), amplifies, and converts the echo into an electrical signal to send to the transceiver. The received acoustic pulse contains information on the impedance of scatterers and backscatter throughout the water column. The temporal delay of the backscatter, which is a function of the sound speed velocity of the mediums, informs on the range of the target, i.e. the distance between the target and the transducer face. The backscatter is also affected by the process of absorption, where some of the sound wave energy is converted to heat, which is a function of range (Francois & Garrison, 1982). The radial location of the target in the acoustic beam can be calculated with a calibrated split-beam transducer. The split-beam transducer records the backscatter through three or four quadrants; the phase difference between the signal from each quadrant can be used to locate the target in the beam (Ehrenberg & Torkelson, 1996). Split-beam technology has had an important impact on fisheries acoustics because the target location can be determined which allows the backscatter to be compensated for the transducer beam pattern. The transducer beam pattern is conical, much like a flashlight beam, with most of the energy concentrated in the centre. Furthermore, information on the target's location in the acoustic beam enables single target tracking, which provides multiple measurements and replicates of a single organism as it travels across the beam and reduces the risk of counting the same individual multiple times. The target tracking technique can be used for echo-counting. An

alternative technique used when the density of targets is too high for echo-counting is echo-integration, for example, in a fish school or aggregation of zooplankton. For echo integration, the backscatter from all targets is measured over the entire acoustic beam for a given depth range; therefore, individual targets do not need to be resolved.



Figure 1.1: Image of a wideband autonomous transceiver (yellow cylinder; Kongsberg Discovery AS, Horten, Norway) with a 38 kHz split-beam transducer (orange). Photo taken by Stig Falk-Petersen.

1.2.2 Quantifying acoustic backscatter

The backscattered energy measured by the transducer during hydroacoustic surveys is typically quantified by the fraction of incident energy scattered back to the transducer, described as the backscattering cross-section, σ_{bs} [m^2]:

$$\sigma_{bs} = \frac{I_{bs}}{I_i} 10^{\alpha R/10} R^2, \quad (1.1)$$

where I_{bs} is the intensity of the backscattered wave in $W m^{-2}$, I_i intensity of the incident wave in $W m^{-2}$, α is the acoustic absorption coefficient in $dB m^{-1}$, and R is the range in m from the target where I_{bs} and I_i are measured (MacLennan et al., 2002). In fisheries acoustics, we often use a logarithmic scale, in decibels, because of the wide dynamic range of acoustic backscatter measured from aquatic organisms, from zooplankton to fish, covers many orders of magnitude (Simmonds & MacLennan, 2008). The decibel [dB] unit is used for the logarithmic terms, and it describes a ratio in terms of a reference, *re* (Medwin & Clay, 1998). The backscattering cross-section is then commonly described as Target Strength (*TS*) [*dB re 1 m²*]:

$$TS = 10 \log_{10} \sigma_{bs}. \quad (1.2)$$

Typically, TS is used to describe the ability of a single target (fish or zooplankton) to reflect sound. However, when considering an aggregation or layer of single targets that are too dense to resolve individuals, it is more appropriate to use the volume backscattering coefficient, s_v [m^{-1}]:

$$s_v = \frac{\sum_{i=1}^N \sigma_{bs}^i}{V}, \quad (1.3)$$

where N is the number of individual in the volume, σ_{bs}^i is the cross-section of each individual in m^2 , V is the sampled volume of the acoustic pulse in m^3 (Simmonds

& MacLennan, 2008). The sampled volume, V [m^3], can be related to the acoustic beam pattern as:

$$V = \frac{c\tau\psi R^2}{2}, \quad (1.4)$$

where the range is R in m, the pulse length is τ in s, and the sound speed velocity is c in m s^{-1} . The sampled volume represents the coverage of the shell thickness of the acoustic pulse across the area of the beam (Simmonds & MacLennan, 2008). The equivalent beam angle, ψ [steradian], indicates the solid angle of an idealized acoustic beam:

$$\psi = \int_{\theta=0}^{\pi} \int_{\phi=0}^{2\pi} b^4(\theta, \phi) \sin(\theta) d\theta d\phi, \quad (1.5)$$

where, for an ideal cylindrical transducer, the beam pattern is expressed as:

$$b = \frac{2 J_1(ka \sin(\theta))}{ka \sin(\theta)}, \quad (1.6)$$

where k is the wavenumber in m^{-1} , a is the transducer radius in m, and J_1 is a Bessel function of the first kind (Medwin & Clay, 1998). Similarly to the backscattering cross section (σ_{bs}), the volume backscattering coefficient is commonly expressed on a logarithmic scale as volume backscatter, S_v [$\text{dB re } 1 \text{ m}^{-1}$]:

$$S_v = 10 \log_{10} s_v. \quad (1.7)$$

The measure of s_v summarizes the aggregation inside the acoustic sampling volume because of the linearity principle of fisheries acoustics (Foote, 1983), which is expressed as:

$$Av \varepsilon = n_o \langle G b^2 \sigma_{bs} \rangle, \quad (1.8)$$

where $Av \varepsilon$ is the mean echo energy of the impinged target, n_o is the number density, and $\langle G b^2 \sigma_{bs} \rangle$ is the ensemble average of the distribution of the characteristics of

the targets; G is the gain factor, b^2 is the product of transit and received beam pattern and σ_{bs} backscatter cross-section of the targets (Foote, 1983). Equation 1.8 states that the echo energy from a volume containing a random distribution of scatterers is, on average, equal to the sum of scattered echo energy from each individual within the volume (Benoit-Bird, 2009; Greenlaw, 1979).

1.2.3 Hydroacoustic surveys

Based on these fundamental fisheries acoustics principles, hydroacoustic surveys commonly use narrowband echosounders (acoustic pulse containing a single frequency) with trawl data to convert acoustic backscatter into biomass estimates (Parker-Stetter et al., 2009). Empirically derived regressions for TS values are calculated based on TS-length or TS-width relationships and the length or width measurements from the trawls. Once the theoretical mean TS is calculated, the total echo energy can then be partitioned and scaled to estimate the density of targets corresponding to the measured S_v (Parker-Stetter et al., 2009). The measured S_v is often integrated between depth layers to get a measure of the nautical area backscattering coefficient (NASC or s_A , [$m^2 nmi^{-2}$]) for a larger area:

$$NASC = 4\pi (1852)^2 \int_{z_1}^{z_2} s_v dz, \quad (1.9)$$

where the 4π is remnants from historic uses of spherical scattering coefficient ($4\pi\sigma_{bs}$, assumes omnidirectional scattering), the integer, 1852, is the conversion for units from meter to nautical mile in $m nmi^{-1}$, and z_1 and z_2 are depths in m (MacLennan et al., 2002). For large-scale hydroacoustic surveys, NASC is a common measure (MacLennan et al., 2002; Parker-Stetter et al., 2009) where, though technically dimen-

sionless, the scaling factors are expressed explicitly to distinguish between different scaling versions of the same measure. However, as demonstrated by the linearity principle, many small weak scattering targets can have the equivalent volume backscatter to fewer targets with a higher impedance. Therefore, narrowband acoustic surveys rely on trawling for species identification and length composition (De Robertis et al., 2021).

Hydroacoustic surveys typically do not increase species richness or biodiversity knowledge, but, in addition to abundance estimates, they can inform vertical migrations and predator-prey interactions (MacAulay et al., 1995; Skaret et al., 2020). Furthermore, a species' life history can be used to target a specific age group of a species with pelagic acoustic surveys. For example, many species are pelagic in their juvenile stage, such as Atlantic cod (*Gadus morhua*) and polar cod (*Boreogadus saida*), and can be detected with pelagic acoustic surveys (Bouchard et al., 2017; Nielsen & Lundgren, 1999). In regions dominated by a single species of a certain size or age class, narrowband hydroacoustic surveys can be used without coincident additional evidence (i.e., trawling) because all the backscatter can be attributed to a single species (De Robertis et al., 2021; Geoffroy et al., 2011; Reiss et al., 2021). However, hydroacoustic surveys typically depend on knowledge of species composition, body size and density data to translate active sonar signals into abundance or biomass (Fernandes et al., 2016; McClatchie et al., 2000).

To increase the information extracted from hydroacoustic data, different discrete narrowband frequencies at wide frequency intervals can be used to isolate the backscatter contribution from targets or the volume backscatter of different classes of targets (Figure 1.2). This method is called multifrequency analysis or dB difference technique

(Korneliussen, 2018). For example, a common technology used for vertical migrations and predator-prey interactions is the Acoustic Zooplankton Fish Profiler (AZFP, ASL Environmental Sciences, Victoria, Canada) because it has a transducer available for different narrowband frequencies (38 to 2000 kHz). The wide range of available frequencies enables the detection of fish (typically detected with lower frequencies ≤ 200 kHz) and zooplankton (typically detected with higher frequencies ≥ 200 kHz) with a single instrument (Simmonds & MacLennan, 2008, p.66). For example, AZFPs can be installed on bottom-mounted moorings or ice-tethered moorings for a high temporal resolution because of their long-term sampling capabilities (Priou et al., 2021; Wilson, 2011).

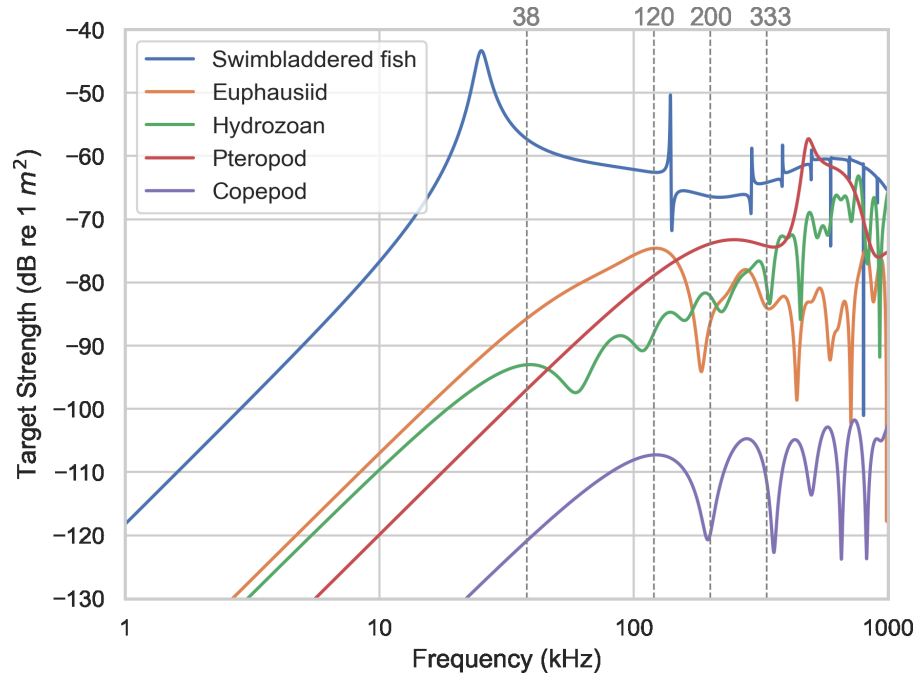


Figure 1.2: Target strength of marine animals at a range of frequencies. Swimbladder fish is representative of a 20 cm Atlantic cod (*Gadus morhua*), euphausiid is representative of a 25 mm *Thysanoessa inermis*, hydrozoan is representative of 15 mm *Aglantha digitale*, pteropod is representative of a 1.5 mm *Limacina retroversa* and copepod is representative of a 5 mm *Calanus* spp. The vertical grey dashed lines indicate commonly used frequencies in fisheries acoustics. The target strength spectra are calculated using the scattering models described in Section 1.4.

1.2.4 Broadband echosounders

Building on the benefits developed with multifrequency analysis, acoustic remote sensing technology has advanced from narrowband to broadband echosounders. The wider bandwidth made available by broadband echosounders returns backscatter mea-

measurements across a wider range of frequencies, offering improved discrimination and characterization of targets (i.e. fish or zooplankton) (Bassett et al., 2019; Benoit-Bird & Waluk, 2020; Lavery et al., 2017; Stanton et al., 1994)(Figure 1.2). The broadband acoustic pulse is called a frequency-modulated chirp, which typically increases linearly throughout the acoustic pulse. Broadband echosounders improve the range resolution and signal-to-noise ratio relative to narrowband echosounders for isolated finite targets. These improvements result from the single processing technique of matched filtering (also called pulse compression). The matched filter output, $y_R(t)$, is calculated by:

$$y_R(t) = \frac{v_R(t) \otimes v_T^*(t)}{|v_T(t)|^2}, \quad (1.10)$$

where v_R is the received pulse, v_T is the transmitted pulse, \otimes is the cross-correlation and $*$ is the complex conjugate (Andersen et al., 2023; Loranger et al., 2022). Finally, the measured target strength is given by (modified from Lavery et al. (2017)):

$$TS(f) = 10 \log_{10} \frac{|Y_R(f)|^2}{|Y_T(f)|^2} - 10 \log_{10} L_{TL}(f)^2 - 10 \log_{10} P_T, \quad (1.11)$$

where f is the acoustic frequency, $Y_R(f)$ and $Y_T(f)$ are the Fourier transform of $y_R(f)$ and $y_T(f)$ (the normalized and autocorrelated transmit signal, $v_T(f)$), respectively. The $L_{TL}(f)$ term is the frequency dependent transmission loss, and P_T accounts for the transmit power.

Through the cross-correlation (Equation 1.10), the matched filter systematically compares the received signal with the pattern of the emitted signal. Stochastic noise does not contain the pattern of the emitted signal; therefore, the match filter results in a

signal with dampened noise. A discrete target, such as a fish, will reflect a reflection of the emitted pulse and result in a narrow peak in the matched filtered signal. However, the broader bandwidth opens up the bandwidth of frequency-dependent noise that can obstruct the target’s backscatter measurements.

Another feature of the matched filter is the improved range resolution. For a narrow-band (NB) system, the range resolution (ability to resolve two vertically separated targets) is given by:

$$\Delta R_{NB} > \frac{c\tau}{2}, \quad (1.12)$$

where ΔR is the range between two resolvable targets (Parker-Stetter et al., 2009; Simmonds & MacLennan, 2008). It is a function of the pulse duration, τ [s], which introduces a trade-off between the range resolution and the amount of energy emitted with the pulse length because two targets cannot be resolved within one narrowband pulse. Broadband systems decouple the range resolution from the pulse length as the match filter uses the bandwidth to resolve targets. The range resolution of a broadband (BB) system is given by:

$$\Delta R_{BB} > \frac{c}{2 BW} \quad (1.13)$$

where BW is the bandwidth in Hz ($f_{max} - f_{min}$) (Ehrenberg & Torkelson, 2000). The order magnitude improvement in range resolution (varies but generally from 10s of cm with narrowband to 10s of mm with broad) opens up a lot of potential for finer scale studies, such as the detection and characterization of individual zooplankton.

Commercial broadband echosounders are relatively new (~ 2011); therefore, developing new processing pipelines to process the broadband signal in a fisheries acoustics context is required (Andersen et al., 2023). For example, the beam width decreases

with increasing frequency within a chirp (Equation 1.6). As a result, the sampling volume is reduced throughout a single frequency modulated up-chirp (i.e., the frequency increasing linearly throughout the pulse duration), which is expressed as a positive trend in volume backscatter with frequency when the s_v is not adjusted (Equation 1.3, 1.4) (Medwin & Clay, 1998; Urmy et al., 2023). Furthermore, the datasets are $\sim 10x$ larger than narrowband datasets. Narrowband data processing methods that require expert scrutiny and visual assessments do not transfer well to broadband datasets because of the size of the files. Therefore, smaller subsamples must be analyzed with expert scrutiny or more powerful algorithms are required.

1.3 Uncrewed ocean monitoring vehicles

Until recently, oceanography was a data-limited field, with data collection solely dependent on research vessels from large survey campaigns. Recent scientific and technological advances are moving physical, chemical and biological oceanography to data-rich fields (Malde et al., 2020). Emerging technologies, particularly uncrewed ocean monitoring vehicles, stem from these scientific and technological advances and can provide a new perspective to regions that have traditionally been surveyed with large research vessels. Uncrewed ocean monitoring vehicles can increase the spatial extent and temporal resolution of environmental monitoring and provide measurements for biophysical assessments (Greene et al., 2014). Indeed, many scientific and technological advancements for ecosystem monitoring with uncrewed vehicles are non-lethal and have minimal impact on the ecosystem (Trenkel et al., 2019).

A prominent benefit to uncrewed vehicles is the reduced disturbance from light and noise. Fish within the epipelagic layer (0 - 100 m) react to light from vessels (Ludvigsen et al., 2018) and vessel noise (Peña, 2019), even when using noise-reducing state-of-the-art research vessels (Ona et al., 2007). Therefore, research vessel surveys report deeper and fewer fish detections for shallowly distributed fish than uncrewed vehicle surveys (De Robertis et al., 2019).

An additional benefit to uncrewed vehicles is their range in size, speed, endurance, depth coverage (Benoit-Bird et al., 2018) and sensor capacity. Diving vehicles, such as gliders, can collect measurements at depths for extended periods of time (Benoit-Bird et al., 2018), whereas surface vehicles can collect undisturbed near-surface data. Typically, hydroacoustic surveys have an acoustic blind zone, the depth at which data collection begins, that can extend ~ 15 m below the surface with a hull-mounted transducer from a research vessel (Scalabrin et al., 2009), but uncrewed surface vehicles tend to be much smaller and have a shallower hull, which reduces the acoustic blind zone to < 5 m.

Despite the clear benefits of uncrewed vehicles, there remains resistance to changing the status quo because of the complexities involved in integrating new data streams (Fujita, 2021; Wilson, 2011). For example, data analysis pipelines for large-scale hydroacoustics surveys have not maintained the same pace as technology advances, causing a bottleneck and a delay in transferring information to end-users of the data (managers and policymakers) (Malde et al., 2020). Uncrewed vehicles equipped with echosounders can be used in areas dominated by a single species because all the backscatter can be estimated from the single dominant species (Bandara et al., 2022; De Robertis et al., 2019). De Robertis et al. (2021) presents the first fully uncrewed

acoustic fisheries survey for stock assessment of walleye pollock (*Gadus chalcogrammus*) without trawling in 2020. Younger pollock, aged 2-4, are more pelagic and can be attributed to the “pre-recruit” biomass for abundance at age indices for fisheries management (De Robertis et al., 2021). However, most regions are not dominated by a single species and hydroacoustic surveys from uncrewed platforms are limited by their inability to collect trawl and net samples. In addition, uncrewed platforms are often small and have limited sensor capacity from the payload limitations and processing power for transmitting data in real time.

The ocean is dynamic and contains diverse species assemblages; therefore, most areas require ancillary sampling of species and size composition. Broadband echosounders are a promising tool for species identification in species assemblages because they can be used to extract a wider backscatter spectrum from a target and, ultimately, to extract identifying features. Nonetheless, broadband acoustics still relies on ancillary sampling to contextualize the backscatter spectra (Benoit-Bird & Waluk, 2020; Cotter et al., 2021; Urmy et al., 2023). Methods applied to broadband echosounder data that could incorporate uncrewed platforms into hydroacoustic surveys could also be used from moorings, drifting platforms and even large vessels to expand the flexibility of surveys depending on monitoring needs.

1.4 Scattering models

Technology and computational developments have also improved numerical and analytical approaches to sound scattering models. Numerical and analytical sound scat-

tering models provide estimates of the acoustic reflectivity of a target (typically fish or zooplankton). These estimates can be used as an alternative technique to estimate target strength when *in situ* measurements are not possible. Sound scattering models range in complexity from approximating the acoustic reflectivity of a sphere, a cylinder or prolate spheroid with homogeneous properties to X-ray images of organisms with complex internal structures (Jech et al., 2015). The organism’s shape, orientation, and material properties are key parameters of sound scattering models. However, these can vary within a population and can be difficult to measure *in situ* (Sakinan et al., 2019; Smith et al., 2010). For example, the sound speed contrast of *Calanus finmarchicus* can vary by more than 10% over the range of environments they occupy, which contributes to the variability of more than 10 dB re 1 m² in their TS measurements (Sakinan et al., 2019). Whereas, gas-bearing organisms, for which the swimbladder accounts for most of the sound scattering, differences between modelled and measured TS greatly depend on tilt angle (Pena & Foote, 2008). Therefore, there are large sources of uncertainty in modelled TS estimates coming from parameter variability, in particular material properties for fluid-like scatterers (Smith et al., 2010) and tilt angles for gas-bearing scatterers (Macaulay et al., 2013).

Several sound scattering models are available depending on the type of acoustic target; each model has limitations and advantages. A summary of available models is published in Jech et al. (2015). The following is a summary of two commonly used scattering models:

Distorted Wave Born Approximation The Distorted Wave Born Approximation (DWBA) is mainly applied to weak scatterers that have material properties

similar to water, e.g., plankton (Stanton & Chu, 2000; Stanton et al., 1996, 1993), and non-swimbladdered fish (Gorska & Ona, 2003). There are a few variants of the DWBA. For example, the stochastic variant (SDWBA), which is commonly used for Antarctic krill (*Euphausia superba*), to account for the stochastic nature of the scattering as the results of body curvature changes while swimming (Calise & Skaret, 2011; Demer & Conti, 2003). Another variant is the phase-compensated version (PC-DWBA), which accounts for the scattering-induced attenuation due to densely aggregated zooplankton (Chu & Ye, 1999) (Figure 1.2, euphausiid, hydrozoan and copepod). Overall, the advantages of the DWBA and its variants are the flexibility to scattering geometry, orientation and acoustic frequency (Jech et al., 2015). The main limitation is that it is only applicable to fluid-like scatterers.

Viscous-elastic model Feuillade & Nero (1998) developed the viscous-elastic scattering model to include the scattering of the swimbladder wall (elastic shell), surrounding flesh (outer shell) and the gas enclosed (inner layer). Together, the shells affect the resonance of the swimbladder and its backscatter. Khodabandeloo et al. (2021) applied the model to mesopelagic fish and compared it with *in situ* measurements. The advantage of the viscous elastic model is that it includes the higher modes of scattering, which is particularly important for higher frequencies (Khodabandeloo et al., 2021) (Figure 1.2, swimbladdered fish and pteropod). As implemented in Khodabandeloo et al. (2021), a prominent limitation of this method is the assumption that the gas enclosure is spherical. The simple sphere shape was chosen to reduce the computational expense, but it ignores the realistic aspect ratios of the swimbladder, which tend to have the shape of a prolate spheroid (Khodabandeloo et al., 2021).

For all models, assumptions have to be made for morphological and material properties parameters, which can affect the shape and amplitude of the results. Sound scattering models can be run as ensembles to capture the study region’s variability in shape, orientation, and material properties. Model ensembles repeat calculations with a random selection of parameters within the given parameter distributions. Model ensembles can be particularly valuable for averaging over orientation for volume backscatter inversions (Amakasu et al., 2017; Stanton et al., 1993).

1.5 Machine learning in fisheries acoustics

From face recognition to self-driving cars, artificial intelligence is increasingly being applied to datasets of all types. Machine learning, a subfield of artificial intelligence, implements models for data-driven decisions in various domains, including fisheries acoustics (Beyan & Browman, 2020). Machine learning supports data-driven learning and results in automated decision-making (Beyan & Browman, 2020), thus potentially reducing human review effort and user subjective bias from visual assessments during data analysis. Statistical algorithms learn from training data by detecting patterns, such as reoccurring characteristics in text or images, to be able to generalize to unseen data (Nguyen & Armitage, 2008; Theodoridis & Koutroumbas, 2006). In particular, machine learning algorithms are practical for sensors and vehicles that collect large amounts of data, like uncrewed vehicles and broadband echosounders.

Machine learning can be categorized into four learning methods: supervised learning, unsupervised learning, semi-supervised learning and reinforcement learning (Zhao et al., 2021). Supervised learning is the most common type of learning, including

in fisheries acoustics. With supervised learning, predictions are made on new data through continuous learning from training data based on predictor features (Kotiantis et al., 2007). Classification and regression type of problems are commonly solved with supervised learning (Zhao et al., 2021). Example uses of supervised learning in fisheries acoustics are predicting the dominant species of an aggregation or school by using multifrequency S_v of acoustic fish school and other fish school descriptions (morphological, bathymetric and positional) (e.g., Fallon et al., 2016; Fernandes, 2009) or, more recently, classifying species using modelled target strength spectra (Cotter et al., 2021; Roa et al., 2022). Unsupervised learning finds patterns and representations in the data without requiring labelled training data (Yassir et al., 2023). Unsupervised learning is predominantly used for clustering or dimensionality reduction. Unsupervised learning may be preferred in fisheries acoustics for studies with minimal supporting biological information, e.g., differentiating between scattering layers based on volume backscatter spectra, $S_v(f)$ (Ross et al., 2013), clustering mesopelagic targets based on their target spectra, $TS(f)$, (Agersted et al., 2021), or optimizing parameters in regression TS to length models (Stevens et al., 2021).

Semi-supervised learning combines supervised and unsupervised learning, where labelled and unlabelled datasets are used to realize a combination of classification, clustering and regression (Zhao et al., 2021). Semi-supervised classification was used by Choi et al. (2021) to delineate sandeel schools in S_v measurements by clustering and classification trained by labelled and unlabelled data. The semi-supervised method requires only 10% of the training data to be labelled, thus reducing the dependency on user expert knowledge and visual assessments (Choi et al., 2021). Meanwhile, reinforcement learning is used for autopilot and uncrewed operations because it is

a complex ML method that constantly interacts with the outside world, i.e., new information (Montague, 1999; Zhao et al., 2021). It is not commonly directly used for fisheries acoustics, but it is used for uncrewed marine vehicles. For example, reinforcement learning has been used for obstacle detection and avoidance (Cheng & Zhang, 2018).

A particular limitation of machine learning is feature engineering. That is the selection, manipulation and transformation of the raw input data into new variables for the ML algorithms. These are predominantly the steps in machine learning where data processing workflow continues to require user manipulation and decisions. Deep learning methods automate the feature engineering component and reduce the need for user data preprocessing (Yassir et al., 2023). The feature engineering components are either predefined between convolutional layers, such as scaling and statistics, or learnt and modified by adjusting to important features in the training dataset (Yassir et al., 2023). Generally, deep learning methods outperform machine learning. However, they are not always used because they require larger amounts of data for training. For example, fish school classification using machine learning methods requires that the input training data set has already identified schools and additional descriptors to be calculated (Proud et al., 2020). In deep learning, these features would be automatically learned (Yassir et al., 2023). Deep learning methods are deemed unnecessary for simpler cases, such as target spectra classification with limited availability for feature manipulation and training data. However, deep learning would become relevant for broadband species identification on field data with an entire echogram (Brautaset et al., 2020; Roa et al., 2022).

1.6 Chapter outline and research objectives

The goal of the present thesis is to contribute to advancing and testing methods that increase the independence of acoustic surveys for monitoring marine ecosystems. The goal was achieved by advancing and testing methods for broadband echosounders compatible with uncrewed platforms, moorings, lowered probes, and ships.

This thesis is structured in 5 chapters. Chapter 1 provides an introduction to the main themes discussed throughout the thesis, Chapters 2, 3, and 4 are core research papers, and Chapter 5 provides the general conclusions.

Chapter 2 aimed to complete a comparative study of the zooplankton and ichthyoplankton density estimates in near-surface sound scattering layers using four different methods. Two of the methods were by direct sampling from a research vessel (mesozooplankton net (MultiNet), macrozooplankton trawl (Tucker trawl)) and the other two methods used data collected from an uncrewed vehicle, one with single frequency data and the other with the broadband data. The main objective of this chapter was to compare the density estimates of the sound scattering layers from these four methods and contextualize the results in terms of each method's expected biases and calculated uncertainties. I discussed the importance of new solutions for surveying ecosystems. This chapter was published with co-authors. I contributed to the conceptualization of the comparative study. I completed the methodology, the data analysis, and wrote the original draft.

Chapter 3 aimed to increase the taxonomic resolution of acoustic surveys by classifying the target spectra of zooplankton using sound scattering models. I trained three conceptually different supervised learning classification algorithms with modelled target

spectra of four different Arctic zooplankton groups. I validated the classification predictions against observations collected in a mesocosm of a known mixed zooplankton community. I discussed the limitations of the tested method and provided recommendations for model-informed classification of zooplankton. This paper is published and co-led with Chelsey McGowan-Yallop. I participated in the conceptualization and data collection. I ran the sound scattering models and the final machine learning algorithms. I participated in the data analysis and co-wrote the original draft.

Chapter 4 aimed to investigate the potential of discriminating between coincident species in the Arctic using only their measured target spectra. I conducted single-species mesocosm experiments to collect the target spectra of free-swimming Atlantic cod, polar cod and northern shrimp. I used the target spectra measurements to train three machine learning classification algorithms. I discussed the feasibility of expanding the supervised classification of mesocosm-informed classification for *in situ* measurements of coincident species from a lowered acoustic probe or glider. Co-authors contributed to the realization of this chapter. I contributed to the conceptualization. I performed the data collection, the data analysis, and wrote the original draft.

In Chapter 5, I summarized the results and contributions of the research from Chapters 2, 3 and 4. I discussed the limited availability of ecosystem monitoring data in the Arctic and the use of uncrewed vehicles equipped with broadband echosounders as a tool to increase the monitoring potential and ecosystem understanding in the Arctic. I propose directions for future research to incorporate acoustic measurements in ecosystem-based fisheries management and discuss the promise and limitations of broadband echosounders in fisheries.

The thesis was funded through Glider II (2 years), Polar Front (1 year) and Bioglider (1

year). This thesis's core research paper chapters contain objectives to develop and/or incorporate new technologies and techniques into traditional monitoring methods. Modernizing ecosystem monitoring methods requires substantial research and development on multiple fronts (technological, management and implementation). The present thesis was part of an incremental process to facilitate incorporating modern technologies in ecosystem monitoring.

Chapter 2

**Inverse method applied to
autonomous broadband
hydroacoustic survey detects
higher densities of zooplankton in
near-surface aggregations than
vessel-based net survey**

Muriel Dunn^{1,2}, Geir Pedersen³, Sünnje L. Basedow⁴, Malin Daase⁴, Stig Falk-Petersen¹,
Loïc Bachelot⁵, Lionel Camus¹, and Maxime Geoffroy^{2,4}

¹ Akvaplan-niva AS, Fram Centre, Postbox 6606, Stakkevollan, 9296 Tromsø, Nor-

way

² Centre for Fisheries Ecosystems Research, Fisheries and Marine Institute of Memorial University of Newfoundland, St. John's, A1C 5R3, NL, Canada

³ Institute for Marine Research, 5005 Bergen, Norway

⁴ Department of Arctic and Marine Biology, UiT The Arctic University of Norway, 9019 Tromsø, Norway

⁵ IFREMER, Laboratoire d'Océanographie Physique et Spatiale, 29280 Plouzané, France

Published in *Canadian Journal of Fisheries and Aquatic Sciences* (2022)

2.1 Abstract

Throughout all oceans, aggregations of zooplankton and ichthyoplankton appear as horizontal sound scattering layers (SSLs) when detected with active acoustic techniques. Quantifying the composition and density of these layers is prone to sampling biases. We conducted a net and trawl survey of the epipelagic fauna in northern Norway (70°N) in June 2018 while an autonomous surface vehicle equipped with a broadband echosounder (283-383 kHz) surveyed the same region. Densities from the autonomous hydroacoustic survey were calculated using forward estimates from the relative density from the net and trawl, and inversion estimates with statistical data-fitting. All four methods (net, trawl, acoustic forward and inverse methods) identified that copepods dominated the epipelagic SSL, while pteropods, amphipods

and fish larvae were present in low densities. The density estimates calculated with the inverse method were higher for mobile zooplankton, such as euphausiid larvae, than with the other methods. We concluded that the inverse method applied to broadband autonomous acoustic surveys can improve density estimates of epipelagic organisms by diminishing avoidance biases and increasing the spatio-temporal resolution of ship-based surveys.

Keywords: broadband acoustics, inversion, machine learning, autonomous surface vehicle, zooplankton

2.2 Introduction

Pelagic zooplankton and ichthyoplankton form dense horizontal aggregations throughout all oceans and represent an easily accessible food source for higher trophic levels. In the North Atlantic, these organisms funnel energy from primary producers to top predators such as marine mammals, seabirds, and the pelagic early life stages of larger fishes targeted by commercial fisheries, e.g., Atlantic cod (*Gadus morhua*) (Falk-Petersen et al., 1981; Solvang et al., 2021). Accurate density estimates of zooplankton and ichthyoplankton are thus needed to calculate and model energy transfer in marine environments.

The density of zooplankton and ichthyoplankton can be calculated for large volumes of water using hydroacoustic surveys because the aggregations appear as sound scattering layers (SSLs) when detected with echosounders (Barham, 1966; Dietz, 1948; Proud et al., 2018). At high latitudes, for example in the Fram Strait, the passage between Greenland and Svalbard, the backscatter from the SSLs is usually much

stronger in the epipelagic zone (< 200 m) than in the mesopelagic zone (> 200 m), suggesting that there is a higher density of biomass near the surface than below 200 m (Gjørseter et al., 2020; Knutsen et al., 2017). Epipelagic SSLs of zooplankton, mainly euphausiids, copepods, amphipods, pteropods, and juvenile fish, have been detected with acoustics over high latitude shelves (Bandara et al., 2022; Knutsen et al., 2017), in fjords in Northern Norway (Falk-Petersen et al., 1981; Falk-Petersen & Kristensen, 1985), and in deeper basins of the Barents Sea (Gjørseter et al., 2020). However, density estimates of epipelagic organisms generally contain several biases because of 1) the draft of research vessels and the near-field of acoustic instruments which form a blind zone in the top ca. 10 m (e.g., Pedersen et al., 2019); 2) variation in detection probability with density and range (Appenzeller & Leggett, 1992; Demer & Hewitt, 1995; Simmonds & MacLennan, 2008); and 3) the sound and light emitted by research vessels (Berge et al., 2020; De Robertis et al., 2012; Peña, 2019; Trevorrow et al., 2005).

New technology can contribute to minimizing uncertainties in the detection and density estimates of epipelagic organisms. The recent development of autonomous surface and subsurface vehicles with compact and energy-efficient active acoustic systems reduces the blind zone as well as artificial noise and light sources compared to traditional acoustic surveys conducted from research vessels. These autonomous platforms also have the potential to increase the temporal and spatial scale of acoustic surveys (e.g., De Robertis et al., 2019; Mordy et al., 2017; Verfuss et al., 2019). Concomitantly, the development of broadband echosounders (Andersen et al., 2023) and scattering models for several taxonomic groups (Jech et al., 2015) have improved our ability to detect and characterize small (<1 cm) acoustic targets at a high vertical resolution.

Two methods can be used to estimate density from the acoustic signal scattered from dense epipelagic aggregations of zooplankton and ichthyoplankton in SSLs: the forward method and the inverse method. The forward method uses the relative density of each taxonomic group based on net and trawl samples from the survey region to allocate a proportion of the backscatter, the sound intensity reflected by the targets, for a density estimate of each taxonomic group (Love, 1975; Simmonds & MacLennan, 2008). However, each net or trawl is inherently selective (Skjoldal et al., 2013) depending on mesh size, net/trawl opening, tow speed, and species density (Battaglia et al., 2006; Moriarty et al., 2018; Pearcy et al., 1983). Ultimately, with the forward method, biases from net and trawl selectivity are transferred to the species density estimates. The inverse method rather directly calculates the density of each taxonomic group from acoustic data by optimising the densities based on the received backscatter and the scattering models of each species (Holliday, 1977). When applying the inverse method to broadband acoustics, the spectrum of the acoustic signal can be fully exploited to optimize the model fitting and calculations of density for each taxonomic group. Applying the inverse method to broadband acoustic data has the potential to reduce the bias from net and trawl selectivity and could increase the value of datasets from autonomous or remotely operated platforms with sparse net validation. However, because the inverse problem is typically an underdetermined problem, it implies that solutions will not be unique (Urmy et al., 2023). For example, two solutions may have similar errors but widely different compositions of taxonomic groups. In this study, we used a least-squares inversion which has been used previously in studies with similar taxonomic groups (Lavery et al., 2007; Trevorrow et al., 2005; Warren et al., 2003). Alternatively, a Bayesian statistical framework could be

used to provide a probability distribution for each solution (Urmy et al., 2023).

This study assessed zooplankton and ichthyoplankton density estimates in a near-surface SSL using four different methods: mesozooplankton net (MultiNet), macrozooplankton trawl (Tucker trawl), and the forward and inverse methods applied to broadband acoustic data collected with an autonomous surface vehicle. The survey was conducted as a case study in the Tromsøflaket area, a bank north of the northern Norwegian Sea (70°N). We deployed nets and trawls from a research vessel while an autonomous surface vehicle equipped with a broadband echosounder surveyed the same region (Camus et al., 2019). We also tested the applicability of using theoretical scattering models (Chu & Ye, 1999; Khodabandeloo et al., 2021) to reduce the dependence on relative density estimates from net and trawl sampling when conducting autonomous hydroacoustic surveys. The limitations of each method are discussed and we provide recommendations on combining sampling methods to increase the accuracy of zooplankton and ichthyoplankton studies.

2.3 Materials and methods

2.3.1 Study area and survey design

Tromsøflaket is comprised of a plateau (150 – 250 m depth) located at the southwestern entrance of the Barents Sea (Figure 2.1). The plateau is an area of high biological activity; some bank areas are heavily trawled as they support a rich community of commercially harvested fish (Olsen et al., 2010). It is a difficult region for traditional ecosystem sampling activity despite the relatively shallow bank because of the strong

and variable currents (Bellec et al., 2008; Kędra et al., 2017).

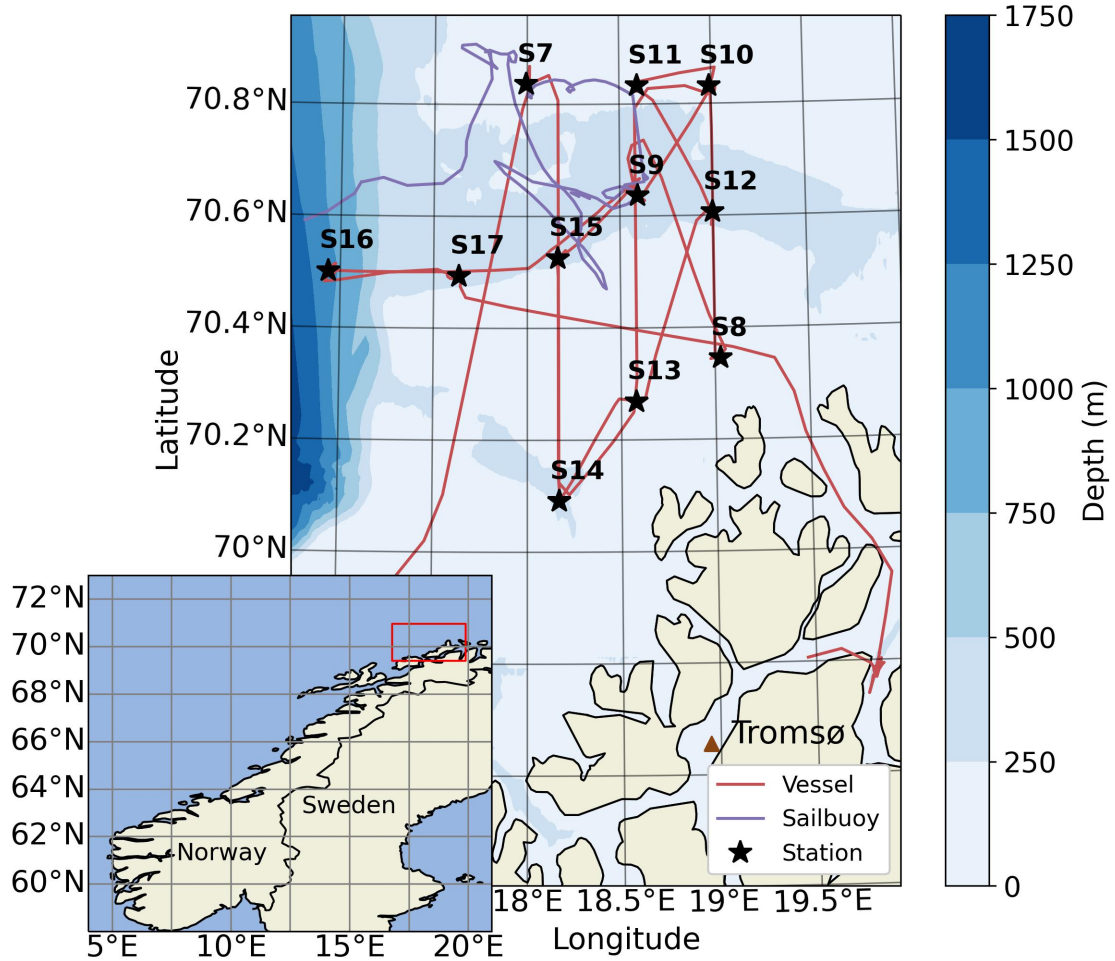


Figure 2.1: Map of the Norwegian Sea and Norway’s coasts. The red box in the inset indicates the area shown in the large bathymetric map of Tromsøflaket. The Tromsøflaket map indicates the vessel-based research cruise track in red as it travelled between sampling stations (black stars). Time and GPS location of stations are described in Table 1, and the Sailbuoy track in purple is the autonomous acoustic survey. Map produced with cartopy (ver. 0.18.0; scitools.org.uk/cartopy) in orthographic projection and the inset in plate carrée projection (UTM coordinate system).

Tromsøflaket was surveyed from June 20th to 29th, 2018, from the R/V *Helmer Hanssen* and an autonomous surface vehicle (Sailbuoy, Offshore Sensing, Bergen, Norway, www.sailbuoy.no). During the R/V *Helmer Hanssen* cruise, environmental data and biological samples were collected at 11 stations to estimate zooplankton and fish composition, density, and vertical distribution (Stations 7 to 17; Table 2.1). The Sailbuoy was deployed from the vessel at Station 7 on June 21st. It was picked up from Station 11 on June 22nd to fix issues with the storage of acoustic data and relaunched on June 24th at Station 9. The Sailbuoy left the study area on June 29th and was recovered south of Lofoten on August 22nd. The ship left the study area on June 25th. For this study, we only used the data from the Tromsøflaket region as delimited in Figure 2.1.

Table 2.1: The location and time of sampling stations within the Tromsøflaket region during the SeaPatches research cruise with R/V Helmer Hanssen.

Station	Date	Time (UTC)	Latitude ($^{\circ}$ N)	Longitude ($^{\circ}$ E)
S7	21/06/2018	03:53:00	70.836	17.996
S8	22/06/2018	03:48:00	70.345	19.028
S9	22/06/2018	17:15:00	70.636	18.595
S10	23/06/2018	01:01:00	70.831	18.988
S11	23/06/2018	05:50:00	70.833	18.597
S12	23/06/2018	13:40:00	70.606	18.999
S13	23/06/2018	22:45:00	70.268	18.581
S14	24/06/2018	02:14:00	70.091	18.169
S15	24/06/2018	10:57:00	70.525	18.166
S16	25/06/2018	05:35:00	70.500	16.936
S17	25/06/2018	20:26:00	70.493	17.636

2.3.2 Biological sampling

Mesozooplankton were sampled by vertical hauls (towing speed of 0.5 m s^{-1}) using a multiple opening/closing net (MultiNet, Hydro-Bios, Kiel, Germany, www.hydrobios.de; mouth opening 0.25 m^2 , mesh size $180 \mu\text{m}$). Five depth strata (bottom-100, 100-30, 30-10, 10-5, and 5-0 m) were sampled at each station, but data below 100 m were not used in this study because it was outside the range of the echosounder mounted on the Sailbuoy. At station 13, samples were taken by a ring net (WP2 net, Hydro-Bios), with the same mouth opening, mesh size and depth strata as the MultiNet, but did

not include the 0-5 m depth stratum. All samples were preserved in 4% formaldehyde-in-seawater solution buffered with hexamine. Taxonomic analyses were completed in the laboratory. Large organisms (total length > 5 mm) were picked out using forceps, identified, and counted from the whole sample. The remainder of the sample was examined by sub-sampling with aliquots obtained with a 5 ml automatic pipette, with the pipette tip cut at 5 mm diameter to allow a free collection of mesozooplankton. The number of subsamples analyzed was chosen so that at least 150 individuals of copepods (*Calanus* spp.) and 300 other organisms were counted. To assess the length frequency distribution of the *Calanus* population, the prosome length of all counted individuals of *Calanus* spp. was measured from the tip of the cephalosome to the distal lateral end of the last thoracic segment. In addition, body length of euphausiids, amphipods, pteropods, and fish larvae were measured from subsamples of Multinet samples taken at stations 8 through 17. Body length of euphausiids and amphipods was measured on stretched animals along the dorsal line from the tip of the rostrum (euphausiids) or the anterior edge of the eye (amphipods) to the tip of the telson. Body length of pteropods was measured as the diameter of their shell. The total length of fish larvae was measured as the most forward point of the head to the farthest tip of the tail with the fish lying on its side. Zooplankton density (individuals per m³) was estimated for each species by stratum by correcting for the mouth-opening area of the net and vertical hauling distance of the stratum, assuming 100% filtration efficiency. The weighted mean density estimate for each species per station over the 0-100 m range was calculated using the following equation:

$$\rho = \frac{\sum_{i=1}^n \rho^i dz^i}{\sum_{i=1}^n dz^i}, \quad (2.1)$$

where n is the number of strata, ρ^i is the density of the species in the stratum i in individuals per m^3 (ind. m^{-3}) and dz^i is the thickness of each stratum i in meters. Macrozooplankton and ichthyoplankton were sampled with a Tucker trawl (1 m^2 opening and 1000 μm mesh size) towed for 15 minutes at 2 knots between 20 to 40 m depth. The targeted depth at each station was determined from the epipelagic SSL identified in the echogram from the vessel's echosounders (Kongsberg Discovery AS, Horten, Norway, www.kongsberg.com; Simrad EK60, 18 and 38 kHz, 1.024 ms pulse duration, 2 Hz pulse repetition). All samples were preserved in a 4% formaldehyde-in-seawater solution buffered with hexamine. Density estimates from the Tucker trawl samples were analyzed per station. Each station was sub-sampled using a plankton splitter and counted until at least 300 individuals were identified. The count of each species was extrapolated to the entire sample size and converted to density by accounting for the mouth-opening area, deployment speed and time. To document the length distribution of dominant macrozooplankton species captured with the Tucker trawl, random subsamples of euphausiids, amphipods, pteropods and fish larvae were taken from samples of stations 7, 8 and 9 and body length was measured as described above.

For both MultiNet and Tucker trawl samples, species were grouped by taxon. Four taxonomic groups were most abundant: copepods, euphausiid larvae, amphipods, and pteropods. Additionally, fish larvae were included in the analysis because of the high sonar reflectivity of their swimbladder and their socio-economic importance.

2.3.3 Acoustic sampling

2.3.3.1 Acoustic data processing

The autonomous hydroacoustic survey was completed using a Sailbuoy equipped with a WBT Mini (Kongsberg Discovery AS) with a 333 kHz transducer (ES333-7CDK split-beam) operating in broadband mode (283-383 kHz, 1.024 ms pulse duration, 0.5 Hz pulse repetition, fast ramping) for 5 minutes every half hour. The transducer was mounted on a gimbal on the bottom of the Sailbuoy keel at 0.5 m depth. The Sailbuoy keel was always in the water and the transducer was always submerged. Echosounder calibration was performed before the deployment and after the retrieval with a 22.0 mm tungsten carbide (6% cobalt binding) calibration sphere (Demer et al., 2015). Broadband calibration parameters were calculated with the EK80 calibration wizard (version 2.0.1, EK80 software, Kongsberg Discovery AS), and the parameter values were linearly interpolated over the inhibition bands that covered the nulls. Data were calibrated and processed in Echoview (version 12.1, Echoview Software Pty Ltd, Hobart, Australia, www.echoview.com). The maximum range for the analysis was set to 50 m (50.5 m depth) because the signal to background noise ratio diminished below 10 dB (for a signal of -70 dB) at greater ranges.

2.3.3.2 Sound scattering layer backscatter spectra

Sound scattering layers forming discrete horizontal bands of backscatter above the background noise (Proud et al., 2015) were identified using k-means clustering, an unsupervised machine learning algorithm (Lloyd, 1982). Each raw data file output from the echosounder was converted into a netCDF4 file with the open-source software

echopype (version 0.5.3; Lee et al., 2021; Figure 2.2a). Data analysis was restricted to the region between the near-field (3 m range) and the signal-to-noise ratio limit (50 m range). In all echograms, a maximum of one SSL was detected by the clustering algorithm in the upper 50.5 m of the water column. The SSL varied in strength, thickness, and depth. The pulse-compressed volume backscattering strength (S_v [dB re 1 m^{-1}]) averaged over the frequency spectrum was pre-processed with a mean filter to smooth the backscatter in time (35 pings; or 70 s) and depth (15 bins; or 0.09 m) (Figure 2.2b). The pre-processing filter revealed the SSL on the depth/ S_v projection, as shown in the comparison between the unfiltered data in Figure 2.2c and the filtered data in Figure 2.2d.

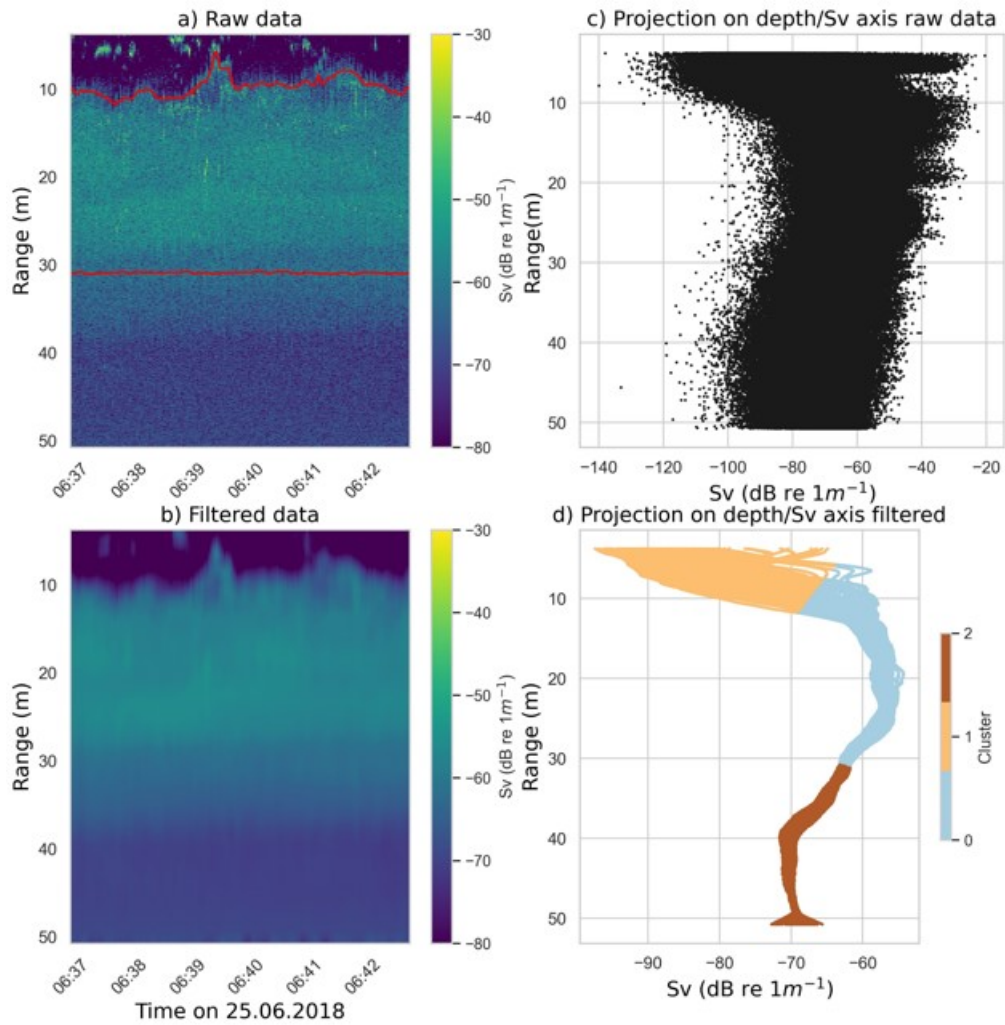


Figure 2.2: Example of a) raw pulse-compressed volume backscattering strength (S_v) echogram data upper and lower boundaries of Cluster 0 in red; b) echogram after the mean filtering in time and depth (70 s and 0.09 m filter, respectively); c) projection of raw data by removing the time dimension; and d) projection of filtered data in the depth/ S_v dimensions classified into clusters ($k=3$ in this example) obtained by k-means clustering. In this example, the cluster corresponding to the SSL is Cluster 0.

After the pre-processing, we applied k-means clustering on the depth/ S_v dimensions of each data file (between 3 to 5 minutes of data, depending on the file size). The k-means clustering algorithm categorizes all the data points into different groups, i.e., clusters. The only parameter adjusted for each SSL was the number of clusters. The other k-means parameters stayed the same for each iteration (k-mean++ initialization, 10 separate runs, tolerance of $1e^{-4}$, and a maximum of 300 iterations). Selecting the optimal number of clusters is an intrinsic challenge with k-means clustering. Here, the number of clusters was optimal when the entire SSL was grouped in a single cluster. The SSLs were easier to delineate by clustering when they were thick, had a high S_v and had a distinct separation from surface bubbles or entrained air (Anderson et al., 2007). We typically selected between 3-7 clusters. For example, in Figure 2.2d where Cluster 0 corresponds to the SSL, we chose to separate the backscatter profile into 3 clusters because of the relatively high S_v within the SSL (i.e., strong backscatter in the SSL relative to the background level).

The upper and lower boundaries of the SSLs identified by the clustering algorithm were imported to Echoview as editable line files to delineate SSL regions (e.g., red lines in Figure 2.2a which delimit the upper and lower boundaries of the SSL associated with Cluster 0). The broadband spectra of pulse-compressed volume backscattering strength ($S_v(f)$) were extracted from each identified SSL using Echoview’s “Wideband Frequency Response” export option. Broadband frequency response values were converted to the linear domain (volume backscattering coefficient spectra, $s_v(f)$ [m^{-1}]). We selected a Fourier transform window size of 0.4 m at a frequency resolution of 100 Hz over the entire bandwidth for a total of 1001 values per SSL. The Fourier transform window size was selected as a compromise between high frequency resolu-

tion and a high range resolution (Benoit-Bird & Waluk, 2020). The median and the interquartile range of $s_v(f)$ from each SSL were calculated for further analysis.

2.3.3.3 Sound scattering models

We ran scattering model ensembles per taxonomic group to calculate the theoretical backscatter for the forward and inverse acoustic density estimates. The taxonomic groups were selected from the net and trawl density data.

Weakly scattering fluid-like zooplankton The weakly scatterers were copepods, euphausiid larvae, and amphipods, which were modelled using a prolate spheroid for the copepods and a finite uniformly-bent cylinder for the euphausiid larvae and amphipods. Weakly scatterers have a sound speed contrast (h) and density contrast (g) of $1 \pm 5\%$. A near-unity sound speed and density contrast implies that the material properties of the scatterers are not significantly different from the surrounding medium (seawater). We chose the phase-compensated distorted wave Born approximation (PC-DWBA) model for the weakly scatterers in our domain because it is specifically adapted to densely aggregated zooplankton (Chu & Ye, 1999). Also, the PC-DWBA is adequate for the range of fluid-like taxonomic groups in the Tromsøflaket epipelagic layer because the parameters are flexible to geometry, material properties, and acoustic frequency changes (Chu & Ye, 1999; Gastauer et al., 2019). We identified the most abundant species of each taxonomic group to determine the model parameters. Copepods were modelled as *Calanus finmarchicus* copepodite stage V (CV) (61% of copepods in the MultiNet samples, Appendix A Table S1), euphausiid larvae were modelled as *Thysanoessa inermis* (100% of euphausiid larvae in the Tucker Trawl

samples, Appendix A Table S2) and amphipods were modelled as *Themisto abyssorum* (100% of amphipods in the MultiNet samples, Appendix A Table S1). We ran 1000 model simulations for each taxonomic group using the ZooScatR package (version 0.5; Gastauer et al., 2019) with varying shape, size, and material properties parameters. These parameters were selected based on literature or net and trawl samples (Table 2.2). The length distribution for euphausiid larvae was calculated using the measurements of *Thysanoessa inermis* in the Tucker trawl subsamples from stations 7, 8 and 9 (Figure 2.1). The length distribution for amphipods was identified by pooling measurements of *Themisto abyssorum* in MultiNet samples from stations 8-17 and Tucker Trawl samples from stations 7, 8 and 9. We repeated 1000 model simulations with random sampling within the distribution of each model parameter (Table 2.2) to calculate the variance in the cross-sectional backscatter across the available frequency spectrum (283-383 kHz) of each weakly scattering taxonomic group.

Table 2.2: PC-DWBA model parameter distributions for each taxonomic group. The distribution used are gamma: $\Gamma(\text{shape}, \text{rate})$, log normal: $L(\text{meanlog}, \text{sigmalog})$ and normal: $N(\text{mean}, \text{sigma})$.

Parameters	Copepods	Euphausiid larvae	Amphipods
Scattering model	DWBA	DWBA	DWBA
	Prolate spheroid	Uniformly-bent cylinder	Uniformly-bent cylinder
Length	$N(2.62, 0.09)^a$	$L(1.5, 0.3)^b$	$\Gamma(10.3, 2.3)^c$
Length-to-width ratio	$N(2.7, 0.2)^a$	$N(10.5, 0.3)^d$	$N(3, 0.5)^d$
Density contrast (g)	$N(0.996, 0.003)^{e,f}$	$N(1.036, 0.005)^e$	$N(1.058, 0.005)^d$
Sound speed contrast (h)	$N(1.027, 0.005)^e$	$N(1.026, 0.005)^e$	$N(1.058, 0.005)^d$
Orientation	$N(90, 30)^g$	$N(20, 20)^d$	$N(0, 30)^d$

^a Santana Hernández (2019)

^b Fit for the length measurements from the Tucker trawl subsamples. The distribution was assessed as the best fit based on a 1:1 line between theoretical and empirical quantiles in Q-Q plots.

^c Fit for the length measurements from MultiNet and Tucker trawl subsamples. The distribution was assessed as the best fit based on a 1:1 line between theoretical and empirical quantiles in Q-Q plots.

^d Lavery et al. (2007)

^e Kögeler et al. (1987)

^f Chu & Wiebe (2005)

^g Blanluet et al. (2019)

Elastic-shelled zooplankton The pteropod taxonomic group was modelled (in Python version 3.7) with a viscous-elastic model (Feuillade & Nero, 1998), as updated by Khodabandeloo et al. (2021). The model is developed for shapes with four layers: gas layer (swimbladder), thin elastic layer (swimbladder wall), thicker viscous layer (fish flesh) and the surrounding medium (seawater). We adjusted the model for pteropods by reducing the thickness of the viscous layer to zero, increasing the thickness of the elastic layer to correspond with the shell thickness, and characterizing the gas layer with the material properties of internal soft tissue. The adjustments to the boundary conditions fitted with the literature description of pteropods, a roughly spherical hard aragonite elastic shell with soft and weakly reflecting internal tissue inside (Lavery et al., 2007; Simmonds & MacLennan, 2008). The model is parameterized by the material properties and size of each layer, including the shape (thickness), density and sound speed properties (Khodabandeloo et al., 2021). As with the weakly scatterers, we identified the most abundant species to represent the taxonomic group in the scattering model. The pteropods were modelled as *Limacina retroversa* (100% of pteropods in the Tucker trawl samples, Appendix A Table S2). We assumed a spherical target for the scattering model. To account for the slightly elongated shape, we determined the radii distributions using both the width and length of the subsampled *Limacina retroversa* from the Tucker Trawl samples at stations 7, 8 and 9. The other shape parameters (radius of viscous layer and radius of gas layer; parameterized as a dense fluid layer) were calculated for each ensemble based on the selected elastic shell radius (Table 2.3). The outer layer was parameterized as aragonite. The internal layer was parameterized as a dense fluid representing the internal tissue with $g = 1.022$ and $h = 1.04$ (Lavery et al., 2007). The variance from the parameter space

of the viscous-elastic model was assessed by repeating 1000 model iterations with random sampling within the distribution of the radius of the elastic shell parameter (Table 2.3).

Table 2.3: Viscous elastic model ensemble shape and material properties parameters for pteropods and fish larvae in Tromsøflaket.

Parameters	Pteropods (two-layer sphere)	Fish larvae (three-layer sphere)
Radius of elastic shell - R_3	$\Gamma(shape = 5.4, rate = 9.17)^a$	$L(-1.46, 0.45)^b$
Radius of viscous layer - R_2	R_3	$(8.77R_3) + 1.62^c$
Radius of gas layer - R_4	$R_3 - (0.023R_3)^d$	$R_3 - 0.01^e$
Density (kg/m³)		
Surrounding medium - ρ_1	1027 ^d	1027 ^d
Viscous layer - ρ_2	n/a	1040 ^e
Elastic layer - ρ_3	2920 ^f	1141 ^g
Gas layer - ρ_4	1050 ^h	325.1 ^e
Sound speed (m s⁻¹)		
Surrounding medium - c_1	1480 ⁱ	1480 ⁱ
Viscous layer - c_2	n/a	1522.92 ^e
Elastic layer - c_3	5219 ^{e,j}	1450 ^e
Gas layer - c_4	1522.92 ^{h,j}	325.1 ^e
Shear viscosity (N/m ²) - μ_2	n/a	0.8571 ^{e,g}
Shear modulus (MPa) of swimbladder wall - μ_3	35800 ^j	0.17 ^e

^a Fit for the length measurements and corresponding widths using length-to-width ratio from Stanton et al. (2000) ($L/a = 1.5$). The distribution was assessed as the best fit based on a 1:1 line between theoretical and empirical quantiles in Q-Q plots.

^b Swimbladder radius was calculated based on the measured total length and the calculated widths using the relationship described by the data in (Chu et al., 2003) and assuming a linear relationship ($R_2 = 0.98$), as shown in Figure S1. The distribution was assessed as the best fit based on a 1:1 line between theoretical and empirical quantiles in Q-Q plots.

^c Linear regression (Supplementary material; Figure S1) established from swimbladder length-to-total length relationship using data from Chu et al. (2003).

^d Subtracted shell layer thickness (2.3% of radius) from elastic shell radius based on value from Lavery et al. (2007)

^e Khodabandeloo et al. (2021)

^f Stanton et al. (2000)

^g Feuillade & Nero (1998)

^h Lavery et al. (2007)

ⁱ Ship-based CTD measurements

^j Liu et al. (2005)

Gas-bearing organisms The fish larvae taxonomic group was modelled with the viscous-elastic model as juvenile/larvae of *Gadus morhua* (70% of fish larvae in the Tucker Trawl, Appendix A Table S2). The main scattering component of a gas-bearing organism is the gas enclosure, in this case the swimbladder. The radius of the elastic shell, the swimbladder, including the swimbladder wall, was calculated

by converting total length measurements to swimbladder length using relationships from juvenile and larval *Gadus morhua* studied by Chu et al. (2003) (Appendix A Figure S1). The corresponding swimbladder widths were also calculated through a swimbladder length-to-volume linear relationship, assuming a prolate spheroid swimbladder shape (Chu et al., 2003). The viscous-elastic model comparison of a sphere and a prolate spheroid at a range of incident angles indicates that the magnitude of the frequency response is dependent on the local radius at the angle of incidence (Figure 10 in Khodabandeloo et al., 2021). The peaks and nulls are horizontally translated, but these are eliminated through averaging for the volume backscatter of an aggregation. Therefore, we assumed a spherical target and determined the distribution of radii of the fish larvae using swimbladder length and width (R_3 in Table 2.3). The radii distributions were determined from the measured juvenile/larval *Gadus morhua* from the Tucker Trawl samples at stations 7, 8 and 9.

The other shape parameters (radius of the viscous layer and the gas layer) were calculated for each model simulation iteration based on the randomly selected elastic shell radius (Table 2.3). The variance from the parameter space of the viscous elastic model was assessed by repeating 1000 model iterations with a random selection of parameters given the distributions in Table 2.3.

2.3.3.4 Density estimates

The acoustic density estimates are based on the linearity principle that the total scattered energy from a volume is equal to the sum of the scattered energy of each randomly distributed individual scatterers within that volume (Foote, 1983; Greenlaw, 1979; Lavery et al., 2007), given by:

$$s_v(f) = \sum_{i=1}^N \sigma_{bs}^i(f) \rho^i \quad (2.2)$$

Where $s_v(f)$ is the volume backscattering coefficient spectra in m^2 per m^3 with measurements at all frequencies f in Hz, N is the number of taxonomic groups in the sampled volume, $\sigma_{bs}^i(f)$ is the cross-sectional backscatter spectra of a given taxonomic group i at all frequencies f in m^2 , and ρ^i is the density in individuals per m^3 (ind. m^{-3}) for each taxonomic group i . Estimates based on this equation assume that the entire volume backscatter is formed by the species or taxonomic groups included in the cross-sectional backscatter term. For the forward and inverse methods, we assumed the intensity of the backscattered signal was solely from the five modelled taxonomic groups.

Forward method The forward method is an approach to calculate density or biomass estimates of taxonomic groups from hydroacoustic-trawl survey data (Davison et al., 2015; Dornan et al., 2022; Love, 1975). The forward method for density estimates, as described in Simmonds & MacLennan (2008), was computed at the nominal frequency (333 kHz) to emulate the results from a narrowband (single frequency) survey, which simplifies Equation 2.2 to:

$$s_v = \langle \sigma_{bs} \rangle \rho^{total} \quad (2.3)$$

where s_v is the volume backscattering coefficient at a given frequency, $\langle \sigma_{bs} \rangle$ is the average predicted cross-sectional backscatter weighted by the relative density, $\rho_{relative}^i$, from net and trawl sampling, and ρ^{total} is the total density in individuals per m^3 (ind.

m⁻³).

The relative density is given by:

$$\rho_{relative}^i = 0.5 \left(\frac{\rho_{net}^i}{\rho_{net}^{total}} + \frac{\rho_{trawl}^i}{\rho_{trawl}^{total}} \right) \quad (2.4)$$

where ρ^i is the density of a given taxonomic group i from the net or trawl samples, and ρ^{total} is the total density, in individuals per m³ (ind. m⁻³).

We extracted the median s_v at the nominal frequency from the median $s_v(f)$ of each SSL. From the scattering model simulations for each taxonomic group, we extracted the weighted average $\langle \sigma_{bs} \rangle$ at the nominal frequency. The weights were calculated by the mean of the relative densities from the MultiNet and Tucker trawl samples (Appendix A Table S3 and Table S4). The calculated ρ^{total} for each SSL was divided among the taxonomic groups based on the relative density.

Inverse method Alternatively, the inversion of the broadband scattering data can be used to solve Equation 2.1 with a least-squares data fitting solver, as in Lavery et al. (2010) (Greenlaw, 1979; Lavery et al., 2007). From the scattering model simulations for each taxonomic group, we calculated the median cross-sectional backscatter, $\sigma_{bs}^i(f)$ (Equation 2.2) and 90% bootstrap interval of the median across the frequency spectrum. To calculate the density of each taxonomic group for the autonomous hydroacoustic survey with the inverse method, we solved Equation 2.2 for density ρ^i as a linear least-squares problem by using a Trust Region Reflective algorithm as described in Branch et al. (1999). The optimizer (Python version 3.7, `scipy.optimize.lsqr_linear`) determined the best solution by minimizing the following problem with the following bounds ($0 \leq \rho^i < \text{inf.}$):

$$0.5 \left(\left| \sigma_{bs}^i(f) \rho^i - s_v(f) \right| \right)^2 \quad (2.5)$$

A sensitivity analysis was conducted to quantify the effect of altering species shape and material properties on the variability of the inverse method density estimates. We ran 500 random permutations of Equation 2.3 with replacement. The permutations were run by selecting the cross-sectional backscatter spectra of each species to be either the median, the 5th or 95th percentile. The $s_v(f)$ of each SSL was also selected between the median, the 5th or 95th percentiles.

2.3.3.5 Comparison analysis

For comparison across all four methods, we performed a Kruskal-Wallis H test. For non-parametric pairwise comparisons, Dunn's tests were computed with p-values adjusted with the Benjamini-Hochberg adjustment (non-negative) to assess the significance of the difference in density estimates between each method pair for each taxonomic group.

2.4 Results

2.4.1 Biological sampling

Copepods dominated the mesozooplankton community sampled with the MultiNet with a mean density with standard error (\pm SE) of 1800 ± 300 ind. m^{-3} (95% of the community, Figure 2.3). Pteropods were the second most abundant taxonomic group in the MultiNet samples, with a mean density of 50 ± 30 ind. m^{-3} (2.8%

of the community). Euphausiid larvae had a low density (9 ± 2 ind. m^{-3} , 0.5% of the community); most of these were represented by euphausiid larvae in furcilia stages (89% of euphausiid larvae over all MultiNet samples). Other species, such as siphonophores and meroplankton, not included in the selected taxonomic group for this study, accounted for 30 ± 5 ind. m^{-3} , or 2%, of the MultiNet catch in the study region. Detailed MultiNet density data are presented in Appendix A Table S1 and Table S3.

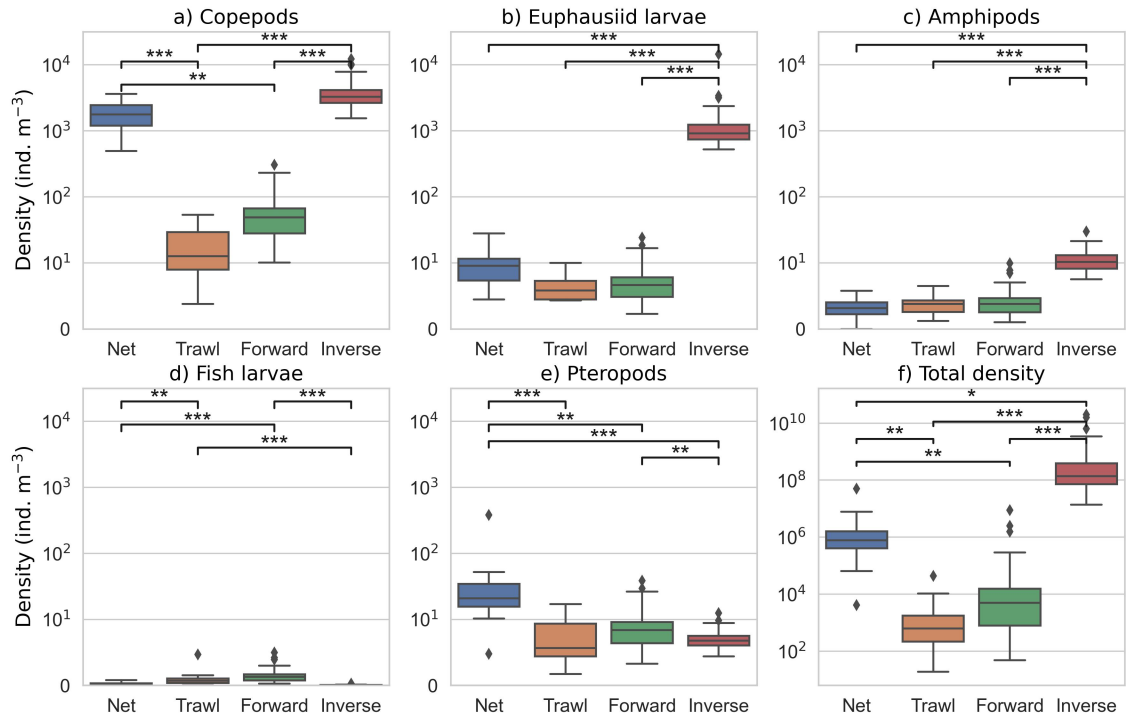


Figure 2.3: a-e) Density estimates in the logarithmic domain for each dominant taxonomic group in Tromsøflaket, in units of base 10 logarithm of individuals per m³. Each box summarises the density measurement from Net (MultiNet; n=11, blue), Trawl (Tucker trawl; n=11, orange), Forward (acoustic forward method; n=70, green) or Inverse (acoustic inverse method; n=70, red). Significant differences are denoted by the number of asterisks (*), with *** p < 0.001, ** p < 0.01 and * p < 0.05 from pairwise Dunn's tests. f) is the total density estimate (sum of all species) for all stations (Net and Trawl) and all SSLs (sound scattering layers) (Forward and Inverse). Note the different y-axis scale in subplot f.

Like the MultiNet samples, the Tucker trawl samples were primarily composed of copepods (54% of the community, Figure 2.4), but the average density was much

lower with 19 ± 5 ind. m^{-3} (Figure 2.3). Small pteropods (mean length = 1.2 mm, Table 4) were the second most abundant taxonomic group in the trawl samples, with a mean density of 5 ± 1 ind. m^{-3} (17% of the community). Euphausiid larvae had comparable density (3.5 ± 0.7 ind. m^{-3} , 16% of the community); most of these larvae were *Thyssanoessa inermis* (99.8% of euphausiid larvae in the Tucker Trawl sample). The mean length of the larvae was 4.7 mm, suggesting they were still young of the year, like the furcilia stages from the MultiNet samples (mean length 4.0 mm; Table 4). Other species not included in the selected taxonomic group for this study, such as siphonophores and decapod crustaceans, accounted for 7% of the Tucker trawl catch in the study region. Detailed Tucker trawl density data are available in Appendix A Table S2 and Table S4.

Table 2.4: The size distribution of the dominant species from each taxonomic group. MultiNet and Tucker trawl length measurements were taken from subsamples. The “acoustics” sampling method shows the mean length and standard deviation (SD) used in the scattering models for the forward and inverse methods.

Taxonomic group	Sampling method	Species	N	Length (mm)	SD (mm)
Pteropods	MultiNet	<i>Limacina retroversa</i>	157	1.5	0.6
	Tucker trawl	<i>Limacina retroversa</i>	70	1.2	0.3
	Acoustics	<i>Limacina retroversa</i>	229	1.4	0.6
Copepods	MultiNet	<i>Calanus finmarchicus CV</i>	^a	2.62 ^b	0.09
	Tucker trawl	<i>Calanus finmarchicus CV</i>	n/a	n/a	n/a
	Acoustics	<i>Calanus finmarchicus CV</i>	^a	2.62 ^b	0.09
Euphausiid larvae	MultiNet	<i>Euphausiacea furcilia</i>	105	4.0	1.0
	Tucker trawl	<i>Thyssanoessa inermis</i>	108	4.7	1.6
	Acoustics	<i>Thyssanoessa inermis</i>	108	4.7	1.6
Amphipods	MultiNet	<i>Themisto abyssorum</i>	75	4.6	1.4
	Tucker trawl	<i>Themisto abyssorum</i>	108	4.3	1.2
	Acoustics	<i>Themisto abyssorum</i>	183	4.4	1.3
Fish larvae	MultiNet	<i>Pisces larvae</i>	8	8.3	5.8
	Tucker trawl	juvenile <i>Gadus morhua</i>	61	9.3	3.2
	Acoustics	juvenile <i>Gadus morhua</i>	61	7.6	3.1

Note: All measurements are of full length unless otherwise specified.

^a Santana Hernández (2019)

^b Prosome Length (PL)

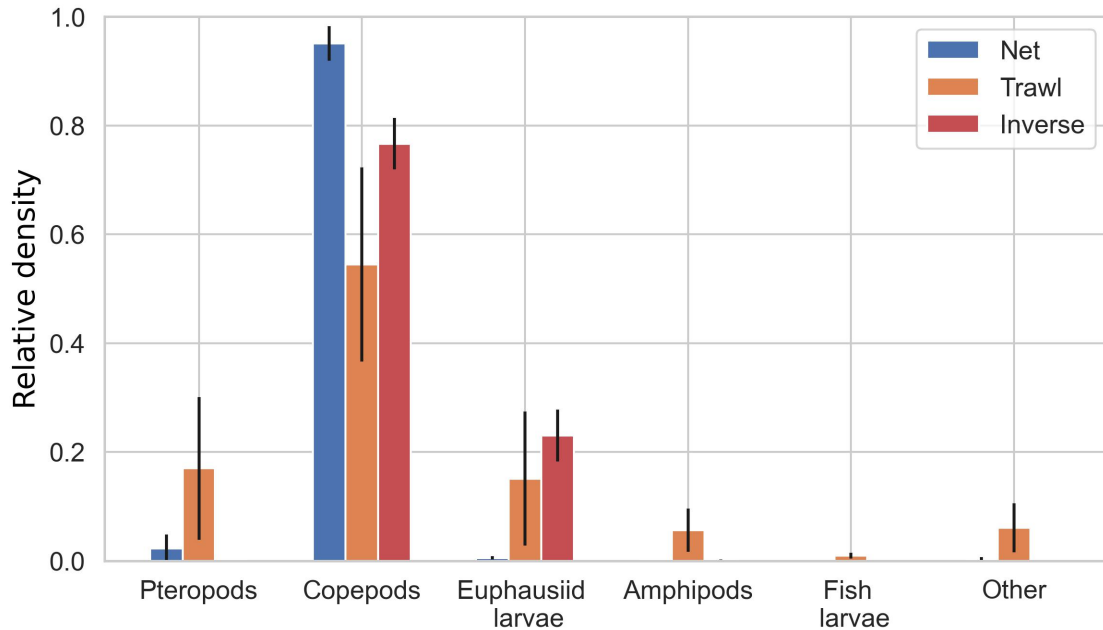


Figure 2.4: Relative density of each taxonomic group as calculated by each sampling method across the whole survey region of Tromsøflaket with standard deviation error bars representing variability between stations (Net and Trawl) or SSLs (Inverse). Taxonomic groups are ordered from smallest (left) to largest (right). Size details of each taxonomic group are described in Table 2.4.

2.4.2 Acoustics

Sound scattering layer detection The k-means clustering algorithm identified a total of 70 SSLs over the autonomous acoustic survey period. The SSLs varied between 1 m to 29 m (min. and max.) in thickness, with the layers centred at an average depth of 20.6 m. The median volume backscattering strength spectra from

all the SSLs varied between -75 to -50 dB re 1 m^{-1} (min. and max.). At the nominal frequency, the median $S_v(f)$ varied between -73 and -56 dB re 1 m^{-1} (min. and max.).

Scattering models The target strength (TS) frequency response varied in strength and shape across the taxonomic groups. The median broadband TS ranged from a minimum of -100 dB re 1 m^2 at the lowest frequency, 283 kHz, for the smallest fluid-like weakly scatterer, copepod taxonomic group, to a maximum of -65 dB re 1 m^2 at 345 kHz from the gas-bearing taxonomic group, fish larvae (Figure 2.5). Copepods, euphausiid larvae and fish larvae TS spectra had a positive slope with TS increasing with frequency, whereas amphipods and pteropods had a negative sloping TS(f) (Appendix A Figure S2, shown as cross-sectional backscatter spectra, i.e., linear form of TS). The cross-sectional backscatter matrix had a rank of 5, suggesting the taxonomic groups were linearly independent and can be distinguished by the least-squares algorithm.

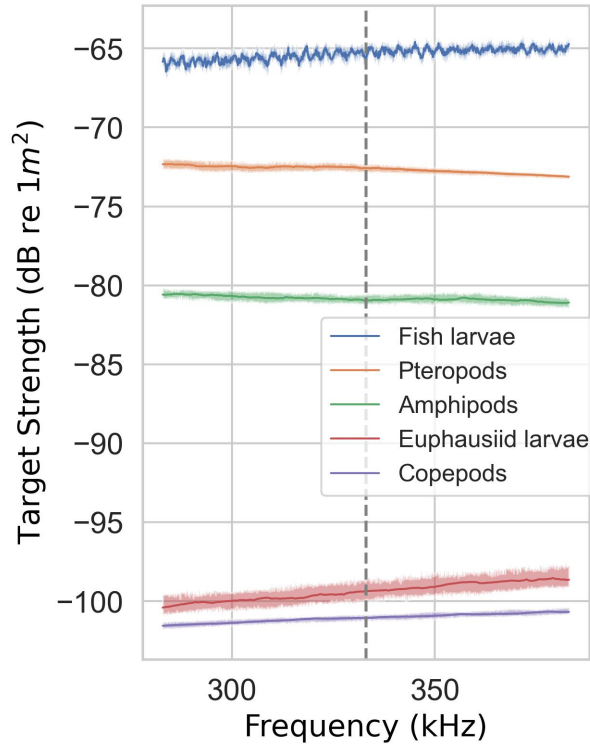


Figure 2.5: Median target strength results of ensemble simulations from the scattering models for each dominant taxonomic group in Tromsøflaket, including the 90% bootstrap confidence intervals of the median as the shaded region. Vertical grey dashed line indicates the nominal frequency (333 kHz).

Forward method density estimates Based on the relative density results from the MultiNet and Tucker trawl, the forward method estimated SSLs dominated by copepods (56 ± 6 ind. m^{-3}) followed by pteropods (7.0 ± 0.7 ind. m^{-3}), euphausiid larvae (4.3 ± 0.5 ind. m^{-3}), amphipods (1.6 ± 0.2 ind. m^{-3}) and fish larvae (0.40 ± 0.04 ind. m^{-3}) (Figure 2.3). The relative density was a fixed input parameter in the calculation; therefore, the forward method was not included in Figure 2.4.

Inverse method density estimates The density estimates measured from the inversion of the autonomous acoustic survey showed an SSL dominated by the copepods ($3700 \pm 200 \text{ ind. m}^{-3}$; 77% of acoustic density estimates), which agreed with the MultiNet results. The second most abundant group in the acoustic results was euphausiid larvae (modelled as *Thyssanoessa inermis* from Tucker trawl), with $1300 \pm 200 \text{ ind. m}^{-3}$, representing 23% of the total taxonomic composition. In the inverse method estimates, amphipods had a higher density than pteropods with $10.3 \pm 0.5 \text{ ind. m}^{-3}$ (0.2%) and $3.9 \pm 0.2 \text{ ind. m}^{-3}$ (0.08%), respectively. The fish larvae had the lowest density as with the other sampling methods, $0.126 \pm 0.001 \text{ ind. m}^{-3}$; 0.002% of the total composition.

The sensitivity analysis showed the variability in the density estimates compared to the variation in the model parameters and the volume backscatter within each SSL (standard deviation). The sensitivity of density estimates was compared to the distribution of densities of the 70 SSLs. For the copepods and euphausiid larvae, the effect of the dispersion in the model parameters and volume backscatter variability was smaller than the standard deviation from the density estimates of all the SSLs (Figure 2.6a,b). Conversely, amphipods, fish larvae and pteropods density estimates had a larger sensitivity to the model parameters and volume backscatter than the variability in density estimates across the study region (Figure 2.6c, d, e). Density estimates of all species showed higher variability in the case of SSLs with high backscatter (e.g., SSL n^o 47-48; Figure 2.6).

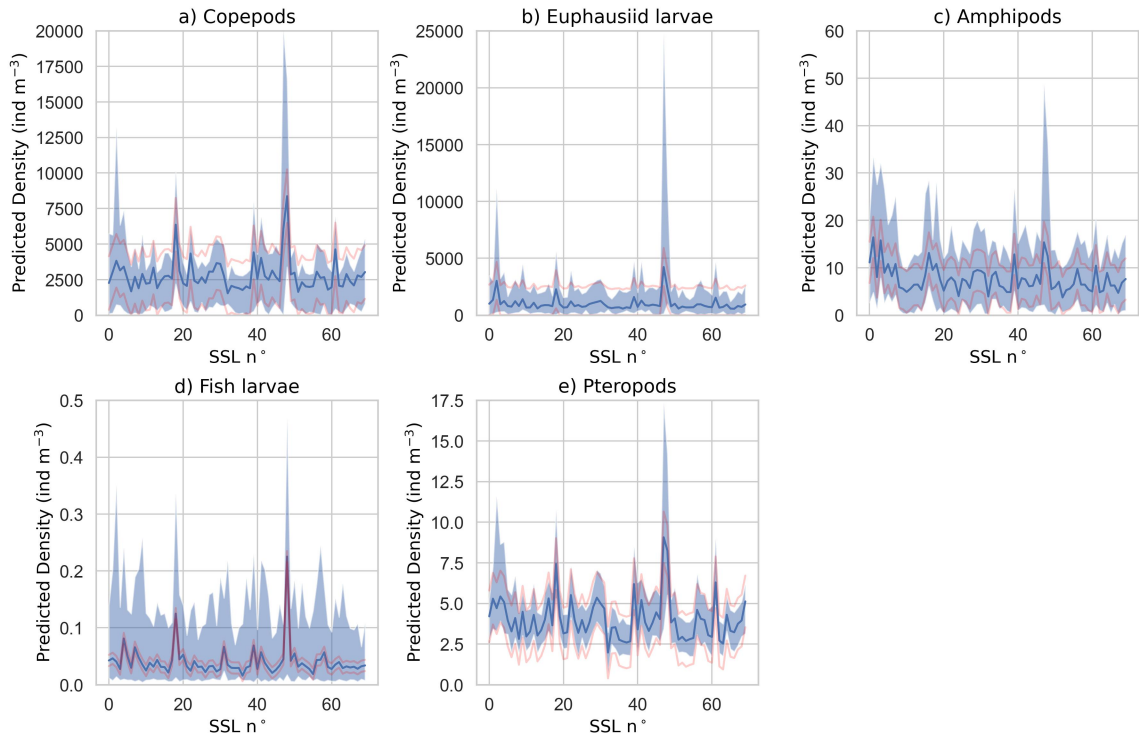


Figure 2.6: The sensitivity analysis results for predicted density estimates of each taxonomic group (a-e) for the inversion of acoustic data with scattering model results varying randomly between median, the 5th and 95th percentiles and the volume backscatter spectra varying randomly between median, and interquartile range for each SSL (x-axis). The blue line in each panel is the median of the sensitivity analysis, and the shaded region displays the extent of the 5th and 95th percentile. The red lines indicate the standard deviation of the density estimates for all the SSLs. Note the difference in scale of the y-axis.

2.4.3 Density analysis across methods

All four methods compared in this analysis (MultiNet, Tucker trawl, and forward and inverse method with autonomous acoustic survey data) showed that copepods dominated the epipelagic SSL across the study area ($> 50\%$ density for all sampling methods, Figure 2.4). However, comparisons of density estimates for all methods were significantly different for each taxonomic group as revealed by a Kruskal-Wallis H test, denoted with degrees of freedom in parenthesis (copepods: $H(3) = 127.87$, $p < 0.0001$; euphausiid larvae: $H(3) = 121.24$, $p < 0.0001$; amphipods: $H(3) = 115.14$, $p < 0.0001$; fish larvae: $H(3) = 118.10$, $p < 0.0001$; pteropods: $H(3) = 31.89$, $p < 0.0001$) (Figure 2.3).

Density estimates were significantly different between the MultiNet and Tucker trawl for copepods, pteropods, and fish larvae (Dunn's test; $p < 0.01$). No significant differences in density estimates between the net and trawl were found for the other taxonomic groups (euphausiid larvae: $p = 0.19$ and amphipods: $p = 0.79$). Results from pairwise comparisons from Dunn's tests are shown in Appendix A Figure S3. Density estimates of euphausiid larvae were almost three times higher based on the MultiNet samples than the Tucker trawl samples. However, the relative density of euphausiid larvae in the Tucker trawl samples was higher (11.1%) than in the MultiNet samples (0.5%) (Figure 2.4). As with the euphausiids, pteropods density was eleven times higher in the MultiNet samples than in the Tucker trawl samples, but pteropods had a lower relative density in the MultiNet (2.8% of the community) than in the Tucker Trawl (16.1%). For amphipods, similar densities were sampled by net and trawl (1.2 ± 0.3 ind. m^{-3} for MultiNet and 1.4 ± 0.3 ind. m^{-3} for Tucker trawl). Fish larvae

were found in low densities, on average 0.05 ± 0.02 ind. m^{-3} in the MultiNet and 0.3 ± 0.2 ind. m^{-3} in the Tucker trawl, and had low relative densities in both net and trawl (<1% of the total catch in both direct sampling methods).

A pairwise comparison of the forward method for acoustic data analysis showed that these density estimates were not statistically different from the Tucker trawl estimates for all taxonomic groups (copepods: $p=0.08$; euphausiid larvae: $p=0.77$; amphipods: $p=0.79$; fish larvae: $p=0.31$; pteropods: $p=0.07$). In contrast, density estimates from the forward method were statistically different from estimates from the MultiNet samples for copepods ($p<0.01$), fish larvae ($p<0.001$) and pteropods ($p<0.01$), but not for the euphausiid larvae ($p=0.18$) and amphipods ($p=0.76$). The density estimates calculated from the autonomous acoustic survey data by the forward and inverse methods were statistically different for all taxonomic groups ($p<0.01$).

Pairwise comparisons indicated that the autonomous acoustic survey density estimates calculated through inversion differed significantly from the other sampling methods for the euphausiid larvae and amphipods (Dunn's test; $p<0.001$). However, for the copepods, the inverse results were not statistically different from the MultiNet ($p=0.06$) but statistically different from the Tucker trawl ($p<0.001$). The results from the inverse method were not statistically different from densities measured from the Tucker trawl for pteropods ($p=0.92$) but were statistically different from the results of the MultiNet and forward method ($p<0.01$). For fish larvae, the densities measured from the MultiNet were not statistically different from the results of the inverse method ($p=0.58$) but were statistically different from the densities measured from the Tucker trawl and forward method ($p<0.001$).

Overall, the inverse method reported the highest total average density of 4987 ind.

m^{-3} , followed by the MultiNet samples (1931 ind. m^{-3}), the forward method (70 ind. m^{-3}) and the Tucker trawl samples (29 ind. m^{-3}).

2.5 Discussion

2.5.1 Comparison of sampling methods

To our knowledge, this study is one of the first implementations of the inverse method from an autonomous broadband acoustic survey with TS estimates informed by locally derived measurements of shape properties. The inverse method yielded higher density estimates. These density estimates are most likely a more accurate representation of the sound scattering layers for the five dominant plankton taxonomic groups in the Norwegian Sea. Net and trawl sampling likely underestimated zooplankton densities within the SSL because of gear-specific biases when assessing species composition across size classes (Hetherington et al., 2022; Skjoldal et al., 2013).

All sampling methods determined that copepods dominated the epipelagic SSL in Tromsøflaket. The relative density of copepods calculated from the inverse method (77%) was between the MultiNet (95%) and Tucker trawl (54%). We suspect that because the copepods were relatively large individuals (mainly *Calanus finmarchicus* CV with a mean length of 2.6 mm) organized in dense swarms, the high frequency and high bandwidth (283-383 kHz) of the acoustic instrument detected most of these copepods. The agreement of the density estimates from the inverse method and MultiNet suggests that the high vertical resolution of the broadband acoustic data could be used to increase the accuracy of copepod density estimates within the epipelagic

layer. In the future, satellite observations of ocean colour could compensate for the blind zone of acoustic measurements near the surface and measure the near-surface density of copepods (Basedow et al., 2019).

Variations in organism size and swimming abilities must be considered when designing surveys and selecting sampling methods. The MultiNet targets small zooplankton species (>0.3 mm), especially weak swimmers aggregating in high densities. The Tucker trawl is designed to catch larger, fast-swimming zooplankton and ichthyoplankton species in the epipelagic layer. Therefore, we did not expect to find higher densities of euphausiid larvae in the MultiNet compared to the Tucker trawl since they are known to avoid MultiNets and similar gear (Brinton, 1967; Greenlaw, 1979). The inverse method estimated densities of euphausiid larvae as more than 100 times higher than the net, trawl, and forward method. Because of the well-known ability of euphausiids to avoid capture by standard oceanographic nets (Wiebe et al., 1982), we suggest that the density estimates of euphausiid larvae based on the inverse method are likely closer to reality than the estimates based on the compared methods. Both the MultiNet and Tucker trawl captured small euphausiids (mean length in MultiNet = 4.0 mm and mean length in Tucker trawl = 4.7 mm, Table 2.4), which did not have the backscattering properties of adults. Young euphausiids have less than 30% of the lipid content of adults, which reduces their density contrast (Kögeler et al., 1987). We expect the density difference of the net, trawl, and forward method to the inverse method to be even larger in the case of adult euphausiids because of their increased avoidance abilities and stronger sound scattering properties.

The relatively high densities of both small (copepods) and larger mobile (amphipods and euphausiids) zooplankton measured with the inverse method suggests that this

approach can accurately sample a larger size spectrum of targets than the other methods. Similar to euphausiids, density estimates of amphipods were higher when calculated with the inverse method. Amphipods are also fairly strong scatterers and mobile swimmers (Skjoldal et al., 2013). We conclude that the inverse method from autonomous acoustic surveys provided the best density estimates for agile organisms that avoid nets and trawls.

The inverse acoustic method could be applied to larger organisms than zooplankton, such as pelagic fish. Sampling efficiency for fish and their vertical distribution in the water column has been widely studied because of the socio-economic importance of fisheries (Handegard & Tjøstheim, 2005). A net comparison study from June 1993 in Storfjorden, Norway, has reported a higher density of ichthyoplankton between 50-100 m than between 0 – 50 m (Skjoldal et al., 2013). The autonomous acoustic monitoring system used in this study had a maximum depth of 50.5 m, limiting the detection of fish larvae in deeper regions of the epipelagic layer. Yet, ichthyoplankton densities were comparable between methods. One way of improving estimates of density and vertical distribution pattern of fish larvae in high latitude shelf areas could be to use the inverse method with a transducer with a deeper detection range (lower frequency band or longer pulse length) or using both surface and underwater vehicles, such as gliders. A lower frequency bandwidth (for example, 185-255 kHz) would also be beneficial for measuring the density of ichthyoplankton and pteropods because they have a stronger acoustic backscatter at lower frequencies.

Zooplankton layers are known to exhibit patchiness; therefore, variability in relative density across the sampling region is expected (Basedow et al., 2006; Trevorrow et al., 2005; Trudnowska et al., 2016). For example, we found high variability in pteropod

densities based on net samples between stations (maximum at station 13 with 379 ind. m^{-3} and minimum at station 17 with 2 ind. m^{-3}), which likely results from their patchy distribution (Elizondo & Vogt, 2022). The Tucker trawl did not capture such a broad variability in densities (maximum at station 8 with 16 ind. m^{-3} and a minimum at station 17 with 0.5 ind. m^{-3}), which may be due to the larger mesh underestimating the small pteropods (mean length of 1.2 mm; Table 2.4). Because the net and trawl sampling and the acoustic measurements are not coincident in time and space in this study, we used a static average relative density to reflect the species composition of the region. In contrast, the inverse method provides continuous measurements and is not dependent on punctual sampling.

2.5.2 Assessment of the autonomous acoustic survey and inverse method for density estimates

Autonomous acoustic surveys require effective data processing methods that limit the introduction of biases and can quickly be applied to large datasets. The results of the k-means clustering algorithm revealed that, despite being ubiquitous over the study area, the sound scattering layer varied in thickness, volume backscattering strength, and depth over time and space. This algorithm restricted the user bias of identifying boundaries and increased reproducibility because the only subjective parameter in this machine learning algorithm was the number of clusters. The successful application of the k-means clustering method for identifying SSLs in the Tromsøflaket area suggests that it can now be tested on more complex vertical structures with multiple discrete SSLs in different regions.

Density estimates were corrected for the sampling volume for each method; however, the differences in sampling depths could influence the results. The acoustic estimates were bounded by the edges of the epipelagic SSLs which were determined by k-mean clustering and typically found between 3.5 – 50 m, whereas the Tucker trawl sampled 0 – 20 or 40 m and the MultiNet sampled 0 – 100 m. The acoustic density estimates did not incorporate volumes with lower densities above and below the epipelagic SSL. In contrast, the densities calculated from nets and trawls were averaged over the entire sampling range. The acoustic inversion was only applicable within the boundaries of the SSL where the density of scatterers is high. If the density of scatterers is too low, the echo statistics are dependent on the target's location in the beam rather than the intensity summation process (Holliday & Pieper, 1995). Under such low-density scenarios, single echo detections and echo counting (Kieser & Mulligan, 1984; Simmonds & MacLennan, 2008) should be used instead of the inverse method. However, if differences in density estimates were driven by differences in sampling depths, we would expect high densities from both acoustic methods, not just the inverse method. In this study, we relied on the size distribution of the dominant species locally derived from nets and trawls to inform the scattering models because the 283-383 kHz bandwidth only detected the geometric scattering of the targets ($ka > 1$; Lavery et al., 2010). However, with a broader frequency spectrum that captures the Rayleigh-to-geometric scattering transition of all taxa, the size classes can be identified within the inverse method (Cotter et al., 2021; Greenlaw, 1979; Lavery et al., 2007). In that case, the scattering transition point determines the resonance frequency, which is inversely proportional to the size of the scatterers and can increase the ability to differentiate among taxa (Benoit-Bird, 2009; Holliday & Pieper, 1995; Warren et al., 2003). Cap-

turing the Rayleigh-to-geometric transition would thus improve the method because it produces a frequency response curve with a more identifiable shape (Cotter et al., 2021). Nonetheless, we demonstrated that relying on a bandwidth covering the transition point is not necessary to determine the density of epipelagic organisms using the inverse method when size distributions are provided by net and trawl samples. The sensitivity analysis tested the variability in the frequency-response curves compared to the variability in the model parameters and showed that the density estimates of the stronger scatterers (amphipods, fish larvae and pteropods) had a larger sensitivity to the model parameters than the weaker scatterers (copepods and euphausiid larvae). The inverse method is based on absolute scattering levels, which rely heavily on calibration (Lavery et al., 2007). A two-sphere calibration covering the entire broadband signal should be carefully completed for future density calculations using the inverse method. Careful calibration across the bandwidth is critical, as with multi-frequency analysis, to avoid artificial trends in the frequency-response curves. In addition, the inverse method requires knowledge of the scattering model parameters for each taxonomic group. Here, some of these parameters were informed by the net and trawl data but others were defined based on previous literature values. Variability in model parameters like orientation or material properties can affect the density estimates, especially for the stronger scatterers as shown by the sensitivity analysis. *In situ* measurements of material properties, sound speed, and density contrasts, and more knowledge about the orientation of the scatterers would restrict the variability of model simulation results and improve the accuracy of the density estimates. Furthermore, the median was used to have a central measure for the tendency of the taxonomic group's cross sectional backscatter spectra from the model

ensembles because of the skewed spread in values, however the mean would be more appropriate measure for the linearity principle (Foote, 1983).

Because of their low taxonomic resolution, both the forward and inverse acoustic methods are dependent on the initial taxonomic group selection. Different statistical or data-fitting approaches with an error term could better account for non-dominant species, such as meroplankton and decapod larvae. In the current study, errors in the taxonomic classification would lead to a positive bias in the density estimates from the acoustic methods. The limited taxonomic resolution of the acoustic inversion method could be improved by the addition of imaging sensors which are already being integrated on autonomous platforms equipped with a wideband echosounder (Reiss et al., 2021; Whitmore et al., 2019). Optical sensors could also provide information on the size and, to some extent, the orientation of the scatterers (Ohman et al., 2019), which would improve the *in situ* scattering models.

2.6 Conclusion

The inverse method was used to quantify aggregations of zooplankton and ichthyoplankton with a broadband autonomous hydroacoustic survey and detected higher densities of abundant mobile zooplankton than the net, trawl, and forward acoustic method. The inverse method also detected similar densities of smaller mesozooplankton to the net samples. We conclude that the inverse method reduced the biases associated with net avoidance in the density estimates for a broad size spectrum of zooplankton. This work built on studies on the inverse method for zooplankton layers (Lavery et al., 2007), autonomous hydroacoustic surveys (De Robertis et al., 2019)

and broadband data processing (Bassett et al., 2019; Benoit-Bird & Waluk, 2020) in recent years. We further advanced the field by offering a solution for the limitation of sparse coexisting biological sampling from autonomous acoustic surveys by using the inverse method with locally derived size measurements.

Accurate density estimates of pelagic organisms with high spatio-temporal resolution are critical to conducting stock assessment surveys and understanding the impact of changes in the epipelagic zone and their effects on food supply to deeper water ecosystems (Rogers, 2015). To this end, we conclude that applying the inverse method to broadband hydroacoustic data can improve the accuracy of acoustic-trawl surveys. We further envision that applying the inverse method to acoustic data collected from autonomous platforms could supplement and extend the spatial resolution of vessel-based surveys at a lower cost than additional ship time.

Chapter 3

Model-informed classification of broadband acoustic backscattering from zooplankton in an *in situ* mesocosm

Muriel Dunn^{1,2}, Chelsey McGowan-Yallop³, Geir Pedersen⁴, Stig Falk-Petersen⁵, Malin Daase⁶, Kim Last³, Tom J. Langbehn⁷, Sophie Fielding⁸, Andrew S. Brierley⁹, Finlo Cottier^{3,6}, Sünnje L. Basedow⁶, Lionel Camus¹, and Maxime Geoffroy^{2,6}

¹ Akvaplan-niva AS, Fram Centre, Postbox 6606, Stakkevollan, 9296 Tromsø, Norway

² Centre for Fisheries Ecosystems Research, Fisheries and Marine Institute of Memorial University of Newfoundland, St. John's, A1C 5R3, NL, Canada

³ Scottish Association for Marine Science, Oban, Argyll PA37 1QA, UK

⁴ Institute for Marine Research, 5005 Bergen, Norway

⁵ Independent scientist, 9012 Tromsø

⁶ Department of Arctic and Marine Biology, UiT The Arctic University of Norway, 9019 Tromsø, Norway

⁷ Department of Biological Sciences, University of Bergen, 5020 Bergen, Norway ⁸ British Antarctic Survey, Natural Environment Research Council, High Cross, Cambridge CB30ET, United Kingdom

⁹ Pelagic Ecology Research Group, School of Biology, Scottish Oceans Institute, Gatty Marine Laboratory, University of St Andrews, St Andrews, KY16 9TS, United Kingdom

Published in *ICES Journal of Marine Sciences - Echosounder to the Cloud Symposium Issue* on December 7th, 2023

3.1 Abstract

Classification of zooplankton to species with broadband echosounder data could increase the taxonomic resolution of acoustic surveys and reduce the dependence on net and trawl samples for ‘ground truthing’. Supervised classification with broadband echosounder data is limited by the acquisition of validated data required to train machine learning algorithms (‘classifiers’). We tested the hypothesis that acoustic scattering models could be used to train classifiers for remote classification of

zooplankton. Three classifiers were trained with data from scattering models of four Arctic zooplankton groups (copepods, euphausiids, chaetognaths, and hydrozoans). We evaluated classifier predictions against observations of a mixed zooplankton community in a submerged purpose-built mesocosm (12 m³) insonified with broadband transmissions (185 to 255 kHz). The mesocosm was deployed from a wharf in Ny-Ålesund, Svalbard, during the Arctic polar night in January 2022. We detected 7,722 tracked single targets which were used to evaluate the classifier predictions of measured zooplankton targets. The classifiers could differentiate the copepod modelled spectra from the other groups, but they could not differentiate euphausiids, chaetognaths, and hydrozoans reliably due to the similarities in their modelled target spectra. We recommend that model-informed classification of zooplankton from broadband acoustic signals be used with caution until a better understanding of *in situ* target spectra variability is gained.

3.2 Introduction

Acoustic target classification of zooplankton is needed to improve our understanding of variability in zooplankton spatio-temporal distribution and community composition. In the past decade, the commercial availability of broadband echosounders has made it possible to characterize the backscattering spectra of aquatic targets over a continuous frequency range (Bassett et al., 2018). Compared to conventional narrowband echosounder methods, the wider bandwidth of frequency-modulated (FM) echosounders offers the potential for improved classification of fish and zooplankton (Benoit-Bird & Waluk, 2020). In addition, pulse-compression signal processing of

broadband data improves the range resolution and the signal-to-noise ratio, enabling weak zooplankton targets to stand out above the stochastic background noise (Chu & Stanton, 1998; Ehrenberg & Torkelson, 2000). These improvements have made it possible to distinguish smaller and acoustically weaker individual targets, such as mesozooplankton (0.2 to 20 mm), offering the potential for target classification using the target strength (TS [db re 1 m²]) - frequency response spectra (TS(f), hereafter ‘target spectra’) as a predictive feature (Bandara et al., 2022).

Machine learning (ML), a field of artificial intelligence, is an increasingly popular tool for target classification in fisheries acoustics, reflecting a broader trend of AI applications in the marine sciences (Beyan & Browman, 2020; Malde et al., 2020). ML methods are objective, efficient, and can handle the large, complex datasets associated with broadband sampling (Malde et al., 2020). In short, supervised classification algorithms are trained to predict the class of new, unidentified samples with reference to scattering spectra from labelled training samples (i.e., samples for which the class is known) to optimize the classification function. In a fisheries acoustics context, the class is typically the species (or a broader functional group, e.g., based on gross anatomical properties) of the target or aggregation. The feature variables used to predict the class of each target may include various acoustic features (e.g., backscattering strength and derived quantities), often in combination with geometric features (e.g., school length and height; Proud et al., 2020) or bathymetric features (e.g., distance from the seabed) (Korneliussen, 2018). Machine learning algorithms improve the potential for real-time target classification and subsequent analysis (such as density estimates; Blackwell, 2020) for the increasing use of autonomous or remotely operated vehicles equipped with echosounders (e.g., De Robertis et al., 2019;

Dunn et al., 2022; Ludvigsen et al., 2018; Malde et al., 2020). However, a significant obstacle to applying supervised classification in fisheries acoustics is the collection of labelled observations to train the algorithms (Handegard et al., 2021).

Labelled observations of TS and target spectra have been measured using various direct sampling or remote sensing methods, all of which have limitations. For example, directed trawl sampling of acoustic targets in areas with high densities of the species of interest has been used for jellyfish (Brierley et al., 2001), Antarctic krill (Hewitt & Demer, 1996) and mesopelagic fish (Sobradillo et al., 2019), but this method is prone to sampling biases like net avoidance and acoustic shadowing of weaker targets (Peña, 2018). Optical verification has been used to validate acoustic targets, for example, krill (Lawson et al., 2006) and salps (Wiebe et al., 2010), but has limited range resolution, especially for small targets (Trenkel et al., 2011) and is further limited by avoidance of the external light source (Geoffroy et al., 2021). Controlled tank experiments with zooplankton (e.g., McGehee et al., 1998; Pauly & Penrose, 1998; Stanton et al., 1998) have typically relied on purpose-built or laboratory sonars (Amakasu & Furusawa, 2006; Conti et al., 2005) because there are physical limits associated with (large and powerful) commercially available echosounders (i.e., beam angle and near-field range; Simmonds & MacLennan, 2008). Controlled cage experiments have been used to measure the acoustic signal of large Antarctic krill (e.g., Foote et al., 1990), jellyfish (Monger et al., 1998) and fish (e.g., Gugele et al., 2021; Legua & Lillo, 2017), but measurements of mesozooplankton remain challenging because detection of weak scatterers requires a cage designed to minimize noise and reverberation (Knutsen & Foote, 1997). Furthermore, tank and cage experiments are limited by the near-field range of each transducer, i.e., the distance from the transducer face where the sound

pulse is not yet linear, for the choice of frequency because the near-field range depends on the transducer size and frequency. Smaller transducers typically have a smaller near-field range.

Model-informed classification theoretically removes the need to collect measurements of known targets for use as labelled training data (e.g., Cotter et al., 2021). Validated scattering models (e.g., Cotter et al., 2021; Korneliussen & Ona, 2003; Peña, 2018) provide theoretical frequency response spectra for each class (e.g., species) expected to be present in the acoustic data. Sound scattering models are considered validated when predictions of acoustic backscatter are comparable to benchmark models (Gastauer et al., 2019). Benchmark models are predictions of acoustic backscatter from exact or approximate analytical models and serve to find the limitations and validity domain of sound scattering models (Jech et al., 2015). These modelled spectra are then used as labelled training data for machine learning classification algorithms (hereafter, ‘classifiers’). This approach has been used to classify scatterers into gross anatomical groups based on their acoustic properties for mesopelagic species (Cotter et al., 2021) and reef fish (Roa et al., 2022). However, to our knowledge, model-informed classification of target spectra has not yet been validated for any species.

This study aims to evaluate the validity and reliability of model-informed classification for the target spectra of zooplankton species with similar gross anatomical properties and size distributions. We applied model-informed classification to a mixed assemblage of Arctic mesozooplankton that was dominated by fluid-like species, i.e., animals with sound scattering properties similar to water (e.g., euphausiids, copepods, and salps) (Stanton & Chu, 2000). The objectives were threefold: (1) to design an *in situ* mesocosm experiment to insonify zooplankton in a near-natural environment

with minimal background noise and reverberation; (2) to evaluate the performance of classifiers trained with scattering models for differentiating weakly backscattering mesozooplankton groups; (3) to validate the classifier predictions on a known community of zooplankton. We conclude by providing recommendations for model-informed classification of target spectra.

3.3 Material and methods

3.3.1 Study area and zooplankton collection

Zooplankton were collected in Kongsfjorden, Svalbard, from the R/V *Helmer Hanssen* using a Tucker trawl (1 m² opening and 1000 µm mesh size, 10 minutes at 3 m s⁻¹) on the night of 15 January 2022 (Figure 3.1). Twelve Tucker trawl tows were taken at the depth of the strongest sound scattering layer (~150 m) as seen from the vessel's echosounder (Kongsberg Discovery AS, Horten, Norway; Simrad EK60, 18 and 38 kHz, 1.024 ms pulse duration, 2 Hz ping rate). Samples from all tows were combined and kept alive for up to 15 hours in running seawater and delivered unsorted to the wharf in Ny-Ålesund on 16 January. The zooplankton samples were stored overnight in three 100 L holding tanks with a low-pressure flow system of filtered ambient seawater (~2°C) at the Kings Bay Marine Laboratory. An additional Tucker trawl sample collected on 15 January was preserved in 4% formaldehyde-in-seawater solution buffered with hexamine and stored for species shape analysis.

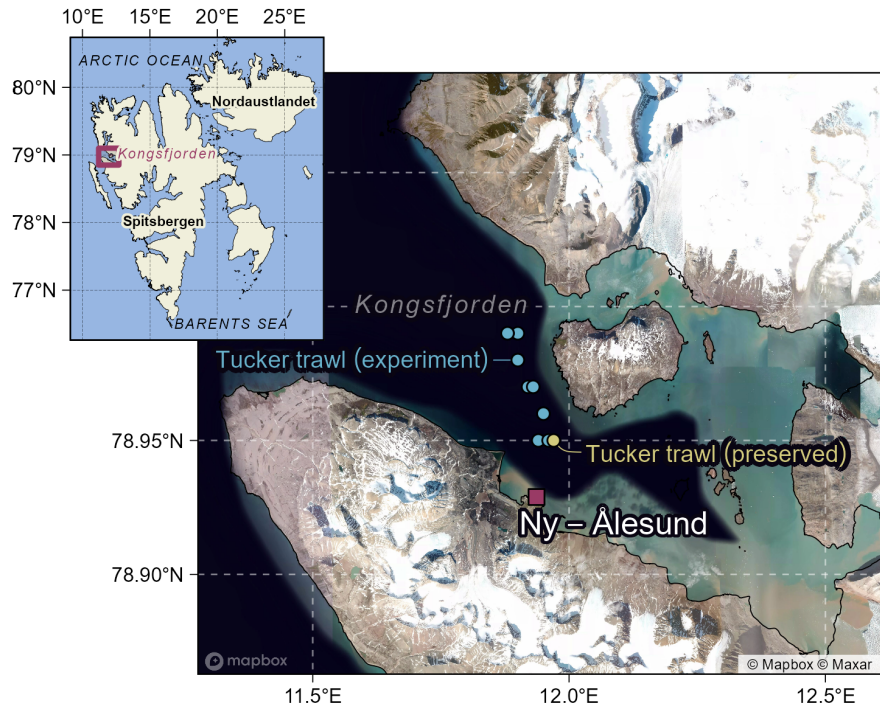


Figure 3.1: Study area in Kongsfjorden with locations of the mesocosm experiment from the wharf in Ny-Ålesund (red square) and Tucker trawl deployments for the experiment (blue circles with some overlap; $n=12$). The yellow circle indicates the Tucker trawl deployment from which zooplankton was preserved for morphometric analyses (yellow circle; $n=1$). The red box in the inset shows the location of the study area within the Svalbard archipelago.

3.3.2 Mesocosm design and experiment

Acoustic data were collected on 17 January 2022 using a mesocosm deployed from a wharf in Ny-Ålesund (Figure 3.1). The mesocosm, or AZKABAN (Arrested Zooplankton Kept Alive for Broadband Acoustics Net experiment), was formed by a cuboid zooplankton net (3 m high, 2 m wide and 2 m long) with a 500 μm -mesh holding a

volume of 12 m^3 (Figure 3.2a). The net was mounted on the top section of an 8 m high by 2 m wide and 2 m long aluminium frame oriented vertically (Figure 3.2a). Ropes attached eyelets on the net to the frame at each corner and along the edges.

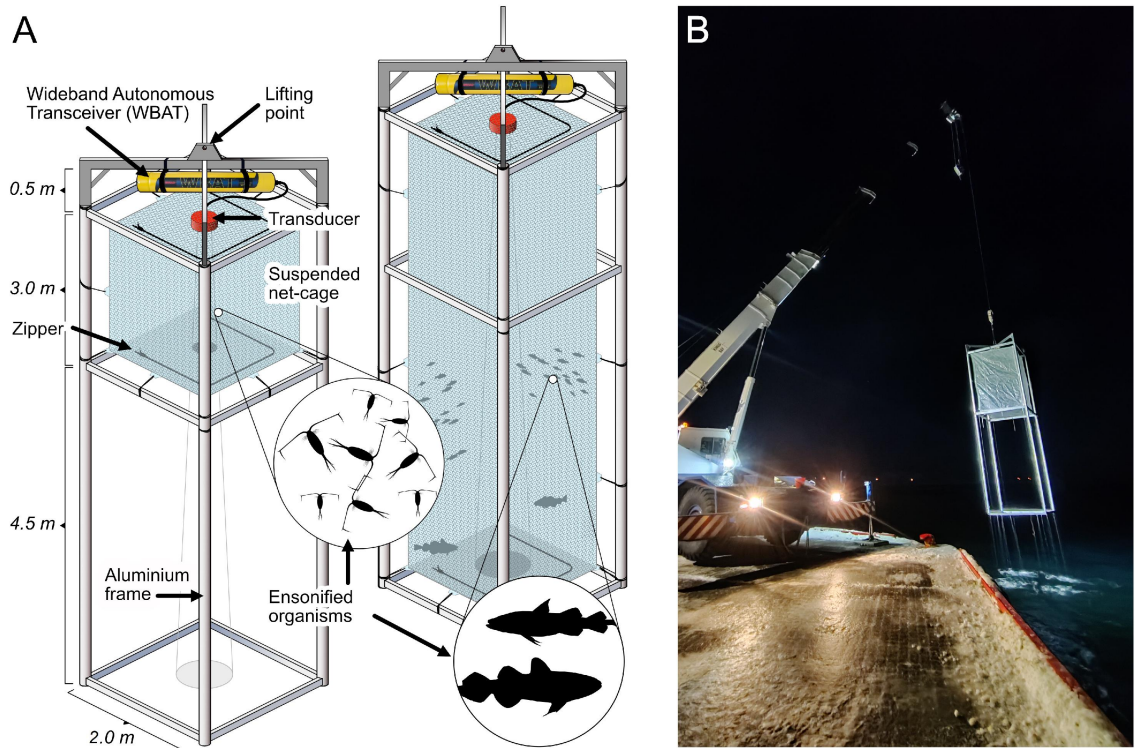


Figure 3.2: A) Schematic of the AZKABAN mesocosm with the small zooplankton net (left) and large fish net (left). Only the configuration with a small net (left) was used for this study to limit the volume of insonified mesozooplankton. The acoustic transceiver (yellow cylinder) is attached to the frame and the transducer (orange cylinder). There is a hole at the top of the net for the transducer face to be unobstructed inside the net. B) The AZKABAN mesocosm was lifted with the crane at the end of the experiment.

A 200 kHz nominal frequency transducer (ES200-7CDK-Split; Kongsberg Discovery AS) was mounted on a plate centred inside the mesocosm through a hole on the top panel of the net with the acoustic axis pointing directly down. A Wideband Autonomous Transceiver (WBAT; Kongsberg Discovery AS) was fastened to the frame to operate the transducer (Figure 3.2). The AZKABAN frame was purpose-built by Havbruksstasjonen (Ringvassøya, Norway) and the frame was designed to contain the entire main lobe of a 7° opening beam angle transducer inside the net.

The AZKABAN mesocosm was deployed by crane and lowered into the sea (Figure 3.2b). Zippers on the top and bottom panels of the net were used to add the alive and active species from the holding tanks into the submerged net. The frame was lowered such that the depth of the transducer face was approximately 0.5 m below the surface for the duration of the experiment. The mesocosm was recovered after three hours of data collection (Appendix B Figure S1). The zooplankton were rinsed off the net and collected for species composition analysis. The species composition of the recovered mesocosm sample was analyzed by identifying and counting 10% of the total sample for all species with more than 1000 individuals. All other species were counted for the entire sample.

The mesocosm experiment was conducted on an unsorted assemblage to maintain a high detection probability (i.e., with large numbers of target animals in the enclosure). The sampling effort required to obtain sufficient animals for single-species experiments was deemed too great in time and hence expense. In addition, separating the live mesozooplankton from a mixed assemblage (as caught) into single species groups would have risked injuring or killing individuals. Using the unsorted mixed population meant that individual animals were handled minimally and that

stress to them was minimized: this left it likely that natural swimming behaviour was preserved.

3.3.3 Acoustic data collection and calibration

During the AZKABAN experiment, the WBAT was programmed to transmit frequency-modulated pulses covering the entire available bandwidth from 185 to 255 kHz. The transmitted pulses had fast ramping, a pulse duration of 512 μ s with 75 W transmit power, and a ping interval of 0.35 s. Simultaneous pinging of two split-beam transducers is not possible with a WBAT, so we had to restrict the bandwidth to that achievable by one transducer alone for the experiment. The simultaneous pinging of two or more transducers would improve the classification potential of broadband signals (Benoit-Bird & Waluk, 2020). Of the available transducers with 7° beam width (120, 200 and 333 kHz), the 200 kHz transducer was chosen to have the greatest signal-to-noise ratio of the targeted species (mesozooplankton) while achieving a small wavelength to detect smaller zooplankton (7 mm; Simmonds & MacLennan, 2008). We used a short pulse length to resolve targets near the net boundary and reduce reverberation volume (Soule et al., 1997).

The acoustic system was calibrated on 19 January 2022 with two spheres made of tungsten carbide (WC) with 6% cobalt binder and diameters of 38.1 mm and 22 mm (Demer et al., 2015). Calibrations were processed with the EK80 software (version 21.15; Kongsberg Discovery AS). The calibration parameters were calculated for each sphere (Appendix B Figure S2) and combined.

3.3.4 Scattering models

The training dataset for the classification was created with scattering models for the most abundant taxonomic groups in the Tucker trawl samples (≤ 1000 individuals). The most abundant were calanoid copepods, euphausiids, chaetognaths, and hydrozoans. All these groups are considered fluid-like scatterers with sound speed contrast (h) and density contrast (g) of $1 \pm 5\%$ (Stanton & Chu, 2000). Near-unity sound speed and density contrasts imply that the material properties of the scatterers are similar to the surrounding medium (seawater). To model the scattering of the zooplankton groups, we chose the phase-compensated distorted wave Born approximation (PC-DWBA) model because the parameters of this model are flexible to geometry, material properties, and acoustic frequency ranges, which makes the model adequate for the broad range of fluid-like zooplankton groups in this study (Chu & Ye, 1999; Gastauer et al., 2019). The DWBA has been extensively tested (Lavery et al., 2007), and PC-DWBA model has been used to infer length or material properties for Antarctic krill, *Euphausia superba* (Amakasu et al., 2017), decapod shrimp, *Palaemonetes vulgaris* (Chu et al., 2000), and eggs of North Atlantic cod, *Gadus morhua* (Chu et al., 2003) by comparison of model outputs with measurements of known species (in controlled laboratory experiments, or concurrent trawl sampling). We ran 1000 model simulations for each zooplankton group using the ZooScatR package (version 0.5, Gastauer et al., 2019) with R (version 4.1.2) with shape, size, and material properties parameters chosen from distributions selected based on the basis of the mesocosm-experiment samples, the preserved sample or literature (Table 3.1). The modelled spectra were calculated with a 0.5 kHz frequency resolution.

Table 3.1: Scattering model parameters distributions for each zooplankton group. The distributions are log-normal: $L(\text{meanlog}, \text{sdlog})$, normal: $N(\text{mean}, \text{sd})$ and gamma: $\Gamma(\text{shape}, \text{rate})$, where sd is the standard deviation.

Parameters	Copepods	Euphausiids	Chaetognaths	Hydrozoans
Modelled species	<i>Calanus glacialis</i>	<i>Thysanoessa inermis</i>	<i>Parasagitta elegans</i>	<i>Aglantha digitale</i>
Length (mm)	$N(3.3, 0.7)^a$	$L(2.4, 0.3)^d$	$\Gamma(10.6, 0.6)^a$	$L(2.4, 0.4)^a$
Length-to-width ratio	$N(5.3, 0.9)^a$	$N(11, 2)^a$	$N(26, 8)^a$	$N(2.8, 0.5)^a$
Density contrast (g)	$N(0.997, 0.005)^b$	$N(1.037, 0.005)^b$	$N(1.030, 0.005)^e$	$N(1.007, 0.005)^f$
Sound speed contrast (h)	$N(1.027, 0.007)^b$	$N(1.026, 0.005)^b$	$N(1.030, 0.005)^e$	$N(1.007, 0.005)^f$
Orientation ($^\circ$)	$N(90, 30)^c$	$N(20, 20)^e$	$N(0, 30)^e$	$N(90, 30)^g$

^a Measurements from the preserved sample with the distribution assessed as the best fit based on a 1:1 line between theoretical and empirical quantile in Q-Q plots.

^b Kögeler et al. (1987); February-March measurements.

^c Blanluet et al. (2019)

^d Measurements from a subsample of the mesocosm experimental sample. The distribution was assessed as the best fit based on a 1:1 line between theoretical and empirical quantiles in Q-Q plots.

^e Lavery et al. (2007)

^f Inferred from a comparison of measurements of hydrozoans from Monger et al.

(1998), Brierley et al. (2001) and Brierley et al. (2004) to model predictions.

^g Monger et al. (1998) from swimming shape analysis.

The preserved Tucker Trawl sample was diluted and subsampled on 22 June 2022 for imaging of copepods (n=70), euphausiids (n=20), chaetognaths (n=70), and hydrozoans (n=70). Images were taken with a Leica M205 C stereomicroscope fitted with a Leica MC170 HD camera, and shape analysis was performed with an image processing software, ImageJ (version 1.53, National Institutes of Health, USA). The shapes were processed with ZooScatR to calculate the length and length-to-width ratio. Large individuals (>16 mm) were measured with a ruler. For the euphausiids, the length distribution was calculated from a subsample of 77 individuals from the mesocosm experiment sample. The processed images were used to create a shape input for each zooplankton group and its scattering model (Appendix B Figure S3). Material properties of copepods vary geographically and seasonally, predominantly because of their lipid reserves required to sustain the winter season (Sakinan et al., 2019). We selected g and h from Kögeler et al. (1987) because of the availability of measurements from the winter season (February-March) and the proximity of their measurements of *Calanus* spp. to the Arctic, hereby Arctic copepods. For hydrozoans, literature values for density and sound speed contrast were limited; therefore, we inferred the values for g and h from a comparison of the measurements from Brierley et al. (2001), Brierley et al. (2004) and Monger et al. (1998) to the model predictions, a method used by Lavery et al. (2007).

3.3.5 Acoustic data processing

All acoustic data were processed in Echoview 13.0 (Echoview Software Pty Ltd, Hobart, Tasmania). Data analysis was restricted to the 1.0 to 2.25 m range to exclude the near-field region (Simmonds & MacLennan, 2008) and the echo from the bottom of the net. The “Single Target Detection - wideband” operator was applied to the pulse-compressed wideband data (Appendix B Table S1). The minimum value for the compensated TS threshold was set to the minimum allowable value, -120 dB re 1 m², to allow for the detection of the weaker scatterers. The identified single targets were grouped into tracks using the “Detect Fish Tracks” algorithm. We used conservative parameters to increase the likelihood of each track containing targets from one individual (Appendix B Table S2). Tracks were visually assessed to remove outlier targets to further ensure that each track originated from only a single zooplankton target.

The target spectra of all single targets assigned to a track were exported from Echoview for analysis. All target spectra were calculated using a Fourier transform window size of 0.33 times the pulse length (0.25 m) with a 0.5 kHz resolution. The Fourier transform window size was selected as a compromise to maximize frequency resolution while minimizing the likelihood of incorporating backscattering from multiple targets (Benoit-Bird & Waluk, 2020).

3.3.6 Noise level

The noise level inside the mesocosm affected the minimum backscatter detectable from organisms. In this case, the noise level is considered all unwanted signals, including background noise and reverberation from the cage. The noise level within AZKABAN was calculated using a 1-minute segment of data collected during a period of low single echo detections (11:25-11:26 UTC). First, single target detection was applied to the pulse-compressed TS with less stringent detection thresholds (Appendix B Table S2) to identify all possible targets. Second, targets were removed from the dataset using a mask. The target masks covered entire pings to avoid contamination by side lobes associated with pulse compression from targets. The remaining signal was designated as noise. Weak targets that were not identified by the single target detection algorithm were included in the noise level estimation. Finally, the noise level was calculated by exporting the median target strength frequency response profile for increments of 0.1 m depth bins.

Thereafter, when selecting single targets for the spectra analysis, targets were flagged (i.e., excluded from the analysis) if their target strength at nominal frequency (200 kHz) had a signal-to-noise ratio (SNR) of less than 10 dB (Simmonds & MacLennan, 2008) when compared to the noise level at nominal frequency at the range of the target. We calculated the proportion of flagged targets below the SNR threshold relative to the total amount of targets.

3.3.7 Classifier training

Various algorithms have been used for acoustic target classification in previous fisheries acoustics studies, including k-Nearest Neighbours (Cotter et al., 2021), decision trees (D’Elia et al., 2014; Fernandes, 2009), random forests (e.g., Gugele et al., 2021; Proud et al., 2020), gradient boosting (Escobar-Flores et al., 2019), support vector machines (Roa et al., 2022; Roberts et al., 2011), and neural networks (e.g., Brautaset et al., 2020; Cabreira et al., 2009; Simmonds et al., 1996). Here, three supervised classifiers that take different approaches to classification were compared (Table 3.2). The algorithm k-Nearest Neighbours (kNN; Goldberger et al., 2004) was chosen as it has been used for model-informed classification previously (Cotter et al., 2021). LightGBM (Ke et al., 2017), implementation of gradient boosting (Friedman, 2001), was considered representative of decision tree-based ensemble methods, with the potential for improved performance compared to random forest (Fernández-Delgado et al., 2014), which is widely used in fisheries acoustics (Fernandes, 2009; Gugele et al., 2021). Finally, the Support vector machine (SVM; Cortes & Vapnik, 1995) was chosen because it is another widely used algorithm that, together with gradient boosting, has been identified as among the best-performing classification algorithms based on comparisons of performance on large data set collections (Fernández-Delgado et al., 2014).

Table 3.2: Overview of the machine learning algorithms compared in this study. The strengths and limitations are detailed for use in fisheries acoustics.

Classifier	Description	Strengths	Limitations
------------	-------------	-----------	-------------

k-Nearest Neighbours (kNN)	Predicts the class of new samples by taking a majority vote of the k training samples which are closest in distance by some metric (e.g., Euclidean distance) (Fix & Hodges Jr., 1951).	Few hyperparameters therefore easy to implement. Interpretable; an “explainable artificial intelligence” algorithm (Islam et al., 2021). Computationally expensive. Limited ability to deal with noise and outliers (Korneliussen, 2018).	Limited ability to identify low abundance groups (Peña, 2018). Vulnerable to overfitting.
LightGBM	Implementation of gradient boosting, a decision tree-based ensemble method similar to random forest (Breiman, 2001; Friedman, 2001). Gradient descent is used to minimise a loss function with the addition of each new tree to the ensemble. Thus, each new tree attempts to correctly classify samples that were previously misclassified (Hastie et al., 2009).	Suitable for large datasets (Ke et al., 2017), robust to outliers (Hastie et al., 2009). Reduced risk of overfitting (Hastie et al., 2009).	Rarely used in fisheries acoustics. Many hyperparameters, optimisation is computationally expensive.

Support Vector Machine (SVM)	Maps data to a higher-dimensional feature space in which classes are linearly separable; the optimal decision boundary (hyperplane) has the maximal distance between itself and the closest training data points (support vectors) of any class. (Cortes & Vapnik, 1995; Hastie et al., 2009).	Few hyperparameters therefore easy to implement. Results are consistent and reproducible between repeat implementations (Bennett & Campbell, 2000).	Sensitive to outliers (Kanamori et al., 2017). Unsuitable for large datasets, as it is very computationally expensive (Cervantes et al., 2008).
------------------------------	--	---	---

3.3.7.1 Training on modelled target spectra

The ML classifier training was completed with Python 3.9 using the Scikit-Learn library (version 1.1.1, Pedregosa et al., 2011). An L^2 -normalization was applied to each target spectra from individuals modelled with the PC-DWBA model simulations so that if the values were to be squared and summed, the sum would equal 1 (Komer et al., 2014). The target variable (i.e., the classification output) was the zooplankton group: copepod, euphausiid, chaetognath, or hydrozoan.

For each classifier described in Table 3.2, we optimized its hyperparameters (Appendix B Code S1, S2 and S3) and estimated its performance on a holdout dataset through cross-validation (CV; Stone, 1974). The dataset was split iteratively into a training subset (90%) and a testing subset (10%). Nested CV (Wainer & Cawley,

2021) was used to optimize the hyperparameters and evaluate the performance of the classifiers (Appendix B Figure S4). Nested CV ensured that separate data were used to train, validate, and test the classifier and provided an estimate of the classifier’s true error with minimal bias (Varma & Simon, 2006). We compared the classifiers’ success using mean class-weighted F1 score (Equation 3.1; Pedregosa et al., 2011) because that is appropriate for scenarios where both false positives and false negatives are equally undesirable.

The F1 score is a measure of overall accuracy calculated as the harmonic mean of precision and recall, defined as:

$$F1 = \frac{2 * Precision_i * Recall_i}{Precision_i + Recall_i} = \frac{2 * TP_i}{2 * TP_i + FP_i + FN_i}. \quad (3.1)$$

Precision reports the relative success of the classifier, expressed as:

$$Precision = \frac{TP_i}{TP_i + FP_i}, \quad (3.2)$$

where TP is the number of true positives and FP is the number of false positives for each class i (each zooplankton group).

Whereas recall is a measure of the sensitivity from repeat detections, expressed as:

$$Recall = \frac{TP_i}{TP_i + FN_i}, \quad (3.3)$$

where FN is the number of false negatives for each class i (each zooplankton group). An F1 score of 1.0 would indicate that a classifier could correctly classify each sample.

Hyperparameter optimization was repeated on the entire modelled dataset (1000 tar-

get spectra for each of the four zooplankton groups) without subsampling to obtain the final trained classifiers.

3.3.7.2 Classifier sensitivity

To determine the optimal frequency bandwidth for model-informed classification of copepods, euphausiids, chaetognaths, and hydrozoans, kNN classifiers were trained and evaluated with modelled target spectra over the bandwidths commonly used in fisheries acoustics (Simmonds & MacLennan, 2008). The selected bandwidths were the individual bandwidths from the 70, 120, 200 and 333 kHz transducers produced by Kongsberg Discovery AS (45-90 kHz, 90-170 kHz, 185-255 kHz and 283-383 kHz) and their continuous bandwidth (45-383 kHz). Only kNN was used for this analysis as it is less computationally expensive than the other algorithms.

A kNN classifier was also trained using modelled cross-sectional backscattering coefficient – frequency spectra, $\sigma_{bs}(f)$, the linear scale of $TS(f)$, for the bandwidth of 185-255 kHz to examine the effect of the logarithmic scale of the modelled target spectra on the classification performance.

Additionally, we evaluated the classifiers’ sensitivities to the parameterization of material properties in the scattering models because this can strongly influence backscattering intensity (Chu & Ye, 1999; Sakinan et al., 2019). A PC-DWBA model was parameterized using literature material properties values for Antarctic copepods (*Calanus* spp.) ($g = 0.995 \pm 0.001$ and $h = 0.959 \pm 0.010$; Chu & Wiebe, 2005). These values are from spring (2 May 2002) but from similar water temperatures (-0.8 to 0.4 °C) as those used for Arctic copepods in this study. All other model parameters for copepods and the other zooplankton groups remained the same.

3.3.8 Classification

The trained and optimized classifiers were used to classify the measured *in situ* target spectra from AZKABAN into zooplankton groups (copepods, euphausiids, chaetognaths, or hydrozoans). The classifier predictions were evaluated by comparing: 1) the predicted class distributions to the species composition of the zooplankton sample recovered from AZKABAN; 2) the class predictions from each classifier (classifier agreement); and 3) the class predictions for targets from the same track (within-track consistency).

3.4 Results

3.4.1 Species composition

The zooplankton sample collected from AZKABAN after the experiment showed that copepods were numerically dominant. Over 20 000 copepods were in AZKABAN, mostly *Calanus* spp. (> 13 000 individuals; Table 3.3). The second most abundant group was euphausiids, which were an order of magnitude less abundant in the samples than copepods. The most common euphausiid was *Thysanoessa inermis*, and the population consisted mainly of small juveniles (median length of 11mm; Table 3.3). The sample contained almost as many chaetognaths as euphausiids, predominantly *Parasagitta elegans*. The fourth most abundant group in the sample were hydrozoans, predominantly *Aglantha digitale*. All other zooplankton and fish sampled had < 100

individuals; therefore, we did not include these species in the classification analysis due to the low likelihood of repeated detections. During the experiment, the AZKABAN mesocosm had a total density of 2203 individual zooplankton per m³.

Table 3.3: Taxonomic group, species, count and proportion of the sample retrieved from the net after the experiment. Samples with <1000 individuals were counted for the entire recovered mesocosm sample. The species with a "Median length" value were modelled to create the labelled training dataset for the classification algorithms.

Taxonomic group	Species	Total individuals	Proportion of sample (%)	Median length (mm) (\pm SD)
Copepoda	<i>Calanus</i> spp.	13380	50.61	3.3 (\pm 0.7)
Copepoda	<i>Metridia</i> spp.	6310	23.87	
Copepoda	<i>Paraeuchaeta</i> spp.	710	2.69	
Copepoda	Other copepods	160	0.61	
Euphausiacea	<i>Thysanoessa inermis</i>	2485	9.40	11.0 (\pm 4.0)
Chaetognatha	<i>Parasagitta elegans</i>	2220	8.40	17.0 (\pm 5.0)
Hydrozoa	<i>Aglantha digitale</i>	1000	3.78	11.0 (\pm 5.0)
Decapoda	juvenile <i>Pandalus</i> spp.	76	0.29	
Decapoda	benthic shrimp	2	0.01	
Pteropoda	<i>Clione limacina</i>	40	0.15	
Amphipoda	<i>Themisto</i> spp.	27	0.10	
Amphipoda	Undetermined	14	0.05	
Fish (larvae)	<i>Leptoclinus maculatus</i>	7	0.03	
Mysidacea	Undetermined	4	0.02	

3.4.2 Scattering models

Copepods were the smallest scatterers in this experiment with a median total length (\pm standard deviation) of 3.3 ± 0.7 mm and an average modelled TS of -113 dB re 1 m^2 across the frequency spectrum. The amplitude of the modelled target spectra was typically lower for the copepods than the other three groups. Modelled Antarctic copepods had similar target spectra results but with a 5 dB mean increase across the spectra compared to the Arctic copepods, with an average TS of -107 dB re 1 m^2 (Figure 3.3a; blue).

Euphausiids and hydrozoans had the same median total lengths of 11 mm (± 4 mm for euphausiids and ± 5 mm for hydrozoans). Despite their similar length distributions, euphausiids had a higher average TS (-89 dB re 1 m^2 for euphausiids and -94 dB re 1 m^2 for hydrozoans) due to differences in their material properties. However, both groups had relatively flat average spectra over the measured bandwidth (Figure 3.3b, d). Lastly, chaetognaths had the longest median length (17 ± 5 mm) but had a relatively low median TS (-98 dB re 1 m^2). The target spectra of chaetognaths had a slight positive slope and a large dispersion of TS intensity (Figure 3.3c, g).

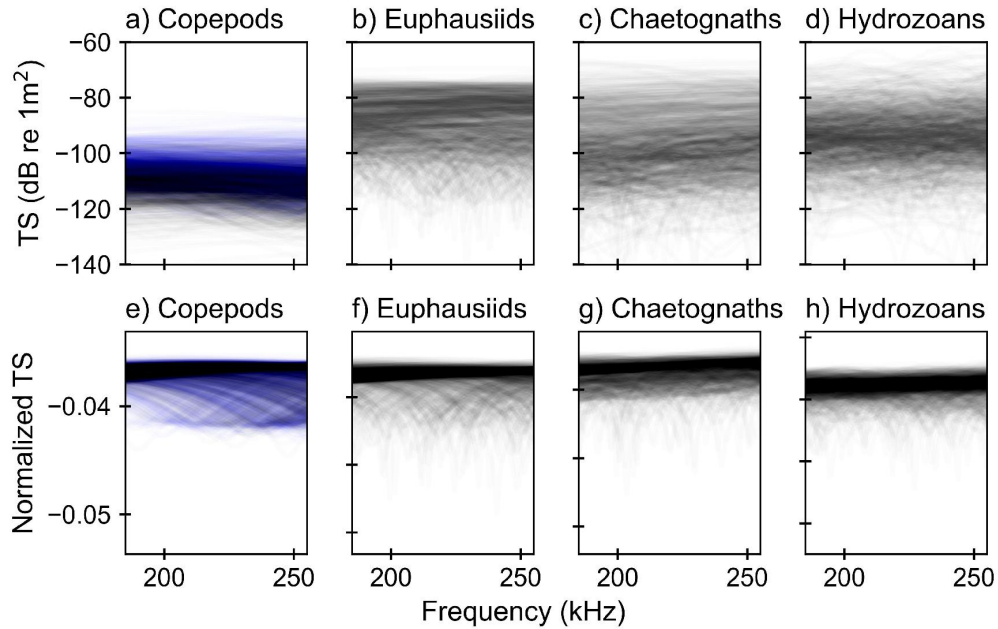


Figure 3.3: a-d) All PC-DWBA model simulation results for each dominant zooplankton group. For copepods (a) the model results are shown for Arctic species (black; Kögeler et al., 1987) and the Antarctic species (blue; Chu & Wiebe, 2005). e-h) L^2 -normalised PC-DWBA model simulation results for each dominant zooplankton group.

3.4.3 Noise level

The noise level inside AZKABAN was low, being below -100 dB re 1 m^2 throughout the mesocosm (Figure 3.4) and across the frequency bandwidth. There were peaks in the noise level profile at 1.1 m, 1.6 m and 1.9 m range from the transducer (Figure 3.4). The noise profile followed a similar magnitude and trend across the bandwidth, with approximately 5 dB re 1 m^2 variability. We found that the signal-to-noise ratio at 200 kHz was less than 10 dB re 1 m^2 for 10.6% of the single targets used for classification,

as shown by the overlaid detected target used for classification analysis in Figure 3.4. This was deemed adequate, and all targets were retained for subsequent analyses. The full noise spectra was assessed (Figure 3.4) and followed the same trend as the nominal frequency.

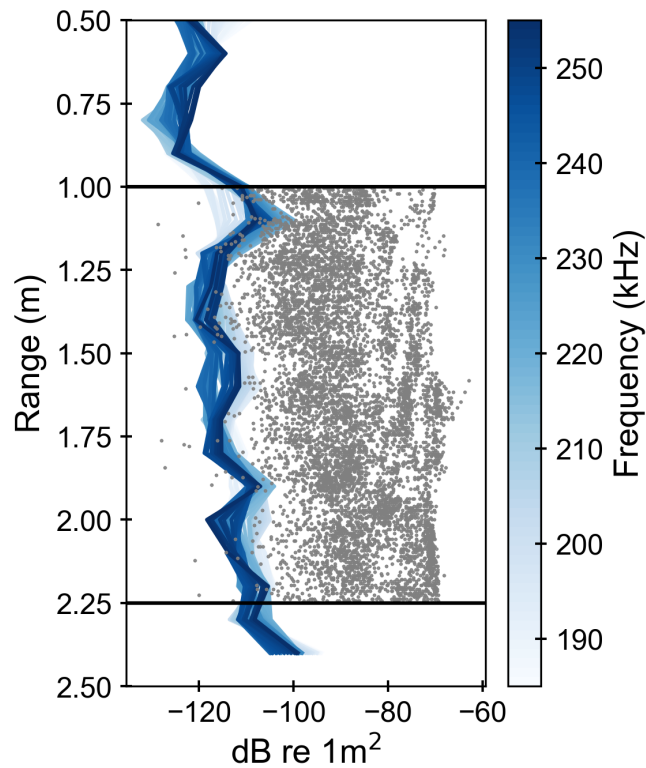


Figure 3.4: Background noise profile inside AZKABAN across the available bandwidth (185-255 kHz; blue lines). The grey dots indicate the TS of each detected tracked target detection at 200 kHz. The detection zone is delimited by the horizontal black lines at 1 m and 2.25 m. The transducer face and top of the net are at 0 m range and the bottom of the net is at 3 m range.

3.4.4 Mesocosm target detections

A total of 7,722 tracked single targets were detected during the three-hour AZKABAN mesocosm experiment. The mesocosm target detections were from a mixed zooplankton assemblage, and individual detections were from targets of unknown identity. There were 777 distinct tracks, with a mean of 10 single target detections per track. The minimum number of detections in a track was 4, and the maximum was 178.

3.4.5 Evaluation of classifier training

The optimized kNN classifier used the KDTree algorithm (Pedregosa et al., 2011) and Euclidean distance as the distance metric. For the kNN classifier, the optimized value for the number of training samples closest in distance to the query sample used for predictions, k , was 1. The optimized SVM classifier used a radial basis function kernel, and the optimized LightGBM comprised 3,400 trees with a maximum tree depth of seven. Full details of the optimized classifiers are provided in the Appendix B Code S1, S2 and S3.

3.4.5.1 Classifier performance

The F1 scores reflect the classifiers' performance at classifying the modelled target spectra. The highest class-weighted F1 score was achieved using LightGBM (0.71 ± 0.02), followed by kNN (0.70 ± 0.03) and SVM (0.59 ± 0.03) for the 185-255 kHz bandwidth. Per-class F1 scores showed consistently highest scores for copepods (0.71-0.87). The lower per-class F1 scores for euphausiids (0.64-0.72), hydrozoans (0.58-0.67) and chaetognaths (0.44-0.58) indicated that the classifiers had limited pre-

cision and/or recall in classifying these groups. The limited precision and recall of the classifiers were reflected in the confusion matrices for each classifier (i.e., the high numbers of misclassifications; Appendix B Table S3, S4 and S5).

Table 3.4: Classifier mean F1 scores estimated through nested cross-validation (mean \pm standard deviation) for the 185-255 kHz bandwidth. A score of 1.0 indicates that a classifier could correctly classify each sample (100% classification success).

Classifier	kNN	LightGBM	SVM
Class-weighted	0.70 \pm 0.03	0.71 \pm 0.02	0.59 \pm 0.03
Copepods	0.87 \pm 0.02	0.87 \pm 0.02	0.71 \pm 0.03
Euphausiids	0.70 \pm 0.03	0.72 \pm 0.03	0.64 \pm 0.03
Chaetognaths	0.58 \pm 0.04	0.58 \pm 0.05	0.44 \pm 0.03
Hydrozoans	0.66 \pm 0.04	0.67 \pm 0.03	0.58 \pm 0.04

3.4.5.2 Classifier sensitivity

The nested CV procedure was conducted for modelled target spectra across five different frequency bandwidths (45-90 kHz, 90-170 kHz, 185-255 kHz, 283-383 kHz, and 45-383 kHz) to test the effect of bandwidth selection on classifier performance. The comparisons were only run with kNN because it was the least computationally expensive algorithm of those used in this study and, based on the results in Table 3.4, provided similar performance to LightGBM. The mean class-weighted F1 score for kNN with the full bandwidth (TS_{45-383kHz}) was 0.92 (\pm 0.02) (Appendix B Table S6). The best score for a single “transducer” was 0.86 (\pm 0.01), using modelled spectra at

the centre bandwidth of the 120 kHz transducer (TS_{70–190kHz}).

The cross-sectional backscatter spectra ($\sigma_{bs185–255kHz}$) (i.e., the linear domain representation of the target spectra) were also used to train a kNN classifier. Using the linear scale of the target spectra brought a slight improvement to classifier performance (mean class-weighted F1 score: 0.73 ± 0.03 in the linear domain compared to 0.70 ± 0.02 in the logarithmic domain).

The performance of the kNN classifier trained with modelled target spectra of Antarctic copepods (Appendix B Code S5) (mean class-weighted F1 score: 0.69 ± 0.03 ; Appendix B Table S7) was not significantly different from the classifier trained with modelled target spectra of Arctic copepods (mean class-weighted F1 score: 0.70 ± 0.02).

3.4.6 Classification of *in situ* measurements

All classifiers predicted a different class distribution to the species composition of the zooplankton sample recovered from AZKABAN (Figure 3.5). For kNN, hydrozoans were predicted to be the most abundant class, followed by chaetognaths, euphausiids, and copepods, which was the inverse of the recovered sample (Figure 3.5). For LightGBM, chaetognaths were predicted as the most abundant class with no copepod detections. The SVM predictions implied a majority of hydrozoans, followed by euphausiids, chaetognaths, and copepods.

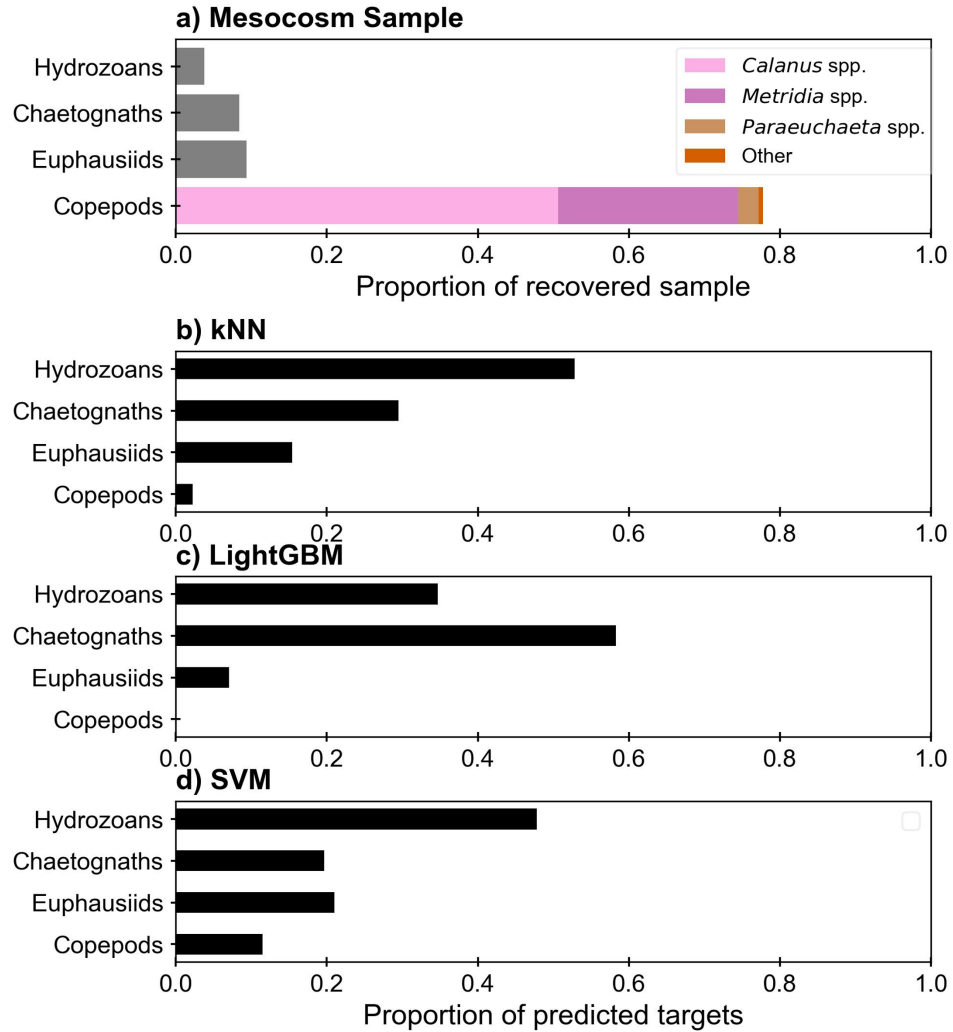


Figure 3.5: a) Composition of the zooplankton sample used in the mesocosm experiment as a proportion of the total sample for the four most abundant groups (n=26,435). b-d) the proportion of predicted targets of the total detections for tracked single targets (n=7,722) assigned to each group by k-nearest neighbours (kNN), LightGBM and support vector machine (SVM) classifiers.

The measured *in situ* target spectra for each class, as classified by kNN and Light-

GBM, were generally consistent with each other and the modelled spectra (Figure 3.6). However, the measured *in situ* target spectra classified as copepods by kNN had a higher target strength than the copepods' modelled target spectra (Figure 3.6). Of the mesocosm targets, those with high intensity and flat target spectra were labelled as copepods by the SVM classifier. However, the target spectra for euphausiids, chaetognaths, and hydrozoans predictions from SVM were in general agreement with the modelled results.

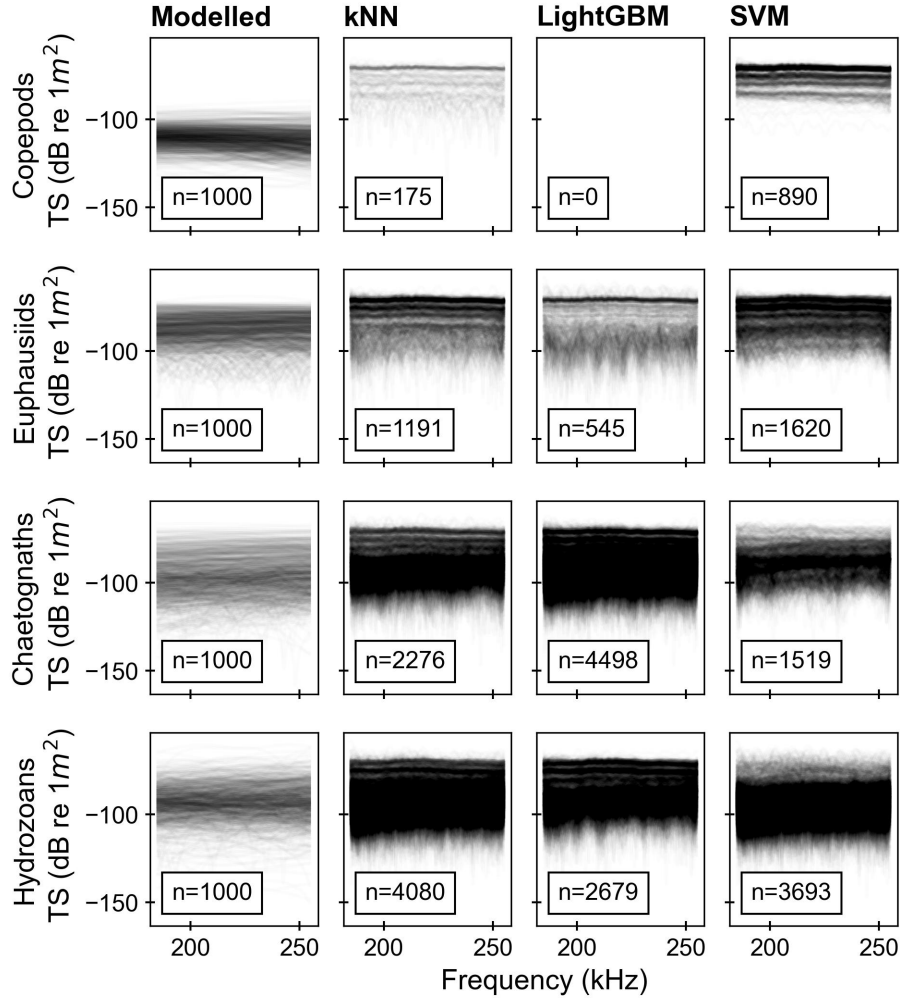


Figure 3.6: *Modelled*: PC-DWBA model simulations (theoretical) target spectra for each zooplankton group. *kNN*, *LightGBM*, and *SVM*: measured target spectra of tracked single targets from the mesocosm experiment as classified by k-Nearest Neighbours (kNN), LightGBM, and support vector machine (SVM). All panels include the number (n) of target spectra in each panel.

Only 18.13% of the measured target spectra (1,400 samples) were classified as the same zooplankton group by all three classifiers: 10.09% were consistently classified

as hydrozoans, 5.93% as chaetognaths, 1.29% as euphausiids, and 0% for copepods because no target spectra were labelled as copepods by LightGBM. Pairwise comparisons of classifiers show that 50.62% of tracked single target spectra (3,909 samples) were classified as the same zooplankton group by kNN and LightGBM, compared to 42.55% (3,286 samples) by kNN and LightGBM, and 29.31% (17,103 samples) by LightGBM and SVM.

SVM had the highest within-track prediction consistency: on average, 75% of targets within a track were assigned the same class label. However, 70% of tracks included at least two different classes. For LightGBM, 67% of detections within a track were assigned to the same class, and 100% of tracks included at least two classes, compared to 62% and 93%, respectively, for kNN.

3.5 Discussion

3.5.1 AZKABAN: A mesocosm for *in situ* broadband acoustic backscatter measurements

AZKABAN was designed to facilitate *in situ* broadband acoustic backscatter measurements of caged fish and zooplankton. The estimated noise level of AZKABAN was sufficiently low to enable the detection of mesozooplankton. Noise and reverberation from mesocosm walls have been a major challenge in past experiments with weak scatterers (Knutsen & Foote, 1997). The successful detection of weak targets in the AZKABAN mesocosm was partly due to the improvements in signal-to-noise ratio and range resolution associated with pulse compression of the broadband received

signal.

The purpose-built mesocosm offered a practical platform for broadband measurements of mesozooplankton. The design enabled the zooplankton sample to be added to the submerged net from a small boat, minimizing stress on the animals. It was also possible to recover the samples after the experiment for enumeration and morphometric analysis. Therefore, this mesocosm could be an effective experimental setup for controlled behavioural experiments, such as reactions to different sources and intensities of light and sound.

3.5.2 Performance of classifiers trained by modelled target spectra

Of the three conceptually different classifiers trained on modelled target spectra, the best-performing classifier was LightGBM, with a mean class-weighted success rate of 0.71. Copepods consistently had the highest mean F1 score (0.71-0.87), indicating that copepods' modelled target spectra could be discriminated from the others. The sensitivity analysis with the copepods parameterized with Arctic or Antarctic material properties demonstrated that changes in g and h have little effect on the normalized target spectra (Figure 3.3a,e) or classification success (Table 3.4, Appendix B Table S7). All the classifiers were limited in their ability to discriminate between euphausiids, chaetognaths and hydrozoans. Despite parameterizing the scattering models with representative parameters and shapes of the different zooplankton group organisms, these groups had overlapping modelled target spectra. Presumably, the overlap in the modelled target spectra of euphausiids, chaetognaths and hydrozoans is due to

the close similarity of the parameter distributions. The model’s inability to resolve the target spectra of different fluid-like zooplankton directly introduces consequences for target detection and classification. This suggests that thresholds should be established to determine possible taxonomic resolution for the classification of species with overlapping model parameter distributions. Ross et al. (2013) report a similar effect with juvenile euphausiids and pteropods and conclude that the similarity in frequency responses of these groups may render them indistinguishable.

Previous studies on supervised classification of target spectra have used coarse taxonomic resolution to manually label measured target spectra to create a training set based on model-informed classes. Cotter et al. (2021) achieved a class-weighted F1 score of 0.90 for the classification of manually labelled fluid-like and gas-bearing targets detected with a broadband echosounder (25-40 kHz) using k-Nearest Neighbours. (Roa et al., 2022) classified six reef fish using scattering models with a wide bandwidth (30-200 kHz) and found high classification accuracy (F1 score > 80%). We also found a wide bandwidth (45-383 kHz) resulted in high classification performance (class weighted mean F1 score of 0.92 ± 0.02). However, the wide bandwidth (45-383 kHz) results were not possible to validate within the mesocosm experimental setup because of the hardware and space requirements of four simultaneously pinging transducers. Furthermore, we achieved higher accuracy with lower frequencies (90-170 kHz; class weighted mean F1 score of 0.86 ± 0.01) than the ones used in the mesocosm (185-255 kHz). Despite the higher F1 scores at lower frequencies (90-170 kHz), we used 185-255 kHz for its smaller wavelength and shorter near-field range. For the classification of *in situ* measurements, physical and practical limitations of target size and echosounder properties (beamwidth, wavelength, transmit power, near-field

range) must be considered in addition to the F1 score of the classifier. While previous model-informed classification studies (Cotter et al., 2021; Roa et al., 2022) may have achieved better classification performances because the classes they used had distinct acoustic properties, in contrast to our study their model-informed classifiers were not validated with *in situ* measurements.

3.5.3 Discrepancies between classifiers predictions and *in situ* measurements

We used the AZKABAN mesocosm experiment to validate the performance of three model-trained classifiers using measurements of a mesozooplankton community sample for which the species composition was known. Overall, the zooplankton community composition determined by the classifiers differed from the actual composition in the mesocosm. Copepods were overwhelmingly the most abundant group in the mesocosm (Figure 3.5a) but were consistently the least abundant class in the classifier predictions (Figure 3.5b-d). Hydrozoans were the least abundant group in the mesocosm but the most abundant predicted class for kNN and SVM. Whereas for LightGBM, chaetognaths were the most abundant class. These major discrepancies show that model-informed classification was not successful on *in situ* target detections.

Small copepods in the mesocosm (3 mm length) were probably not detected, given the spatial resolution of the wavelength (7 mm at 200 kHz; Simmonds & MacLennan, 2008). The classifier predictions reflected this, with few copepod predictions and the target strength mismatch between the modelled and predicted results (Figure 3.6)

despite the relatively high F1 scores for copepods. Therefore, while the larger copepods were detected acoustically, the majority of copepods were likely not identified by the echosounder. A higher frequency range (283-383 kHz) with a shorter wavelength would theoretically resolve the issue, but previous noise level tests (not presented here) showed that the increased noise level higher frequencies would not allow the detection of individual weak scatterers (< -100 dB re 1 m^2). Future studies testing model-informed classification of zooplankton with the 200 kHz transducer should only select the zooplankton fraction > 7 mm. In that case, if the model-informed classification is successful the proportion of each zooplankton group calculated from *in situ* target detections may match the real proportion in the zooplankton sample.

The *in situ* target detections were also used to assess the within-track consistency of predictions between classifiers. The target tracking algorithm associates many single target detections to an individual organism as it travels across the acoustic beam. There was a high variability of zooplankton groups assigned to each track, highlighting the large variability in target spectra from an individual organism. The inhomogeneity of predictions per track and poor agreement between classifiers provide compelling evidence that model-informed classification of fluid-like mesozooplankton is unreliable.

3.5.4 Recommendations to improve model-informed classification of zooplankton

Our results on classifier training with modelled target spectra suggest that the classification performance is highly dependent on the choice of algorithm when the groups

cannot be reliably differentiated. Good practice for machine-learning-based science typically requires that a classifier’s performance is evaluated on a test set ‘drawn from the distribution of scientific interest’ (Kapoor & Narayanan, 2022). Model-informed acoustic target classification is appealing because it avoids the practical challenges and cost of obtaining labelled measurements of known species empirically (by sampling in the field or tank). However, using model-informed classification inevitably means that the samples used to train, validate, and test a classifier are not drawn from the distribution of scientific interest.

This study used a scattering model flexible to geometry, material properties, and acoustic frequency changes to generate training data for supervised machine learning classifiers. For future studies, we suggest that model-informed classification could be useful in assessing the theoretical classification potential of different bandwidths. However, classifier performance must be considered in the context of factors such as the target strength of the species of interest at a given frequency and the frequency’s range resolution for the classification of *in situ* measurements. We conclude that a better understanding of the variability in the acoustic measurements from individuals is required before model-informed classification of target spectra can be implemented reliably. Features in broadband spectra, such as the locations of nulls and peaks, can provide insight into morphological characteristics of individuals (Kubilius et al., 2020; Reeder et al., 2004). A better understanding of these features could increase classification potential and the information we can extract from target spectra.

3.6 Summary and conclusions

This study evaluated a model-informed classification of zooplankton from broadband echosounder data using *in situ* measurements (185 to 255 kHz) of a mixed Arctic mesozooplankton assemblage in a purpose-built mesocosm. Acoustic scattering models generated modelled target spectra for the four most abundant zooplankton groups in the mesocosm: copepods, euphausiids, chaetognaths and hydrozoans. Three different supervised machine learning algorithms were trained using modelled target spectra, and then compared in terms of their ability to classify the *in situ* measured target spectra obtained from the mesocosm experiment. Investigations of the classifier training using modelled target spectra showed that kNN and LightGBM classifiers could not differentiate euphausiids, chaetognaths, and hydrozoans reliably. The classifier training results were confirmed by their inconsistent predictions within-track and between classifiers for the *in situ* mesocosm measurements. The lack of consistent predictions within a track suggests that the variability in target spectra per class is greater than in the target spectra between the different zooplankton groups from the sound scattering models. The outstanding challenge remaining is to understand the ping-to-ping variability in the spectra of individual scatterers (Dunning et al., 2023; Martin et al., 1996).

Another remaining challenge for this method is the requirement to model the dominant taxa that are expected to be found in the study area. An Arctic fjord was selected as the study location in part because of the low species diversity. For regions with higher diversity, similar taxa could be grouped based on their material properties and shape to expand model-informed classification. In addition, *in situ* imaging

could complement the acoustic measurements to increase the taxonomic resolution of model-informed classification (Ohman et al., 2019).

The mesocosm design used in this study was an effective platform for measurements of fluid-like scatterers, which could be used to develop a better understanding of measured variability in target spectra. For example, mesocosm experiments with fewer individuals or a series of single species experiments could improve model validation for broadband echosounder measurements of freely swimming individuals. However, a semi-permanent installation for longer experiment periods, visual validation through video or imaging for swimming behaviour information and repeat experiments would be required to complete such comparative studies.

Chapter 4

Classification of three coinciding species (Atlantic cod, polar cod, and northern shrimp) using broadband hydroacoustics

Muriel Dunn^{1,2}, Geir Pedersen³, Malin Daase^{4,5}, Jørgen Berge^{4,5}, Emily Venables⁴, Sünne L. Basedow⁴, Stig Falk-Petersen⁶, Jenny Jensen¹, Tom J. Langbehn⁷, Lionel Camus¹, and Maxime Geoffroy^{2,4}

¹ Akvaplan-niva AS, Fram Centre, Postbox 6606, Stakkevollan, 9296 Tromsø, Norway

² Centre for Fisheries Ecosystems Research, Fisheries and Marine Institute of Memorial University of Newfoundland, St. John's, A1C 5R3, NL, Canada

³ Institute for Marine Research, 5005 Bergen, Norway

⁴ Department of Arctic and Marine Biology, UiT The Arctic University of Norway, 9019 Tromsø, Norway

⁵ Department of Arctic Biology, The University Centre in Svalbard, 9171 Longyearbyen, Norway

⁶ Independent scientist, 9012 Tromsø

⁷ Department of Biological Sciences, University of Bergen, 5020 Bergen, Norway

4.1 Abstract

The northern shrimp (*Pandalus borealis*) fishery, an important commercial fishery in the eastern Canadian Arctic and the Barents Sea, is reporting increasing bycatch of polar cod (*Boreogadus saida*), a key Arctic forage fish species. Furthermore, northern shrimp and polar cod spatial distributions increasingly coincide with that of Atlantic cod (*Gadus morhua*). Discrimination between the acoustic signals of Atlantic cod, polar cod and northern shrimp could provide more information on the risk of polar cod bycatch in the northern shrimp fishery and improve the accuracy of stock assessment surveys. We conducted a series of single-species mesocosm experiments for target strength measurements of Atlantic cod, polar cod and northern shrimp to assess the potential for species discrimination using their target strength spectra, TS(f). Mesocosm experiments were completed with a Wideband Autonomous Transceiver (WBAT) and collected broadband TS(f) (90-170 kHz and 185-255 kHz) of individual targets. Hundreds of TS(f) were extracted for each species and used to train machine-

learning classification algorithms (“classifiers”). We found that a simple classifier, k-Nearest Neighbor, and a single 200 kHz transducer operating in broadband mode are sufficient to achieve high classification performance (97%). The promising results from mesocosm-trained acoustic classifiers are an important step towards classifying coinciding marine species *in situ* and increasing the sustainability of fisheries.

4.2 Introduction

The northern shrimp fishery, *Pandalus borealis*, is one of the most valuable fisheries in the Northwest Atlantic, the eastern Canadian Arctic, and the Barents Sea. It generates 90% of Greenland’s export value (Garcia, 2007), and is the most valuable invertebrate fishery in the Barents Sea (Berenboim et al., 2000). However, shrimp fisheries are associated with bycatch problems (Grimaldo & Larsen, 2005; Howell & Langan, 1992). Currently, bycatch reduction strategies in the shrimp trawl fishery focus on gear modification, such as rigid sorting grids (Hannah & Jones, 2007), which has a limited effect on separating small gadoids (Grimaldo & Larsen, 2005; Isaksen et al., 1992), in particular Atlantic cod (*Gadus morhua*) and polar cod (*Boreogadus saida*) (Walkusz et al., 2020). Atlantic cod is an important predator of northern shrimp and influences the stock size (Garcia, 2007). Polar cod can account for > 95% of the pelagic fish assemblage in the Arctic and has a pivotal role in the Arctic food web as a key forage fish species (Geoffroy et al., 2023). A better understanding of the spatial dynamics of Atlantic cod, polar cod, and northern shrimp would help forecast stock changes and bycatch risk. Hydroacoustic surveys are widely used for expanding the spatial footprint of ecosystem assessments (Bassett et al., 2018). They support

high-resolution fish abundance, biomass, and movement estimates and are less invasive than traditional trawl monitoring (Trenkel et al., 2019). Because the acoustic scattering of a target, which depends on size, orientation, and acoustic properties, is also dependent on frequency, broadband echosounders have been increasingly used to infer species composition (e.g., Loranger et al., 2022; Ross et al., 2013). However, broadband acoustic scattering measurements of an individual target, conventionally recorded as target strength spectra (TS(f) [dB re 1 m²]; hereby target spectra), has been found to have large variability, which cannot be explained by length or orientation (Briseño-Avena et al., 2015; Dunning et al., 2023). The increased variability, complexity and size of broadband data have required powerful data analysis tools, such as machine learning algorithms (Malde et al., 2020). However, supervised machine learning algorithms require training datasets containing measurements of known targets. Schooling pelagic fish has been a common test for acoustic classification of monospecific aggregations (e.g., Bassett et al., 2020; Brautaset et al., 2020) because of the possibility of validation by trawl. Less invasive measures applicable to individual targets, such as camera validation (Benoit-Bird & Waluk, 2020), have successfully classified acoustic signals. However, these methods are limited by the ability to identify the acoustically detected individuals when multiple species are present. Mesocosm classification of target spectra has been successfully used to differentiate between two coincident swim-bladdered fish species: whitefish (*Coregonus wartmanni*) and stickleback (*Gasterosteus aculeatus*) (Gugele et al., 2021). A mesocosm-trained classification approach represents a promising avenue to improve taxonomic resolution from broadband hydroacoustics because a high number of detections can be collected for a known population with semi-natural swimming behaviours for a range of dif-

ferent species. For the shrimp fishery, the classification of coincident species could help assess the bycatch risk of fishing grounds prior to setting the trawls or to inform policy and models on ecosystem distribution patterns. Remote target classification with broadband acoustics could also benefit stock assessment surveys and estimates by increasing spatial resolution, access to remote areas, and sustainability by reducing survey time and costs. This study reports on a series of single-species mesocosm experiments with broadband hydroacoustics to classify the acoustic backscatter from three coinciding species: Atlantic cod, polar cod, and northern shrimp. In addition, these experiments further improve our understanding of the potential use of mesocosm-trained classification of broadband acoustic backscatter.

4.3 Methods

4.3.1 Species collection

The three coinciding species (Atlantic cod, polar cod, and northern shrimp) were collected from R/V *Helmer Hanssen* using a Harstad pelagic trawl (8 mm mesh) and bottom trawl (Campelan 1800 shrimp trawl with rockhopper gear) at 3 knots for 15 to 20 minutes in three fjords in Svalbard (Billefjorden, Krossfjorden, and Kongsfjorden) (Figure 4.1) on 17 and 19 January 2023 (Table 4.1). The trawled depth was selected based on the depth of the strongest scattering layer seen on the vessel's echosounder (Kongsberg Discovery AS; Simrad EK60, 18 and 38 kHz, 1.024 ms pulse duration, 2 Hz pulse repetition). A FISH-LIFT, an aquarium attached to the trawl codend that reduces turbulence and minimizes the impact of trawling on the caught

animals (Holst & McDonald, 2000), was used to maximize the fitness and health of the live fish and shrimp. The fish and shrimp were kept on board in large tanks (1 m³) with running seawater and delivered to the wharf in Ny-Ålesund in Kongsfjorden. At the Kings Bay Marine Laboratory, the fish and shrimp were sorted by species and stored in 6 m³ holding tanks with a flow-through system of filtered ambient seawater ($\sim 1^{\circ}\text{C}$) for 2 to 7 days, depending on weather and experiment priority.

Table 4.1: Overview of the trawling when the catch was used for single species mesocosm experiments. The pelagic trawl was used unless otherwise noted. All dates are in 2023.

Trawl date (UTC)	Location (°N, °E)	Collection depth (m)	Experiment date	Species (n)	Experiment duration (h)
17 Jan 22:26	Billefjorden (78.62, 16.54)	102	19 Jan	Polar cod (90)	6
			24 Jan	Polar cod (133)	6.5
19 Jan 00:10	Outer Krossfjorden (79.05, 11.35)	150	26 Jan	Northern shrimp (100)	5.25
			20 Jan	Atlantic cod (5)	8
19 Jan 19:54	Outer Kongsfjorden (79.04, 11.34)	352*			

* Bottom depth – bottom trawl was used.

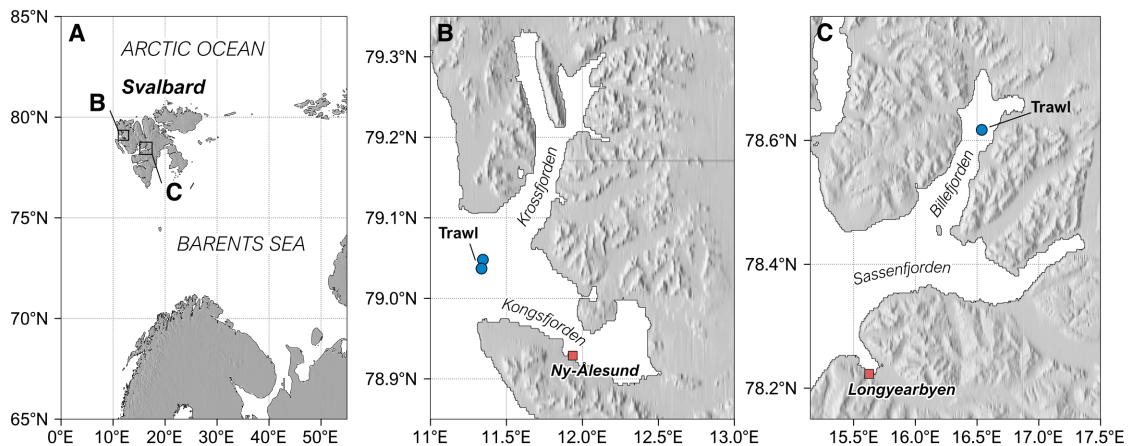


Figure 4.1: A) Map of the Svalbard archipelago. B) Map of two species collection location (blue circles) and experiment location at the Ny-Ålesund wharf (red square) in Outer Krossfjorden and Outer Kongsfjorden. C) Map of a species collection location in Billefjorden in relation to Longyearbyen (red square).

4.3.2 Mesocosm experiment

Broadband target strength data of single species were collected during four experiments in January 2023 (Table 4.1) using a mesocosm deployed from a wharf in Ny-Ålesund, Svalbard (red square; Figure 4.1B). The mesocosm, or AFKABAN (Arrested Fish Kept Alive for Broadband Acoustics Net experiment), was fitted with a large cuboid fish net (H7 x W2 x L2 m) with a 6 mm by 3 mm oval mesh or a small cuboid zooplankton net (H3 x W2 x L2 m) with a 500 μm -mesh (Figure 4.2A). The net was mounted on an 8 m high by 2 m wide and 2 m long aluminium frame oriented vertically (Figure 4.2A). Ropes with hook and loop straps attached the eyelets on the net to the frame at each corner and along the edges. A zipper on the top panel was

opened to introduce species into the submerged mesocosm.

The transducers (ES120-7CD and ES200-7CDK-split; Kongsberg Discovery AS, Horten, Norway) were mounted side by side on a plate centred inside the mesocosm through a hole on the top panel of the net with the acoustic axis pointing directly down. The smaller transducer (ES200-7CDK-split) was mounted on raisers to level the transducer faces. The transducer plate was fixed to the frame to ensure the transducer, the frame, and the net moved as a unit under the stress of currents. AFKABAN was suspended from a crane and lowered into the sea (Figure 4.2B) until the depth of the transducer face was approximately 1 m below the surface. A Wideband Autonomous Transceiver (WBAT, SN:253120; Kongsberg Discovery AS) was fastened horizontally to the frame to operate the transducers (Figure 4.2). The AFKABAN frame was purpose-built by Havbruksstasjonen (Ringvassøya, Norway) and wide enough to have two side-by-side beams of 7° opening angle transducers inside the net.

The acoustic data were collected using a WBAT programmed to emit frequency-modulated chirps multiplexing between bandwidths 90-170 kHz and 185-255 kHz. The emitted pulse had a fast taper, a pulse duration of 0.512 ms with 200 and 113 W emitted power for the 120 kHz and 200 kHz transducers, respectively. The ping interval was set to the minimum allowable value, between 2 and 2.5 s, to maximize the number of single detections and tracks; it was limited by factors such as the internal processing time and range. We selected a fast taper to have the maximal bandwidth available at full power for the classifier. A short pulse length was selected to resolve targets near the net boundary, reduce reverberation volume (Soule et al., 1997), and increase the chances of sampling clean echoes from single targets in the mesocosm (Gugele et al., 2021). Data collection for analysis started at least 25 minutes after the

mesocosm was fully submerged with the species inside the net to leave enough time for the organisms to acclimate and bubbles to disperse. Continuous conductivity, temperature, and pressure data measurements were collected during all experiments with a Sea-Bird SBE19plus (SN 01908096) for the fish experiments and SeaBird 37SI MicroCAT CTD (SN 37SI31215-2767) for the northern shrimp experiment.

Immediately after the experiment, the frame was lifted to the wharf and the species were removed from the net via a zipper on the bottom panel. The shrimp and fish were euthanized in an overdose of Finquel MS-222 (tricaine methane sulfonate) compound solution (500-600 mg l⁻¹). Length and weight measurements were taken on the euthanized individuals after the experiment. The treatment and use of species in these experiments were approved by the Norwegian Food Safety Authority (FOT 29801, 22/231325) (Appendix C).

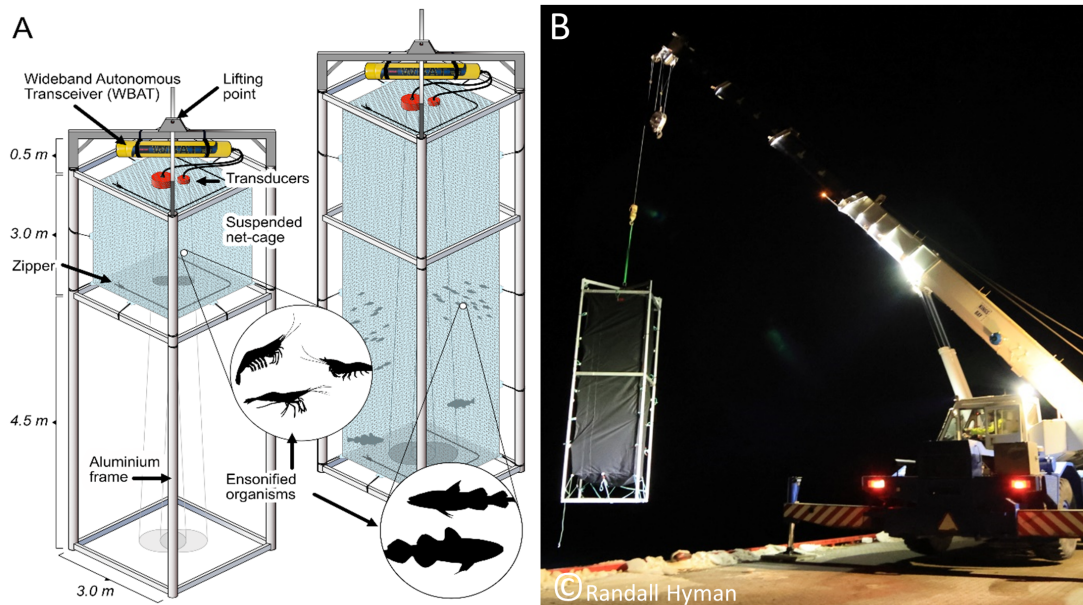


Figure 4.2: A) Schematic of the frame with the small zooplankton net (left; northern shrimp experiment) and large fish net (right; Atlantic cod and polar cod experiments). The acoustic transceiver (yellow cylinder) is attached to the frame and the transducers (orange cylinder, two in this experiment). There is a hole at the top of the net for the transducer faces to be unobstructed inside the net. B) The AFKABAN mesocosm with the large fish net lifted with the crane at the end of the experiment.

4.3.3 Acoustic data analysis

Acoustic data were calibrated using the sphere method adapted to broadband echosounders (Andersen et al., 2023; Demer et al., 2015). The calibrations required two spheres for each transducer (38.1 mm and 22 mm) to collect calibration parameters for the available frequency bandwidths (Appendix D Figure S1, S2). Calibrations were performed on 26 January 2023 in Ny-Ålesund, Svalbard. The theoretical nulls of the 38.1 mm

sphere did not match the measurements during the calibration. Therefore, the 22 mm calibrations parameters were preferred over the 38.1 mm values (Appendix D Figure S3). Since the 38.1 mm sphere had been used for a successful calibration previously (Appendix B Figure S2) and the magnitude of the target spectra match reasonably well, these calibrations values were used when values from the 22 mm sphere were unavailable due to the inhibition bands. All acoustic data were processed in Echoview 13.1 (Echoview Software Pty Ltd, Hobart, Tasmania). The data analysis range was bounded by the near-field region (Simmonds & MacLennan, 2008), and by the echo from the bottom of the net (i.e., 1.0 m - 6.8 m for the fish experiments and 1.0 m - 2.4 m for the shrimp experiments). The “Single target detection – wideband 1” operator was applied to select qualifying targets for each transducer (Table 4.2). The target strength, TS, threshold was adjusted for the different experimental species; all other parameters were consistent between experiments.

Table 4.2: Single echo detection - wideband 1 detector settings, where TS is target strength.

Parameter	Value
TS threshold (dB re 1 m ²)	fish: -75 shrimp: -120
Pulse length determination level (dB re 1 W ²)	8
Normalized pulse length (min, max)	(0.5, 1.5)
Minimum target separation (m)	0
Off-axis angle filter (degrees)	4

¹ Dunning et al. (2023).

All the single targets accepted by single echo detection (SED) parameters of both transducers were merged for manual target selection. The selected single echo detections were manually organized into tracks by visual assessment to ensure each track had a high probability of being from a single organism (Khodabandeloo et al., 2021). We selected isolated SEDs that did not contain adjacent targets in the Fourier transform window (0.25 m above and below) (Figure 4.3D-F). Adjacent targets can distort the frequency response because of interference between the backscattered signals. Target spectra graphs (Figure 4.3G-I) were used to assess the presence of adjacent targets; these can be identified by regularly spaced nulls (Khodabandeloo et al., 2021; Reeder et al., 2004; Stanton et al., 1996). The single target tracks were formed by following SEDs traces from ping to ping and verifying the location sequence of the single target tracks across the acoustic beam. We ensured each selected track had a minimum of 4 SEDs to have enough information for the target trajectory across the acoustic beam. Only one SED per ping could be selected, in the case of multiple SED candidates in a single ping, the center, strongest SED was selected for the track. A single organism likely formed each track because we used both frequency response patterns and target tracking location in the acoustic beam to select targets and create tracks (Figure 4.3).

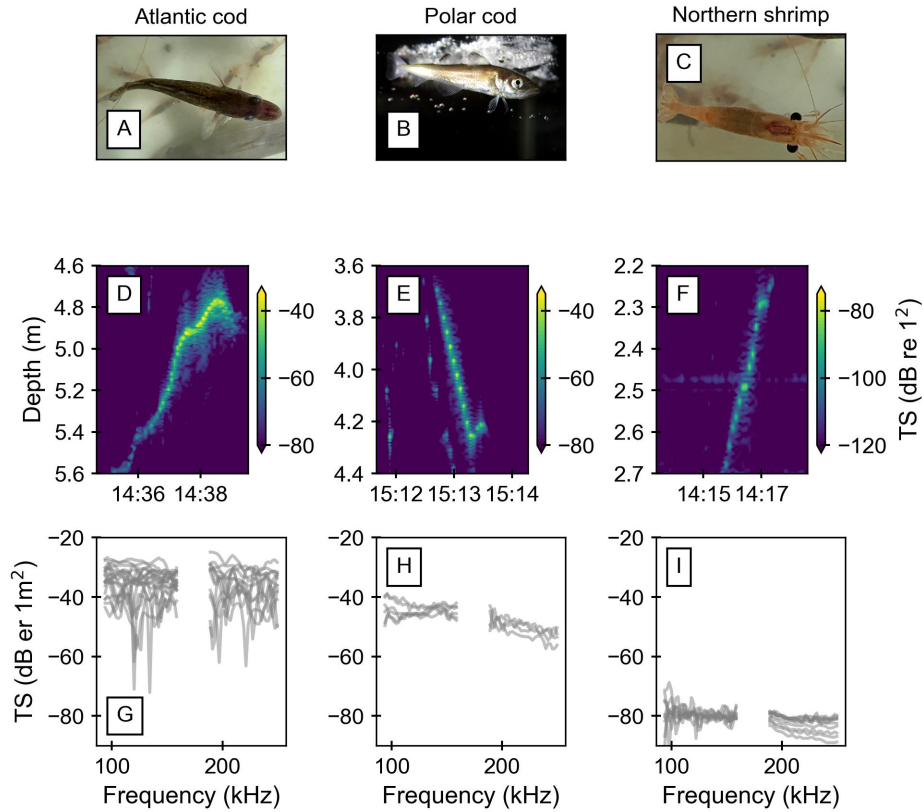


Figure 4.3: Examples of the target spectra of each selected detection from an individual track of each species using multiplexing broadband echosounders. An image of the species from the experiment: A) Atlantic cod (*Gadus morhua*), B) polar cod (*Boreogardus saida*) C) northern shrimp (*Pandalus borealis*). D-F) Echogram of a selected isolated track from each species labelled above. Measured target spectra of the selected tracks; G) Atlantic cod with 19 detections in the 94-158 kHz bandwidth and 13 detections in the 189-249 kHz bandwidth (grey lines), H) polar cod track with 6 in the 94-158 kHz bandwidth and 4 target spectra in the 189-249 kHz bandwidth, I) northern shrimp track with 9 target spectra in the 94-158 kHz bandwidth and 10 target spectra in the 189-249 kHz bandwidth. Photo in Panel B was taken by Hauke Flores.

All target spectra were calculated using a Fourier transform window length of 0.33 times the pulse length (i.e., 0.25 m) and exported from Echoview with a 2 kHz frequency resolution, determined by the pulse duration (Khodabandeloo et al., 2021; Medwin & Clay, 1998). The Fourier transform window size was selected to maximize the information from the echo while reducing the risk of contamination from nearby targets.

The first and last 5% of each target spectra were removed to eliminate the effects of the pulse taper. The frequency band from 162-170 kHz was removed because of inconsistent calibration results at this frequency range (Appendix D Figure S2). The trimmed target spectra were used to train the classifiers.

4.3.4 Classifier training

Classifier training was performed in Python (version 3.9.15) using the Scikit-Learn library (version 1.1.3, Pedregosa et al., 2011) and Hyperopt-Sklearn library (version 1.0.3; Komer et al., 2014). An L^2 -normalization was applied to each target spectra so that if the values were to be squared and summed, the sum would equal 1 (Komer et al., 2014). Preprocessing with normalizing by observation removed the influence of intensity on the off-axis compensation of the target spectra. The normalization is a standard data preparation step for machine learning to stabilize training, reduce the impact of outliers and improve performance. The number of target spectra per class was balanced by applying an over-sampling technique. Over-sampling was used to avoid removing samples and the classes were not severely unbalanced (6:1). The

samples in the minority classes (Atlantic cod and northern shrimp) were resampled randomly until they were balanced with the majority class (polar cod) to reduce the risk of bias in the model predictions (Goodfellow et al., 2016), reaching a total of 695 and 699 samples per class for the 94-158 kHz and 189-249 kHz bandwidths, respectively.

Three classifiers, K-Nearest Neighbours (kNN; Goldberger et al., 2004), LightGBM (Ke et al., 2017), and support vector machine (SVM; Cortes & Vapnik, 1995), were trained and Bayesian hyperparameter optimization was used for parameter selection. The classifiers were trained using a 10-fold cross-validation method (Stone, 1974) to split the data iteratively into a training subset (90%) and a testing subset (10%) of the single species target spectra from the mesocosm experiments. Classifier performance was evaluated using a mean class-weighted F1 score because it is an evaluation metric that penalizes false positives and false negatives equally. The class-weighted F1 score was averaged by class and weighted by the number of true instances for each class (Pedregosa et al., 2011).

4.4 Results

4.4.1 Species composition

The 16 Atlantic cod in AFKABAN had a mean length of 52 ± 8 cm ($L \pm$ standard deviation (SD)), and their mean weight was 978 ± 346 g ($W \pm$ SD). The individuals were smaller for both polar cod experiments than for the Atlantic cod experiment. The first polar cod experiment had fewer but larger individuals ($n = 90$; $L = 19 \pm$

2 cm; $W = 50 \pm 10$ g), whereas the second experiment had more individuals that were, on average, smaller ($n = 133$; $L = 18 \pm 2$ cm; $W = 30$ g; weighed as a group and divided by the number of individuals). For the shrimp experiment, we added 100 shrimps with an average length of 8 ± 1 cm (measured from eye to telson) inside the small mesocosm configuration of AFKABAN (Figure 4.1A left). The shrimps were weighed as a group and divided by the number of individuals, which resulted in an average individual weight of 6 g.

4.4.2 Single species target spectra

There were 60 selected tracks in the Atlantic cod dataset, comprised of 345 target spectra in the 94-158 kHz bandwidth and 273 target spectra in the 189-249 kHz bandwidth (Figure 4.4A). The first polar cod experiment resulted in 62 selected tracks with 345 target spectra in the 94-158 kHz bandwidth frequency bandwidth and 362 target spectra in the 189-249 kHz frequency bandwidth (Figure 4.4B). The second polar cod experiment was slightly shorter in length but had more individuals in the net (Table 4.1) and had slightly more tracks, a total of 66 tracks with 350 target spectra in the 94-158 kHz bandwidth and 337 target spectra in the 189-249 kHz bandwidth (Figure 4.4C). Lastly, the northern shrimp experiment had the fewest tracks because of the low number of individuals, the shorter duration of the experiment and the small size of the individuals (Table 4.1). There were 25 selected tracks composed of 108 target spectra in the 94-158 kHz bandwidth and 180 target spectra in the 189-249 kHz bandwidth (Figure 4.4D).

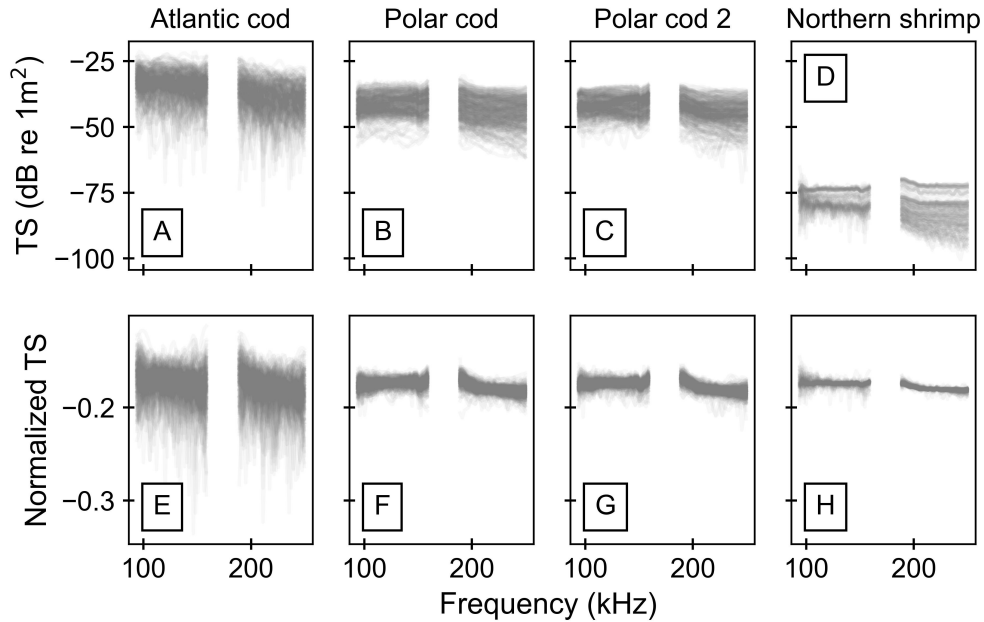


Figure 4.4: Target spectra of all single target detections from all single species experiments. Each target spectra was recorded as target strength (TS) over the 94-158 kHz or the 189-249 kHz bandwidth. *Panel A-D*: target spectra of single echo detections organized by species. *Panel E-H*: L^2 -normalized target spectra, each target spectra have a unit norm.

The classification analysis used all the selected target spectra and, in the case of Atlantic cod and northern shrimps, the replicates added to achieve balanced classes (Figure 4.4). Atlantic cod had the strongest average echo intensity with a mean target strength of -34 dB re 1 m² for the 94-158 kHz bandwidth and -38 dB re 1 m² for the 189-249 kHz bandwidth. Both polar cod experiments resulted in similar target strength values with a mean target strength of -41 dB re 1 m² for the 94-158 kHz bandwidth for the first polar cod experiment with the slightly larger individuals and

-42 dB re 1 m² for the 94-158 kHz bandwidth for the smaller polar cod experiment. In the 189-249 kHz bandwidth, both polar cod experiments resulted in an average target strength of -44 dB re 1 m². The northern shrimp had the weakest echo intensity with a mean target strength of -78 dB re 1 m² and -82 dB re 1 m² in the 94-158 kHz and 189-249 kHz bandwidth, respectively. All species had a mean target strength that decreased in the higher frequency range.

Atlantic cod had the largest variability in target strength intensity per individual (i.e., among pings forming a track) with a maximum range of 43 dB re 1 m² at the nominal frequency, 120 kHz, and 33 dB re 1 m² at the nominal frequency, 200 kHz. The variability in target strength intensity per track at the nominal frequency for the polar cod and northern shrimps were largest at 200 kHz but smaller than the Atlantic cod target strength intensity variability. During the second polar cod experiment, the polar cod had a maximum target strength intensity range within a track of 21 dB re 1 m² at 200 kHz, and for northern shrimp it was 8 dB re 1 m² at 200 kHz.

4.4.3 Classifier training

The three classifiers trained on the normalized target spectra (Figure 4.4E-H) showed a high performance in classifying the frequency response of polar cod, Atlantic cod, and northern shrimp across both the 94-158 kHz and 189-249 kHz bandwidths (mean class-weighted F1 scores: >95%; Tables 4.3). The northern shrimp target spectra had the highest mean per-class classification performance in the 94-158 kHz bandwidth for all three classifiers ($\geq 98\%$; Table 4.3). Atlantic cod had a slightly higher performance

than polar cod (up to 0.03 increase) in both bandwidths. Both complex and computationally expensive classifiers, LightGBM and SVM, did not have notably higher performance than kNN, and the kNN classifier required at least 10x less computing time to train. The preprocessing with an L^2 -normalization resulted in a marginal overall improvement to the classification results, ~ 0.02 increase in F1 scores.

Table 4.3: Classifier F1 scores estimated by classifier training (mean \pm SD) of the normalized target spectra collected with the 120 kHz and 200 kHz transducer.

	120 kHz			200 kHz		
	kNN	LightGBM	SVM	kNN	LightGBM	SVM
Mean						
class-weighted	0.96 ± 0.01	0.97 ± 0.02				
Atlantic cod	0.95 ± 0.02	0.98 ± 0.01	0.96 ± 0.02	0.98 ± 0.01	0.96 ± 0.02	0.96 ± 0.04
Polar cod	0.94 ± 0.02	0.95 ± 0.02	0.95 ± 0.02	0.96 ± 0.01	0.95 ± 0.03	0.96 ± 0.03
Northern shrimp	0.98 ± 0.01	0.97 ± 0.01	0.99 ± 0.01	0.98 ± 0.0	0.99 ± 0.01	1.0 ± 0.0

4.5 Discussion

4.5.1 Species-specific patterns

The high classification performance (mean class-weighted F1 score of 97%) for three coincident species is a promising result for *in situ* classification of targets from broadband echosounders. The results show that three coincident species, Atlantic cod,

polar cod, and northern shrimp, can be differentiated using their target spectra with a single transducer and a relatively simple classification algorithm. Presumably, the range of target spectra complexity and morphological differences of the three species ensured the high performance of the classifiers.

Atlantic cod's target spectra were found to be the most complex, defined by closer and more intense peaks and null across the bandwidth. The spectral complexity observed in the Atlantic cod target spectra could have suggested that the SED contained interference from other targets (Figure 4.3G; Khodabandeloo et al., 2021; Stanton et al., 1996). However, the rigorous manual target selection process ensured that only one individual was included per SED and no adjacent targets were included in the Fourier transform window (~ 0.25 m above and below the target). Therefore, the multiple scattering features (constructive and destructive interference) within the individual Atlantic cod targets must have originated from the backscatter of different organs interfering with each other (Demer et al., 2017; Reeder et al., 2004). We thus expect that discriminating and classifying several morphologically complex targets, such as Atlantic cod, will be more challenging (Au & Benoit-Bird, 2003; Clay, 1991, 1992).

In contrast, polar cod target spectra had an intermediate complexity with some ripples and a relatively consistent slope across the spectra. During the target selection of polar cod, there was only one central dominant SED per ping, which suggested each individual had a single dominant scattering feature (i.e., the swimbladder) and explained the absence of large nulls and peaks (Figure 4.3H). The northern shrimp had a mixed spectral complexity in the target spectra with some ripples in the 94-158 kHz bandwidth but predominantly flat normalized target spectra, especially in the 189-249 kHz bandwidth (Figure 4.4D). The emitted chirp from the 120 kHz trans-

ducer had a 10 kHz wider bandwidth than the 200 kHz transducer, which increased the spatial resolution to 9 mm (compared to 11 mm for the 200 kHz). The finer temporal resolution from the wider bandwidth may have revealed finer-scale scattering features, which are typically only discernible with higher frequencies (Reeder et al., 2004).

Target spectra complexity was used by Cotter et al. (2021) to scrutinize target spectra into four classes based on selected scattering models (i.e., above, at, or below resonance for gas-bearing organisms or fluid-like organisms). These categories were used to classify mesopelagic fish into size classes with a mean F1 score of 0.90. Similarly, Roa et al. (2022) had a high performance (the best mean class-weighted F1 score was 0.96) with classifiers trained on scattering models for six different reef fish. They found that the nodes or “ripples”, typically found at higher frequencies, were the prominent source of discriminating information. Discriminating nodes and ripples were not found in three of the four modelled zooplankton groups in Dunn et al. (2023), which resulted in moderate performance for the classifiers (best mean class-weighted F1 score was 0.71). Based on previous studies and the results from this study, we conclude that classifying targets with different spectral complexity can positively impact classification performance.

4.5.2 Intensity variability of broadband target spectra

Broadband acoustic backscattering signals exhibit large unexplained variability between detections of a single target (Dunning et al., 2023; Gugele et al., 2021; Reeder et al., 2004). For example, an Atlantic cod target spectra study recorded a maximum

target strength variation of 30 dB re 1 m² within a track of a single fish at 38 kHz (Dunning et al., 2023). Here, we observed a comparable maximum variation in target strength of 33 dB re 1 m² at 200 kHz with an Atlantic cod track. However, polar cod and northern shrimp exhibited a smaller variation of target strength per track. The target strength variability in broadband acoustics for a single target was found to be greater than could be explained with tilt angle or fish length (Dunning et al., 2023), which are traditionally used to explain the variability in narrowband target strength measurements (Khodabandeloo et al., 2021; Zhang et al., 2021). Presumably, the stochasticity found in the Atlantic cod target spectra tracks could be due to variations in the section of the fish being ensonified from ping to ping. In particular, the Atlantic cod had a similar length to the beam width; therefore, different parts of the fish body were likely impinged separately, adding variability to the measurements. Different target spectra could be obtained at a farther detection range in the wild. A mesocosm experiment, similar to this study but with fewer individuals with a larger measurement range and optical verification, could develop a better understanding of broadband acoustic target strength variability.

In the classification, the normalizing preprocessing algorithm removes the intensity component of the target spectra (Figure 4.4I-L). Normalizing the target spectra had the largest effect on the intensity variability of northern shrimp spectra. Though northern shrimp had the smallest maximum variability per track, 7 dB re 1 m² at 120 kHz and 8 dB re 1 m² at 200 kHz, the intensity between individuals varied greatly, especially over the 189-249 kHz bandwidth (Figure 4.4D). The normalized shrimp target spectra reduced variance, which showed that the northern shrimp had the most consistent target spectra pattern despite the large variability in target strength

intensity.

4.5.3 Classification of *in situ* targets

The high performance of the classifiers in a controlled experiment is an important step towards *in situ* target classification. However, fundamental challenges should be addressed before *in situ* target classification can be achieved with mesocosm-trained classifiers. A significant limitation of supervised classification is the dependence on collecting training datasets for all classes (Handegard et al., 2021). Collecting target spectra from mesocosm experiments for all species and size groups in complex and dynamic environments such as the ocean, even in Arctic regions with relatively low species diversity, is unrealistic. A series of ship-based downward-looking lowered acoustic probe experiments were completed as part of this study, attempting to classify *in situ* targets using the trained classifiers. However, the trawls showed the community was dominated by herring and capelin among the Atlantic cod, polar cod and northern shrimps, which prevented validation of *in situ* classification. One method to validate the classifiers would be to repeat the lowered acoustic probe experiments in an enclosed region, such as a lake or smaller fjord, dominated by a single species to assess the error for that class. Single species-dominated regions are commonly used in fisheries acoustics to associate the backscatter to a single species (e.g., De Robertis et al., 2019; Geoffroy et al., 2016). A more widespread method to use mesocosm-trained classifiers would be to have broader classes and to group species based on morphological features and expected backscattering (Gugele et al., 2021). However, better knowledge of the impact of multiple scattering features and

their contribution to target spectra complexity will also be necessary to successfully classify *in situ* broadband acoustic signals.

Another practical limitation to *in situ* broadband acoustic target classification is the rigorous track selection requirements. Better tracking algorithms for broadband data with reduced risk of interference from contaminating targets within the Fourier transform window will need to be developed. Currently, tracks tend to be manually selected in broadband acoustics studies (Dunning et al., 2023; Khodabandeloo et al., 2021), which is time-consuming and subjective. Manual selection of single echoes and tracks halts the potential of automation and reproducibility. With automatic and reproducible track selections, classifiers could be quickly applied to new datasets for large-scale analysis of hydroacoustic survey datasets (Chawarski et al., *In prep*).

Another challenge with applying mesocosm results to *in situ* measurements is the limited possible replicates of target spectra available from the enclosed species. There is a much wider range of shapes and swimming behaviour found in naturally occurring individuals. For the Atlantic cod experiment, only 16 individuals were enclosed in the mesocosm. Therefore, there were limited detection replicates possible from the experiment and their swimming behaviour, which may have been affected by the handling and transport, is a limited representation of that from fish in the wild. The repeatability of the results from the two polar cod experiments showed consistency in the target spectra results between two groups of the same species; however, they were from the same fjord and trawl haul. Further mesocosm experiments with populations from different fjords could improve our understanding of the interspecies variability of target spectra and limit pseudoreplication (Hurlbert, 1984). Furthermore, the results were possibly biased because of the occurrence of detections from tracks being used

for testing and training at the same time. The potential autocorrelation risk could be mitigated by using all detections from a track either in the testing or the training set. The individual detections were used for the study because target spectra were variable within a track, and the spectral complexity factors from the target spectra would be flattened by combining multiple detections from a track. However, tracks could be added as a feature to the classifiers to test if detections within a track are more similar than between tracks. Incidentally, this type of test could inform on intraspecies variability.

4.6 Conclusion

Three coincident species (Atlantic cod, polar cod, and northern shrimp) were found to have distinct enough target spectra relative to each other in monospecific mesocosm experiments, despite their intraspecies variability. The high performance of the machine learning classifiers was due to the different levels of target spectra complexity observed across the selected species. Further mesocosm studies will determine the taxonomic resolution to which mesocosm-trained classifiers can be used for *in situ* classification, either by adding new classes of additional coinciding species, such as herring and capelin, or by joining new classes in the existing ones based on their target spectra complexity. This study paves the way toward automating *in situ* species classification using lowered acoustic probes or autonomous underwater vehicles equipped with broadband echosounders, which opens the possibility to real-time warnings of bycatch risks to reduce cost and trawling impact. Forecasting bycatch risks could greatly impact the shrimp fishery because excessive retention of non-regulated bycatch can

increase fuel costs, loss of revenue, and practical problems of onboard with sorting the catch (Jacques et al., 2022). Finally, automated acoustic classification methods could increase our ability to measure ecosystem changes and distribution shifts of fish species, for instance in the North Atlantic and the Barents Sea (Fosheim et al., 2015; Morato et al., 2020; Morley et al., 2018).

Chapter 5

General conclusions

5.1 Overview of research goal

The overarching goal of the present thesis is to contribute to advancing and testing methods that increase the independence of acoustic surveys for monitoring marine ecosystems. The goal was achieved by contributing the three methods below:

- reducing the dependence on relative density estimates of sound scattering layers from net and trawl sampling by using scattering models for hydroacoustic surveys with uncrewed vehicles;
- training classification algorithms with scattering models to classify the target spectra of individual zooplankton;
- training classification algorithms with mesocosm measurement of target spectra to discriminate morphologically different species.

These methods addressed some of the key challenges in fisheries acoustics research,

such as increasing the value of acoustic data when concomitant trawl or net data is not possible or limited (Fernandes et al., 2016; Horne, 2000) and utilizing target spectra patterns from scattering models and mesocosm measurements for classification and determining their limitations (Gugele et al., 2021; Roa et al., 2022).

The methods studied in this thesis were advanced while keeping in mind the unique challenges of monitoring the Arctic, such as behavioural effects of lights from vessels during polar night (Berge et al., 2020) and rapid ecosystem changes (Florko et al., 2021; Kebir et al., 2023). To sustainably fish, develop industries and advance research in the Arctic, we need to increase and improve the monitoring and baseline assessments. Some of these assessments can be done by complementing traditional vessel-based surveys with uncrewed vehicles equipped with broadband echosounders. In addition, the Arctic was a practical region to advance and test multispecies discrimination methods because of the relatively low species diversity and the relatively larger size structure of zooplankton at higher latitudes (Brandão et al., 2021). However, the limitations and recommendations resulting from this thesis are not restricted to Arctic waters nor uncrewed vehicles. They are relevant and can be modified for use in different marine environments. The results emerging from this thesis demonstrate the potential for incorporating hydroacoustic surveys with broadband echosounders for ecosystem research, ecosystem-based fisheries management, and commercial fishing in the Arctic and beyond.

5.2 The role of acoustic surveys with uncrewed vehicles in fisheries

5.2.1 Ecosystem-based fisheries management

A successful implementation of ecosystem-based fisheries management requires more information than single-species stock assessments, especially in light of climate change stressors (Andersson et al., 2015; Kebir et al., 2023). Active acoustic methods, including echosounders, have been identified as having a strong potential to contribute to implementing ecosystem-based management (Trenkel et al., 2011). In particular, echosounders can be used to study organisms ranging from euphausiids and large copepods to large fish, depending on the selected frequency, and can provide high spatial resolution compared to traditional station-based sampling.

Acoustic-trawl surveys are currently implemented for a few pelagic fisheries stock assessments (e.g., capelin and herring, (Toresen et al., 1998), anchovy (Trenkel et al., 2009)) to provide an estimate of biomass and provide valuable samples to infer age, diet and other information. The methods explored in this thesis can complement traditional surveys by allowing more independence to uncrewed vehicles for the acoustic transects while the ship can do more extensive direct biological sampling work (Chapter 2, Dunn et al., 2022). There is a high potential and low threshold for uncrewed vehicles equipped with broadband echosounders to complement vessel-based acoustic-trawl surveys. Furthermore, vessel-based surveys can be complemented with moorings equipped with broadband echosounders to increase the temporal extent of surveys (De Robertis et al., 2018; Ross et al., 2013), and lowered acoustic probes or

towed lowered platforms can be used for close proximity high range resolution measurements of organisms at depth (Khodabandeloo et al., 2021).

Broadband echosounders can be used on uncrewed vehicles, acoustic probes, or research vessels to extend temporal and spatial coverage of density estimates when concurrent species and size composition sampling is available through validation with nets and trawls (Chapter 2, forward method, Dunn et al., 2022). When it is not possible to obtain information on the community composition directly from nets and trawls, the inverse method can help to optimize the density solution from modelled target spectra of the species expected to be present (Chapter 2, inverse method, Dunn et al., 2022). The inversion still requires a strong knowledge of the species composition and length distributions for the study region and, therefore, still depends on some level of traditional net and trawl sampling. However, it can allow for more flexibility in the survey transects in well studied regions. The inverse method with broadband target spectra has also been simulated under a Bayesian framework, which requires auxiliary information (biological knowledge or nets and trawls) to be explicitly expressed as priors (Urmy et al., 2023) as opposed to the frequentist approach used in Chapter 2. Extending the spatial and temporal coverage increases the information on the state and functioning of the ecosystems which reduces the uncertainty in fisheries assessments and improves management strategies (Chen et al., 2003).

In addition, uncrewed vehicles, mooring and lowered probes can be outfitted with different sensors to contextualize acoustic data with environmental (e.g., PAR, chlorophyll a) or chemical data streams (e.g., pH). The present thesis focused on methods to increase the independence of broadband echosounders, but concomitant data can provide additional insights for ecosystem-based management. Future works should

enable acoustic data to be coupled to other data streams for additional information on the ecosystem and its environment rather than for validating the acoustic signal. Ecological, oceanographic, and climate variability can substantially impact stocks. A source of parallel data streams to collect measurements for these factors, in addition to biomass estimates, could facilitate the quantitative incorporation of ecosystem-based considerations in fisheries assessments (Boyce et al., 2021).

5.2.2 Commercial fishing

My research has shown that northern shrimp, polar cod and Atlantic cod can be discriminated remotely using their target spectra (Chapter 4), which can be valuable for commercial fishing to reduce the operational and environmental concerns. These results are also valuable in increasing the possibilities for scientific monitoring. These findings pave the way for uncrewed acoustic surveys of fishing grounds before setting the trawls to assess the risk of bycatch. Mesocosm-informed classification could be tested for other commercially important species with high bycatch risks to reduce impacts on the environment, associated costs and fishing grounds closures. Mesocosm-informed classification (Chapter 4) demonstrated that a single transducer and simple machine learning classification algorithm were sufficient for a high classification performance. These results indicate that on-board processing of acoustic data for the classification of morphologically different species could be implemented for species discrimination of commercially important species.

Alternatively, the TS intensity discrepancy between the fish (polar cod, Atlantic cod) and northern shrimp found in Chapter 4 suggests that, in this case, thresholding nar-

rowband echosounder measurements may be enough to discriminate between these species because the mean TS of each species is strongly different. Thresholding narrowband TS is an accessible method to be implemented with fish finders mounted on fishing or research vessels for a rough idea of the community composition of dominant species.

5.3 The promise of broadband fisheries echosounders

5.3.1 The use of broadband echosounders

Broadband echosounders are an encouraging technology development for fisheries acoustics because of the spectra resolution, range resolution and dampening of stochastic noise (Bassett et al., 2020; Benoit-Bird & Waluk, 2020). The promise of broadband fisheries echosounders is rooted in the anticipation that it will resolve the grand challenge of species identification through the spectra resolution (MacLennan & Menz, 1996). However, the increase in size and complexity of the data collect by broadband echosounders requires new methods and standards for data processing and analysis procedures (Benoit-Bird & Waluk, 2020). The promise of broadband acoustics is tested in the present thesis through model-informed (Chapter 3, (Dunn et al., 2023)) and mesocosm-informed (Chapter 4) classification methods. These methods leverage the large volume datasets output from broadband echosounders to train supervised classification algorithms. Through controlled mesocosm experiments, we tested and explored the advantages and limitations of broadband echosounders.

5.3.2 Broadband sensitivity

One of the promising properties of broadband echosounders is the fine-scale range resolution from the matched filtering. With this technique, the range resolution is not dependent on the pulse length, as with narrowband systems, but rather on the bandwidth (Equation 1.13). Targets closer to each other than the transmit pulse length or a strong boundary (e.g., seafloor, a net) can be resolved with pulse compression. However, the processing side lobes are a side effect of the match filtering technique that are dependent on the pulse length (Lavery et al., 2017) (Figure 5.1A). When these processing sidelobes of nearby targets overlap, they contaminate the target spectra by introducing evenly spaced peaks and nulls (Demer et al., 2017)(Figure 5.1B,D). Therefore, even though targets closer than the pulse length can be resolved spatially, their target spectra may be distorted (Khodabandeloo et al., 2021)(Figure 5.1D). Processing sidelobe contamination was particularly problematic while selecting targets for analysis where the large fish targets had strong processing sidelobes in the pulse-compressed target strength echogram (Chapter 4). The processing sidelobes can be reduced with a slow amplitude ramping (gradual increase to full power of the broadband chirp), but the slow ramping reduces the available bandwidth, which in turn reduces the spectral range and range resolution. The standard single echo detection and target tracking algorithms were no longer robust enough to ensure the selection of isolated and uncontaminated target spectra. Recent works with broadband echosounders and target spectra have had to manually select targets and tracks (Chapter 4, Dunning et al., 2023; Khodabandeloo et al., 2021) which is a significant limitation to upscaling broadband echosounder and data processing methods to sur-

veys with uncrewed vehicles.

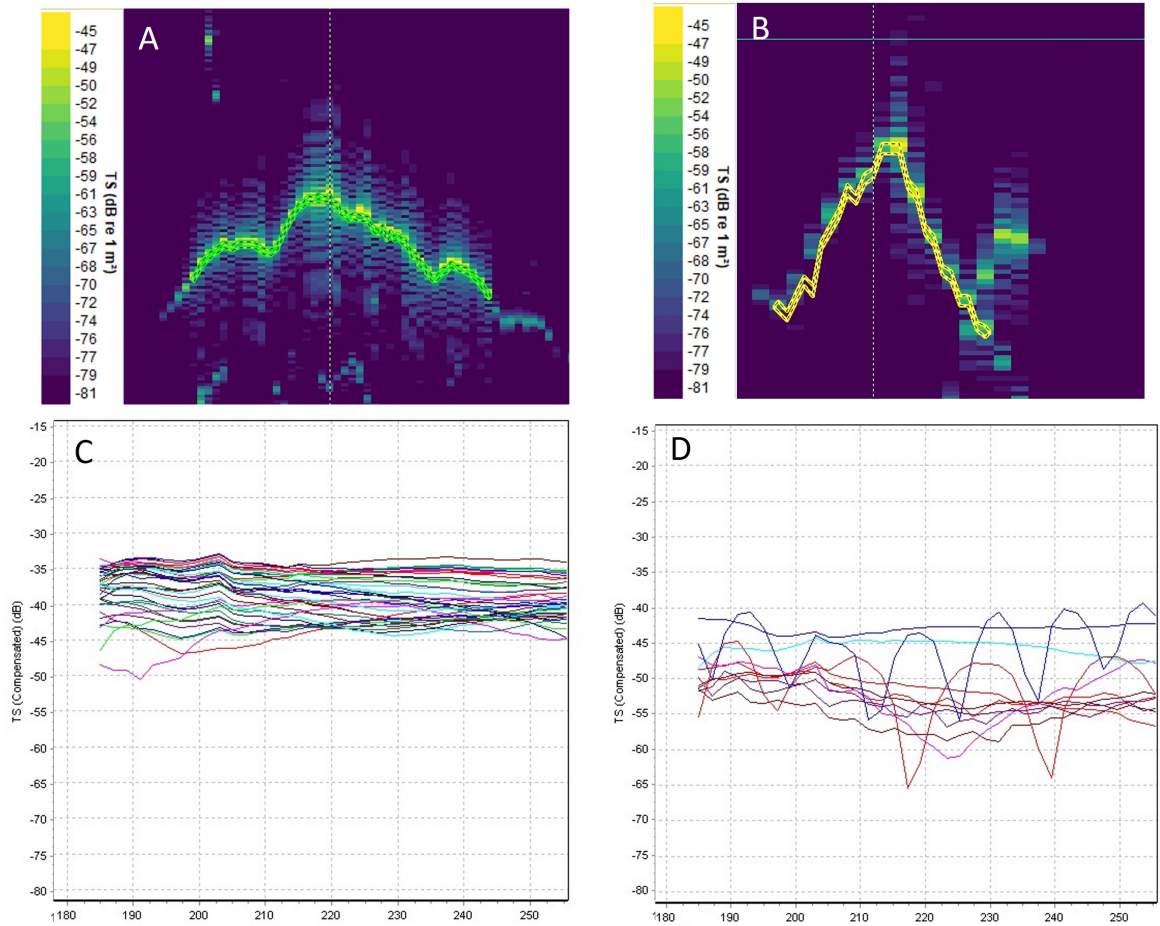


Figure 5.1: A) Echogram of a single fish track with clear processing sidelobes above and below the track. B) Echogram of a single fish track that is intercepted by another fish on the right end of the track, last two selected single echos. C) Target spectra of each selected single echo of the single fish. D) Target spectra of each selected single echo of the single fish with interference in two of the target spectra.

Another unexpected feature of the broadband echosounder system's high resolu-

tion is the ability to resolve the echo of different parts of a fish. On one hand, the echoes from the different acoustic boundaries found in a fish (e.g., seawater to flesh, flesh to swimbladder) can be studied in the time-domain to estimate the fish size (Kubilius et al., 2020, 2023). On the other hand, when studied in the frequency domain, the multiple neighbouring echoes for a single fish return target spectra that have properties indicative of being contaminated (e.g., Figure 4.3G). This interference can be observed for an *in situ* single target spectrum which tends to appear considerably more complex than the relatively smooth output from scattering models (Reeder et al., 2004). The sensitivity and high range resolution of broadband systems lead to high variability and complexity in target spectra measurements (Dunning et al., 2023). Understanding and testing the benefits and limits of broadband systems is a critical component of advancing the grand challenge of species identification.

5.4 Limitations of study and recommendations for future research

In Chapter 2, I present promising results for the inversion of aggregations of fluid-like species in an SSL using scattering models as the input for the least-squares algorithm. However, in Chapter 3, I present that model-informed classification of individual fluid-like species was unreliable based on a mesocosm validation of the method. I concluded that the poor classifier performance was due to the large variability and complexity in the measured *in situ* target spectra versus the relatively smooth modelled spectra.

Both can be valid when considering that the variability of a single individual's target spectra, $TS(f)$, has the potential to be larger than the volume backscatter spectra, $S_v(f)$, of a large number of individuals, where orientation, material properties and shape differences are averaged (Stanton et al., 1993). Therefore, an important consideration is the effect of the interference from neighbouring targets in an aggregation and the impacts on volume backscatter spectra (Demer et al., 2017). Then, the applicability of using modelled target spectra for individuals and for aggregations should be explored in more detail with experiments with reduced complexity, such as single species *in situ* aggregations or schools. Furthermore, the models may need to include the effects of multiple scattering on the attenuation and the spectra for aggregations (Chu & Ye, 1999) and for the acoustic boundaries of individual larger targets. Together, these chapters highlight the limitations of our current knowledge and reveal an important area of future work for continuing to integrate broadband systems in fisheries.

Finally, to maximize the potential of uncrewed vehicles equipped with broadband echosounders, the ability to combine data streams from different sensors should be developed. A limitation of the methods developed in this thesis is that only broadband echosounder data was considered, all complimentary datasets were collected by ships using nets and trawls. To use the benefits of uncrewed vehicles to the fullest, there needs to be further research in identifying other sensors that could provide near-coincident complimentary data to broadband echosounders. A promising complementary data stream would be optical sensors such as UVP6 (Hydroptic, France, www.hydroptic.com) for extending the size range of target detections Ponçon et al. (2023) or camera systems for quantifying and identifying species (Ohman et al., 2019).

The technology developments of sensors, machine learning algorithms and novel monitoring platforms will continue to evolve, and establishing methods and standard processing tools that maximize the potential of these technologies will give us a better chance at keeping up with the rapidly changing Arctic ecosystem.

Bibliography

Agersted, M. D., Khodabandeloo, B., Liu, Y., Melle, W., & Klevjer, T. A. (2021). Application of an unsupervised clustering algorithm on in situ broadband acoustic data to identify different mesopelagic target types. *ICES Journal of Marine Science*, 78(8), 2907–2921.

URL <https://doi.org/10.1093/icesjms/fsab167>

Amakasu, K., & Furusawa, M. (2006). The target strength of antarctic krill (*euphausia superba*) measured by the split-beam method in a small tank at 70 khz. *ICES Journal of Marine Science*, 63, 36–45.

URL <https://doi.org/10.1016/j.icesjms.2005.07.012>

Amakasu, K., Mukai, T., & Moteki, M. (2017). Measurement of the volume-backscattering spectrum from an aggregation of antarctic krill and inference of their length-frequency distribution. *Polar Science*, 12, 79–87.

URL <https://doi.org/10.1016/j.polar.2017.02.007>

Andersen, L. N., Chu, D., Handegard, N. O., Heimvoll, H., Korneliussen, R., Macaulay, G. J., Ona, E., Patel, R., & Pedersen, G. (2023). Quantitative processing of broadband data as implemented in a scientific split-beam echosounder.

Methods in Ecology and Evolution.

URL <https://doi.org/10.1111/2041-210X.14261>

Anderson, C. I. H., Horne, J. K., & Boyle, J. (2007). Classifying multi-frequency fisheries acoustic data using a robust probabilistic classification technique. *The Journal of the Acoustical Society of America*, *121*(6), EL230–EL237.

URL <https://doi.org/10.1121/1.2731016>

Andersson, A., Meier, H. M., Ripszam, M., Rowe, O., Wikner, J., Haglund, P., Eilola, K., Legrand, C., Figueroa, D., Paczkowska, J., et al. (2015). Projected future climate change and baltic sea ecosystem management. *Ambio*, *44*, 345–356.

URL <https://doi.org/10.1007/s13280-015-0654-8>

Appenzeller, A. R., & Leggett, W. C. (1992). Bias in hydroacoustic estimates of fish abundance due to acoustic shadowing: evidence from day–night surveys of vertically migrating fish. *Canadian Journal of Fisheries and Aquatic Sciences*, *49*(10), 2179–2189.

URL <https://doi.org/10.1139/f92-240>

Aronica, S., Fontana, I., Giacalone, G., Bosco, G. L., Rizzo, R., Mazzola, S., Basilone, G., Ferreri, R., Genovese, S., Barra, M., et al. (2019). Identifying small pelagic mediterranean fish schools from acoustic and environmental data using optimized artificial neural networks. *Ecological Informatics*, *50*, 149–161.

URL <https://doi.org/10.1016/j.ecoinf.2018.12.007>

Au, W. W., & Benoit-Bird, K. J. (2003). Acoustic backscattering by hawaiian lutjanid snappers. ii. broadband temporal and spectral structure. *The Journal of the*

- Acoustical Society of America*, 114(5), 2767–2774.
URL <https://doi.org/10.1121/1.1614257>
- Bandara, K., Basedow, S. L., Pedersen, G., & Tverberg, V. (2022). Mid-summer vertical behavior of a high-latitude oceanic zooplankton community. *Journal of Marine Systems*, 230, 103733.
URL <https://doi.org/10.1016/j.jmarsys.2022.103733>
- Barham, E. G. (1966). Deep scattering layer migration and composition: observations from a diving saucer. *Science*, 151(3716), 1399–1403.
URL <https://doi.org/10.1126/science.151.3716.1399>
- Basedow, S., McKee, D., Lefering, I., Gislason, A., Daase, M., Trudnowska, E., Ege-land, E., Choquet, M., & Falk-Petersen, S. (2019). Remote sensing of zooplankton swarms. *Scientific Reports*, 9(1), 1–10.
URL <https://doi.org/10.1038/s41598-018-37129-x>
- Basedow, S. L., Edvardsen, A., & Tande, K. S. (2006). Spatial patterns of surface blooms and recruitment dynamics of calanus finmarchicus in the ne norwegian sea. *Journal of plankton research*, 28(12), 1181–1190.
URL <https://doi.org/10.1093/plankt/fbl048>
- Bassett, C., De Robertis, A., & Wilson, C. D. (2018). Broadband echosounder measurements of the frequency response of fishes and euphausiids in the gulf of alaska. *ICES Journal of Marine Science*, 75(3), 1131–1142.
URL <https://doi.org/10.1093/icesjms/fsx204>

- Bassett, C., Lavery, A., & Stanton, T. (2019). Broadband measurements of the acoustic target strength of mesopelagic fishes. *The Journal of the Acoustical Society of America*, *146*(4), 2772–2772.
URL <https://doi.org/10.1121/1.5136601>
- Bassett, C., Lavery, A. C., Stanton, T. K., & Cotter, E. D. (2020). Frequency-and depth-dependent target strength measurements of individual mesopelagic scatterers. *The Journal of the Acoustical Society of America*, *148*(2), EL153–EL158.
URL <https://doi.org/10.1121/10.0001745>
- Battaglia, A., Trenkel, V., & Rochet, M. (2006). Estimating end effects in trawl catches. *ICES Journal of Marine Science*, *63*(5), 956–959.
URL <https://doi.org/10.1016/j.icesjms.2006.03.002>
- Bellec, V., Wilson, M., Bøe, R., Rise, L., Thorsnes, T., Buhl-Mortensen, L., & Buhl-Mortensen, P. (2008). Bottom currents interpreted from iceberg ploughmarks revealed by multibeam data at tromsøflaket, barents sea. *Marine Geology*, *249*(3-4), 257–270.
URL <https://doi.org/10.1016/j.margeo.2007.11.009>
- Bennett, K. P., & Campbell, C. (2000). Support vector machines: hype or hallelujah? *ACM SIGKDD explorations newsletter*, *2*(2), 1–13.
URL <https://doi.org/10.1145/380995.380999>
- Benoit-Bird, K. (2009). The effects of scattering-layer composition, animal size, and numerical density on the frequency response of volume backscatter. *ICES Journal*

of Marine Science, 66(3), 582–593.

URL <https://doi.org/10.1093/icesjms/fsp013>

Benoit-Bird, K., Patrick Welch, T., Waluk, C., Barth, J., Wangen, I., McGill, P., Okuda, C., Hollinger, G., Sato, M., & McCammon, S. (2018). Equipping an underwater glider with a new echosounder to explore ocean ecosystems. *Limnology and Oceanography: Methods*, 16(11), 734–749.

URL <https://doi.org/10.1002/lom3.10278>

Benoit-Bird, K., & Waluk, C. (2020). Exploring the promise of broadband fisheries echosounders for species discrimination with quantitative assessment of data processing effects. *The Journal of the Acoustical Society of America*, 147(1), 411–427.

URL <https://doi.org/10.1121/10.0000594>

Berenboim, B. I., Dolgov, A. V., Korzhev, V. A., & Yaragina, N. A. (2000). The impact of cod on the dynamics of barents sea shrimp (*Pandalus borealis*) as determined by multispecies models. *Journal of Northwest Atlantic Fishery Science*, 27, 69–75.

URL <https://doi.org/10.2960/J.v27.a6>

Berge, J., Daase, M., Renaud, P. E., Ambrose, W. G., Darnis, G., Last, K. S., Leu, E., Cohen, J. H., Johnsen, G., Moline, M. A., et al. (2015a). Unexpected levels of biological activity during the polar night offer new perspectives on a warming arctic. *Current Biology*, 25(19), 2555–2561.

URL <https://doi.org/10.1016/j.cub.2015.08.024>

Berge, J., Geoffroy, M., Daase, M., Cottier, F., Priou, P., Cohen, J., Johnsen, G.,

- McKee, D., Kostakis, I., Renaud, P., & Vogedes, D. (2020). Artificial light during the polar night disrupts arctic fish and zooplankton behaviour down to 200 m depth. *Communications Biology*, 3(1), 1–8.
URL <https://doi.org/10.1038/s42003-020-0807-6>
- Berge, J., Renaud, P. E., Darnis, G., Cottier, F., Last, K., Gabrielsen, T. M., Johnsen, G., Seuthe, L., Weslawski, J. M., Leu, E., et al. (2015b). In the dark: a review of ecosystem processes during the arctic polar night. *Progress in Oceanography*, 139, 258–271.
URL <https://doi.org/10.1016/j.pocean.2015.08.005>
- Beyan, C., & Browman, H. I. (2020). Setting the stage for the machine intelligence era in marine science. *ICES Journal of Marine Science*, 77(4), 1267–1273.
URL <https://doi.org/10.1093/icesjms/fsaa084>
- Blackwell, R. (2020). *Real-time reporting of marine ecosystem metrics from active acoustic sensors*. Ph.D. thesis, University of East Anglia.
URL <https://ueaeprints.uea.ac.uk/id/eprint/79527>
- Blanluet, A., Doray, M., Berger, L., Romagnan, J., Le Bouffant, N., Lehuta, S., & Petitgas, P. (2019). Characterisation of sound scattering layers in the bay of biscay using broadband acoustics, nets and video. *PloS one*, 14(10), e0223618.
URL <https://doi.org/10.1371/journal.pone.0223618>
- Bouchard, C., Geoffroy, M., LeBlanc, M., Majewski, A., Gauthier, S., Walkusz, W., Reist, J. D., & Fortier, L. (2017). Climate warming enhances polar cod recruitment,

- at least transiently. *Progress in Oceanography*, 156, 121–129.
URL <https://doi.org/10.1016/j.pocean.2017.06.008>
- Boyce, D. G., Fuller, S., Karbowski, C., Schleit, K., & Worm, B. (2021). Leading or lagging: How well are climate change considerations being incorporated into canadian fisheries management? *Canadian Journal of Fisheries and Aquatic Sciences*, 78(8), 1120–1129.
URL <https://doi.org/10.1139/cjfas-2020-0394>
- Branch, L. (1867). Consolidated federal laws of canada. *The Constitution Acts*.
URL <https://laws-lois.justice.gc.ca/eng/acts/o-2.4/>
- Branch, M. A., Coleman, T. F., & Li, Y. (1999). A subspace, interior, and conjugate gradient method for large-scale bound-constrained minimisation problems. *SIAM Journal on Scientific Computing*, 21(1), 1–23.
URL <https://doi.org/10.1137/s1064827595289108>
- Brandão, M. C., Benedetti, F., Martini, S., Soviadan, Y. D., Irisson, J.-O., Romagnan, J.-B., Elineau, A., Desnos, C., Jalabert, L., Freire, A. S., et al. (2021). Macroscale patterns of oceanic zooplankton composition and size structure. *Scientific Reports*, 11(1), 15714.
URL <https://doi.org/10.1038/s41598-021-94615-5>
- Brautaset, O., Waldeland, A. U., Johnsen, E., Malde, K., Eikvil, L., Salberg, A., & Handegard, N. O. (2020). Acoustic classification in multifrequency echosounder data using deep convolutional neural networks. *ICES Journal of Marine Science*,

- 77, 1391–1400.
URL <https://doi.org/10.1093/icesjms/fsz235>
- Breiman, L. (2001). Random forests. *Machine Learning*, 45, 5–32.
URL <https://doi.org/10.1023/a:1010933404324>
- Brierley, A. S., Axelsen, B. E., Boyer, D. C., Lynam, C. P., Didcock, C. A., Boyer, H. J., & Sparks, C. A. (2004). Single-target echo detections of jellyfish. *ICES Journal of Marine Science*, 61, 383–393.
URL <https://doi.org/10.1016/j.icesjms.2003.12.008>
- Brierley, A. S., Axelsen, B. E., Buecher, E., Sparks, C. A., Boyer, H., & Gibbons, M. J. (2001). Acoustic observations of jellyfish in the namibian benguela. *Marine Ecology Progress Series*, 210, 55–66.
URL <http://dx.doi.org/10.3354/meps210055>
- Brinton, E. (1967). Vertical migration and avoidance capability of euphausiids in the california current. *Limnology and Oceanography*, 12(3), 451–483.
URL <https://doi.org/10.4319/lo.1967.12.3.0451>
- Briseño-Avena, C., Roberts, P. L., Franks, P. J., & Jaffe, J. S. (2015). Zoops-o2: A broadband echosounder with coordinated stereo optical imaging for observing plankton in situ. *Methods in Oceanography*, 12, 36–54.
URL <https://doi.org/10.1016/j.mio.2015.07.001>
- Brodziak, J., & Link, J. (2002). Ecosystem-based fishery management: what is it and how can we do it? *Bulletin of Marine Science*, 70(2), 589–611.

URL <http://pascal-francis.inist.fr/vibad/index.php?action=getRecordDetail&idt=13880112>

Cabreira, A. G., Tripode, M., & Madirolas, A. (2009). Artificial neural networks for fish-species identification. *ICES Journal of Marine Science*, *66*, 1119–1129.

URL <https://doi.org/10.1093/icesjms/fsp009>

Calise, L., & Skaret, G. (2011). Sensitivity investigation of the sdwba antarctic krill target strength model to fatness, material contrasts and orientation. *Ccamlr Sci*, *18*, 97–122.

Camus, L., Pedersen, G., Falk-Petersen, S., Dunlop, K., Daase, M., Basedow, S., Bandara, K., Tverberg, V., Pederick, J., Peddie, D., & Langeland, T. (2019). Autonomous surface and underwater vehicles reveal new discoveries in the arctic ocean. *OCEANS 2019-Marseille*, (pp. 1–8).

URL <https://doi.org/10.1109/oceanse.2019.8867089>

Cervantes, J., Li, X., Yu, W., & Li, K. (2008). Support vector machine classification for large data sets via minimum enclosing ball clustering. *Neurocomputing*, *71*, 611–619.

URL <https://doi.org/10.1016/j.neucom.2007.07.028>

Chadwick, E., Brodie, W., Colbourne, E., Clark, D., Gascon, D., & Hurlbut, T. (2007). History of annual multi-species trawl surveys on the atlantic coast of canada. *Atlantic Zonal Monitoring Program Bulletin*, *6*, 25–42.

Chawarski, J., Coté, D., & Geoffroy, M. (????). Improved precision in target strength

- and density estimation of mesopelagic fish through detection of anomalous acoustic broadband signals. In preparation. Not peer-reviewed.
- Chen, Y., Chen, L., & Stergiou, K. I. (2003). Impacts of data quantity on fisheries stock assessment. *Aquatic Sciences*, *65*(1), 92–98.
URL <https://doi.org/10.1007/s000270300008>
- Cheng, Y., & Zhang, W. (2018). Concise deep reinforcement learning obstacle avoidance for underactuated unmanned marine vessels. *Neurocomputing*, *272*, 63–73.
URL <https://doi.org/10.1016/j.neucom.2017.06.066>
- Choi, C., Kampffmeyer, M., Handegard, N. O., Salberg, A.-B., Brautaset, O., Eikvil, L., & Jenssen, R. (2021). Semi-supervised target classification in multi-frequency echosounder data. *ICES Journal of Marine Science*, *78*(7), 2615–2627.
URL <https://doi.org/10.1093/icesjms/fsab140>
- Chu, D., & Stanton, T. K. (1998). Application of pulse compression techniques to broadband acoustic scattering by live individual zooplankton. *The Journal of the Acoustical Society of America*, *104*, 39–55.
URL <https://doi.org/10.1121/1.424056>
- Chu, D., & Wiebe, P. (2005). Measurements of sound-speed and density contrasts of zooplankton in antarctic waters. *ICES Journal of Marine Science*, *62*(4), 818–831.
URL <https://doi.org/10.1016/j.icesjms.2004.12.020>
- Chu, D., Wiebe, P., & Copley, N. (2000). Inference of material properties of zooplankton from acoustic and resistivity measurements. *ICES Journal of Marine Science*,

57, 1128–1142.

URL <https://doi.org/10.1006/jmsc.2000.0800>

Chu, D., Wiebe, P., Copley, N., Lawson, G., & Puvanendran, V. (2003). Material properties of north atlantic cod eggs and early-stage larvae and their influence on acoustic scattering. *ICES Journal of Marine Science*, 60(3), 508–515.

URL [https://doi.org/10.1016/s1054-3139\(03\)00047-x](https://doi.org/10.1016/s1054-3139(03)00047-x)

Chu, D., & Ye, Z. (1999). A phase-compensated distorted wave born approximation representation of the bistatic scattering by weakly scattering objects: Application to zooplankton. *The Journal of the Acoustical Society of America*, 106(4), 1732–1743.

URL <https://doi.org/10.1016/j.icesjms.2004.12.020>

Clay, C. S. (1991). Low-resolution acoustic scattering models: Fluid-filled cylinders and fish with swim bladders. *The Journal of the Acoustical Society of America*, 89(5), 2168–2179.

URL <https://doi.org/10.1121/1.400910>

Clay, C. S. (1992). Composite ray-mode approximations for backscattered sound from gas-filled cylinders and swimbladders. *The Journal of the Acoustical Society of America*, 92(4), 2173–2180.

URL <https://doi.org/10.1121/1.405211>

Conti, G., Demer, D. A., & Brierley, A. S. (2005). Broad-bandwidth, sound scattering, and absorption from krill (*meganctiphanes norvegica*), mysids (*praunus flexuosus* and *neomysis integer*), and shrimp (*crangon crangon*). *ICES Journal of Marine*

Science, 62, 956–965.

URL <https://doi.org/10.1016/j.icesjms.2005.01.024>

Cortes, C., & Vapnik, V. (1995). Support-vector networks. *Machine learning*, 20, 273–297.

URL <https://doi.org/10.1007/BF00994018>

Cotter, E., Bassett, C., & Lavery, A. (2021). Classification of broadband target spectra in the mesopelagic using physics-informed machine learning. *The Journal of the Acoustical Society of America*, 149(6), 3889–3901.

URL <https://doi.org/10.1121/10.0005114>

Davison, P., Koslow, J., & Kloser, R. (2015). Acoustic biomass estimation of mesopelagic fish: backscattering from individuals, populations, and communities. *ICES Journal of Marine Science*, 72(5), 1413–1424.

URL <https://doi.org/10.1093/icesjms/fsv023>

De Robertis, A., Lawrence-Slavas, N., Jenkins, R., Wangen, I., Mordy, C., Meinig, C., Levine, M., Peacock, D., & Tabisola, H. (2019). Long-term measurements of fish backscatter from saildrone unmanned surface vehicles and comparison with observations from a noise-reduced research vessel. *ICES Journal of Marine Science*, 76(7), 2459–2470.

URL <https://doi.org/10.1093/icesjms/fsz124>

De Robertis, A., Levine, M., Lauffenburger, N., Honkalehto, T., Ianelli, J., Monnahan, C. C., Towler, R., Jones, D., Stienessen, S., & McKelvey, D. (2021). Uncrewed surface vehicle (usv) survey of walleye pollock, *gadus chalcogrammus*, in response

- to the cancellation of ship-based surveys. *ICES Journal of Marine Science*, 78(8), 2797–2808.
- URL <https://doi.org/10.1093/icesjms/fsab155>
- De Robertis, A., Levine, R., & Wilson, C. D. (2018). Can a bottom-moored echosounder array provide a survey-comparable index of abundance? *Canadian Journal of Fisheries and Aquatic Sciences*, 75(4), 629–640.
- URL <https://doi.org/10.1139/cjfas-2017-0013>
- De Robertis, A., Wilson, C., & Williamson, N. (2012). Do silent ships see more fish? comparison of a noise-reduced and a conventional research vessel in alaska. In *The Effects of Noise on Aquatic Life*, (pp. 331–334). New York, NY: Springer.
- URL https://doi.org/10.1007/978-1-4419-7311-5_74
- D’Elia, M., Patti, B., Bonanno, A., Fontana, I., Giacalone, G., Basilone, G., & Fernandes, P. G. (2014). Analysis of backscatter properties and application of classification procedures for the identification of small pelagic fish species in the central mediterranean. *Fisheries Research*, 149, 33–42.
- URL <https://doi.org/10.1016/j.fishres.2013.08.006>
- Demer, D., Berger, L., Bernasconi, M., Bethke, E., Boswell, K., Chu, D., Domokos, R., Dunford, A., Fassler, S., Gauthier, S., & Hufnagle, L. (2015). Calibration of acoustic instruments.
- URL <https://doi.org/10.23919/oceans40490.2019.8962778>
- Demer, D., & Hewitt, R. (1995). Bias in acoustic biomass estimates of euphausia superba due to diel vertical migration. *Deep Sea Research Part I: Oceanographic*

- Research Papers*, 42(4), 455–475.
URL [https://doi.org/10.1016/0967-0637\(94\)e0005-c](https://doi.org/10.1016/0967-0637(94)e0005-c)
- Demer, D. A., Andersen, L. N., Bassett, C., Berger, L., Chu, D., Condiotty, J., Cutter, G. R., et al. (2017). 2016 usa–norway ek80 workshop report: Evaluation of a wideband echosounder for fisheries and marine ecosystem science. *ICES Cooperative Research Report*, (336), 69.
URL <https://doi.org/10.17895/ices.pub.2318>
- Demer, D. A., & Conti, S. G. (2003). Validation of the stochastic distorted-wave born approximation model with broad bandwidth total target strength measurements of antarctic krill. *ICES Journal of Marine Science*, 60(3), 625–635.
URL [https://doi.org/10.1016/S1054-3139\(03\)00063-8](https://doi.org/10.1016/S1054-3139(03)00063-8)
- Dietz, R. (1948). Deep scattering layer in the pacific and antarctic oceans. *Journal of marine research*, 7(3), 430–442.
- Doney, S. C., Ruckelshaus, M., Emmett Duffy, J., Barry, J. P., Chan, F., English, C. A., Galindo, H. M., Grebmeier, J. M., Hollowed, A. B., Knowlton, N., et al. (2012). Climate change impacts on marine ecosystems. *Annual review of marine science*, 4, 11–37.
URL <https://doi.org/10.1146/annurev-marine-041911-111611>
- Dornan, T., Fielding, S., R.A., S., & Genner, M. (2022). Large mesopelagic fish biomass in the southern ocean resolved by acoustic properties. *Proceedings of the Royal Society B*, 289(1967), 20211781.
URL <https://doi.org/10.1098/rspb.2021.1781>

Dunn, M., McGowan-Yallop, C., Pedersen, G., Falk-Petersen, S., Daase, M., Last, K., Langbehn, T. J., Fielding, S., Brierley, A. S., Cottier, F., et al. (2023). Model-informed classification of broadband acoustic backscatter from zooplankton in an in situ mesocosm. *ICES Journal of Marine Science*.

URL <https://doi.org/10.1093/icesjms/fsad192>

Dunn, M., Pedersen, G., Basedow, S. L., Daase, M., Falk-Petersen, S., Bachelot, L., Camus, L., & Geoffroy, M. (2022). Inverse method applied to autonomous broadband hydroacoustic survey detects higher densities of zooplankton in near-surface aggregations than vessel-based net survey. *Canadian Journal of Fisheries and Aquatic Sciences*.

URL <https://doi.org/10.1139/cjfas-2022-0105>

Dunning, J., Jansen, T., Fenwick, A. J., & Fernandes, P. G. (2023). A new in-situ method to estimate fish target strength reveals high variability in broadband measurements. *Fisheries Research*, *261*, 106611.

URL <https://doi.org/10.1016/j.fishres.2023.106611>

Ehrenberg, J. E., & Torkelson, T. C. (1996). Application of dual-beam and split-beam target tracking in fisheries acoustics. *ICES Journal of Marine Science*, *53*(2), 329–334.

URL <https://doi.org/10.1006/jmsc.1996.0044>

Ehrenberg, J. E., & Torkelson, T. C. (2000). Fm slide (chirp) signals: a technique for significantly improving the signal-to-noise performance in hydroacoustic assessment

- systems. *Fisheries research*, *47*, 193–199.
URL [https://doi.org/10.1016/S0165-7836\(00\)00169-7](https://doi.org/10.1016/S0165-7836(00)00169-7)
- Elizondo, U., & Vogt, M. (2022). Individual-based modeling of shelled pteropods. *Ecological Modelling*, *468*, 109944.
URL <https://doi.org/10.1016/j.ecolmodel.2022.109944>
- Escobar-Flores, P. C., Ladroit, Y., & O’Driscoll, R. L. (2019). Acoustic assessment of the micronekton community on the chatham rise, new zealand, using a semi-automated approach. *Frontiers in Marine Science*, *6*, 1–22.
URL <https://doi.org/10.3389/fmars.2019.00507>
- Falk-Petersen, S., Gatten, R., Sargent, J., & Hopkins, C. (1981). Ecological investigations on the zooplankton community in balsfjorden, northern norway: seasonal changes in the lipid class composition of meganyctiphanes norvegica (m. sars), thysanoessa raschii (m. sars), and t. inermis (krøyer). *Journal of Experimental Marine Biology and Ecology*, *54*(3), 209–224.
URL [https://doi.org/10.1016/0022-0981\(81\)90158-1](https://doi.org/10.1016/0022-0981(81)90158-1)
- Falk-Petersen, S., & Kristensen, . (1985). Acoustic assessment of krill stocks in ullsfjorden, north norway. *Sarsia*, *70*(1), 83–90.
URL <https://doi.org/10.1080/00364827.1985.10420620>
- Fallon, N. G., Fielding, S., & Fernandes, P. G. (2016). Classification of southern ocean krill and icefish echoes using random forests. *ICES Journal of Marine Science*, *73*(8), 1998–2008.
URL <https://doi.org/10.1093/icesjms/fsw057>

- FAO (2003). The ecosystem approach to fisheries. fao technical guidelines for responsible fisheries. *Food and Agriculture Organization of the United Nations Rome*.
- Fernandes, P. G. (2009). Classification trees for species identification of fish-school echotraces. *ICES Journal of Marine Science*, *66*, 1073–1080.
URL <https://doi.org/10.1093/icesjms/fsp060>
- Fernandes, P. G., Copland, P., Garcia, R., Nicosevici, T., & Scoulding, B. (2016). Additional evidence for fisheries acoustics: small cameras and angling gear provide tilt angle distributions and other relevant data for mackerel surveys. *ICES Journal of Marine Science*, *73*(8), 2009–2019.
URL <https://doi.org/10.1093/icesjms/fsw091>
- Fernandino, G., Elliff, C. I., & Silva, I. R. (2018). Ecosystem-based management of coastal zones in face of climate change impacts: Challenges and inequalities. *Journal of environmental management*, *215*, 32–39.
URL <https://doi.org/10.1016/j.jenvman.2018.03.034>
- Fernández-Delgado, M., Cernadas, E., Barro, S., & Amorim, D. (2014). Do we need hundreds of classifiers to solve real world classification problems? *The Journal of Machine Learning Research*, *15*, 3133–3181.
URL <https://dl.acm.org/doi/abs/10.5555/2627435.2697065>
- Feuillade, C., & Nero, R. (1998). A viscous-elastic swimbladder model for describing enhanced-frequency resonance scattering from fish. *The Journal of the Acoustical Society of America*, *103*(6), 3245–3255.
URL <https://doi.org/10.1121/1.423076>

Fix, E., & Hodges Jr., J. (1951). Discriminatory analysis, nonparametric discrimination: Consistency properties. *International Statistical Review*, (4), 261–279.

URL <https://doi.org/10.2307/1403797>

Florko, K. R., Tai, T. C., Cheung, W. W., Ferguson, S. H., Sumaila, U. R., Yurkowski, D. J., & Auger-Méthé, M. (2021). Predicting how climate change threatens the prey base of arctic marine predators. *Ecology Letters*, 24(12), 2563–2575.

URL <https://doi.org/10.1111/ele.13866>

Foote, K. (1983). Linearity of fisheries acoustics, with addition theorems. *The Journal of the Acoustical Society of America*, 73(6), 1932–1940.

URL <https://doi.org/10.1121/1.389583>

Foote, K. G., Everson, I., Watkins, J. L., & Bone, D. G. (1990). Target strengths of antarctic krill (*euphausia superba*) at 38 and 120 khz. *The Journal of the Acoustical Society of America*, 87, 16–24.

URL <https://doi.org/10.1121/1.399282>

Fossheim, M., Primicerio, R., Johannesen, E., Ingvaldsen, R. B., Aschan, M. M., & Dolgov, A. V. (2015). Recent warming leads to a rapid borealization of fish communities in the arctic. *Nature Climate Change*, 5(7), 673–677.

URL <https://doi.org/10.1038/NCLIMATE2647>

Frainer, A., Primicerio, R., Kortsch, S., Aune, M., Dolgov, A. V., Fossheim, M., & Aschan, M. M. (2017). Climate-driven changes in functional biogeography of arctic marine fish communities. *Proceedings of the National Academy of Sciences*, 114(46),

12202–12207.

URL <https://doi.org/10.1073/pnas.1706080114>

Francois, R., & Garrison, G. (1982). Sound absorption based on ocean measurements: Part i: Pure water and magnesium sulfate contributions. *The Journal of the Acoustical Society of America*, *72*(3), 896–907.

Friedman, J. H. (2001). Greedy function approximation: a gradient boosting machine. *Annals of statistics*, *29*, 1189–1232.

URL <https://doi.org/10.1214/aos/1013203451>

Fujita, R. (2021). The assessment and management of data limited fisheries: Future directions. *Marine Policy*, *133*, 104730.

URL <https://doi.org/10.1016/j.marpol.2021.104730>

Garcia, E. G. (2007). The northern shrimp (*Pandalus borealis*) offshore fishery in the northeast atlantic. *Advances in marine biology*, *52*, 147–266.

URL [https://doi.org/10.1016/S0065-2881\(06\)52002-4](https://doi.org/10.1016/S0065-2881(06)52002-4)

Gastauer, S., Chu, D., & Cox, M. (2019). Zooscatr—an r package for modelling the scattering properties of weak scattering targets using the distorted wave born approximation. *The Journal of the Acoustical Society of America*, *145*(1), EL102–EL108.

URL <https://doi.org/10.1121/1.5085655>

Geoffroy, M., Bouchard, C., Flores, H., Robert, D., Gjørseter, H., Hoover, C., Hop, H., Hussey, N. E., Nahrgang, J., Steiner, N., & Bender, M. (2023). The circumpolar impacts of climate change and anthropogenic stressors on arctic cod (*Boreogadus*

- saida) and its ecosystem. *Elementa: Science of the Anthropocene*, 11(1).
URL <https://doi.org/10.1525/elementa.2022.00097>
- Geoffroy, M., Langbehn, T., Priou, P., Varpe, ., Johnsen, G., Le Bris, A., Fisher, J. A., Daase, M., McKee, D., Cohen, J., & Berge, J. (2021). Pelagic organisms avoid white, blue, and red artificial light from scientific instruments. *Scientific Reports*, 11, 14941.
URL <https://doi.org/10.1038/s41598-021-94355-6>
- Geoffroy, M., Majewski, A., LeBlanc, M., Gauthier, S., Walkusz, W., Reist, J. D., & Fortier, L. (2016). Vertical segregation of age-0 and age-1+ polar cod (*Boreogadus saida*) over the annual cycle in the canadian beaufort sea. *Polar Biology*, 39, 1023–1037.
URL <https://doi.org/10.1007/s00300-015-1811-z>
- Geoffroy, M., Robert, D., Darnis, G., & Fortier, L. (2011). The aggregation of polar cod (*boreogadus saida*) in the deep atlantic layer of ice-covered amundsen gulf (beaufort sea) in winter. *Polar Biology*, 34(12), 1959–1971.
URL <https://doi.org/10.1007/s00300-011-1019-9>
- Gjørseter, H., Ingvaldsen, R., & Christiansen, J. (2020). Acoustic scattering layers reveal a faunal connection across the fram strait. *Progress in Oceanography*, 185, 102348.
URL <https://doi.org/10.1016/j.pocean.2020.102348>
- Goldberger, J., Hinton, G. E., Roweis, S., & Salakhutdinov, R. R. (2004). Neighbourhood components analysis. *Advances in neural information processing systems*,

17, 513–520.

URL https://proceedings.neurips.cc/paper_files/paper/2004/file/42fe880812925e520249e808937738d2-Paper.pdf

Goodfellow, I., Bengio, Y., Courville, A., & Bengio, Y. (2016). *Deep Learning*, vol. 1. Cambridge: MIT Press.

Gorska, N., & Ona, E. (2003). Modelling the effect of swimbladder compression on the acoustic backscattering from herring at normal or near-normal dorsal incidences. *ICES Journal of Marine Science*, 60(6), 1381–1391.

URL [https://doi.org/10.1016/S1054-3139\(03\)00142-5](https://doi.org/10.1016/S1054-3139(03)00142-5)

Greene, C. H., Meyer-Gutbrod, E. L., McGarry, L. P., Hufnagle Jr, L. C., Chu, D., McClatchie, S., Packer, A., Jung, J.-B., Acker, T., Dorn, H., et al. (2014). A wave glider approach to fisheries acoustics: transforming how we monitor the nation's commercial fisheries in the 21st century. *Oceanography*, 27(4), 168–174.

URL <https://www.jstor.org/stable/24862221>

Greenlaw, C. (1979). Acoustical estimation of zooplankton populations 1. *Limnology and Oceanography*, 24(2), 226–242.

URL <https://doi.org/10.4319/lo.1979.24.2.0226>

Grimaldo, E., & Larsen, R. B. (2005). The cosmos grid: A new design for reducing bycatch in the nordic shrimp fishery. *Fisheries research*, 76(2), 187–197.

URL <https://doi.org/10.1016/j.fishres.2005.06.010>

Gugele, S. M., Widmer, M., Baer, J., DeWeber, J. T., Balk, H., & Brinker, A. (2021). Differentiation of two swim bladdered fish species using next generation wideband

- hydroacoustics. *Scientific reports*, *11*, 10520.
URL <https://doi.org/10.1038/s41598-021-89941-7>
- Handegard, N., & Tjøstheim, D. (2005). When fish meet a trawling vessel: examining the behaviour of gadoids using a free-floating buoy and acoustic split-beam tracking. *Canadian Journal of Fisheries and Aquatic Sciences*, *62*(10), 2409–2422.
URL <https://doi.org/10.1139/f05-131>
- Handegard, N. O., Eikvil, L., Jenssen, R., Kampffmeyer, M., Salberg, A., & Malde, K. (2021). Machine learning+ marine science: Critical role of partnerships in norway. *Journal of Ocean Technology*, *16*, 1–9.
- Hannah, R. W., & Jones, S. A. (2007). Effectiveness of bycatch reduction devices (brds) in the ocean shrimp (*Pandalus jordani*) trawl fishery. *Fisheries Research*, *85*(1-2), 217–225.
URL <https://doi.org/10.1016/j.fishres.2006.12.010>
- Hastie, T., Tibshirani, R., & Friedman, J. H. (2009). *The elements of statistical learning: data mining, inference, and prediction*. New York: Springer, 2nd ed.
URL <https://doi.org/10.1007/978-0-387-84858-7>
- Hetherington, E., Choy, C., Thuesen, E., & Haddock, S. (2022). Three distinct views of deep pelagic community composition based on complementary sampling approaches. *Frontiers in Marine Science*, *9*.
URL <https://doi.org/10.3389/fmars.2022.864004>
- Hewitt, R. P., & Demer, D. A. (1996). Lateral target strength of antarctic krill. *ICES*

- Journal of Marine Science*, 53, 297–302.
URL <https://doi.org/10.1006/jmsc.1996.0038>
- Hilborn, R., Punt, A. E., & Orensanz, J. (2004). Beyond band-aids in fisheries management: fixing world fisheries. *Bulletin of Marine Science*, 74(3), 493–507.
- Holliday, D. (1977). Extracting bio-physical information from the acoustic signature of marine organisms. (pp. 619–624).
URL <https://cir.nii.ac.jp/crid/1573387450188531456>
- Holliday, D., & Pieper, R. (1995). Bioacoustical oceanography at high frequencies. *ICES Journal of Marine Science*, 52(3-4), 279–296.
URL [https://doi.org/10.1016/1054-3139\(95\)80044-1](https://doi.org/10.1016/1054-3139(95)80044-1)
- Holst, J. C., & McDonald, A. (2000). Fish-lift: a device for sampling live fish with trawls. *Fisheries Research*, 48(1), 87–91.
URL [https://doi.org/10.1016/S0165-7836\(00\)00116-8](https://doi.org/10.1016/S0165-7836(00)00116-8)
- Horne, J. K. (2000). Acoustic approaches to remote species identification: a review. *Fisheries oceanography*, 9(4), 356–371.
URL <https://doi.org/10.1046/j.1365-2419.2000.00143.x>
- Howell, W. H., & Langan, R. (1992). Discarding of commercial groundfish species in the gulf of maine shrimp fishery. *North American Journal of Fisheries Management*, 12(3), 568–580.
URL [https://doi.org/10.1577/1548-8675\(1992\)012<0568:DOCGSI>2.3.CO;2](https://doi.org/10.1577/1548-8675(1992)012<0568:DOCGSI>2.3.CO;2)
- Hurlbert, S. H. (1984). Pseudoreplication and the design of ecological field experi-

- ments. *Ecological monographs*, 54(2), 187–211.
URL <https://doi.org/10.2307/1942661>
- Isaksen, B., Valdemarsen, J. W., Larsen, R. B., & Karlsen, L. (1992). Reduction of fish bycatch in shrimp trawl using a rigid separator grid in the aft belly. *Fisheries Research*, 13(3), 335–352.
URL [https://doi.org/10.1016/0165-7836\(92\)90086-9](https://doi.org/10.1016/0165-7836(92)90086-9)
- Islam, S. R., Eberle, W., Ghafoor, S. K., & Ahmed, M. (2021). Explainable artificial intelligence approaches: A survey. *arXiv*. Preprint: not peer reviewed.
URL <https://doi.org/10.48550/arXiv.2101.09429>
- Jacques, N., Pettersen, H., Cerbule, K., Herrmann, B., Ingólfsson, . A., Sistiaga, M., Larsen, R. B., Brinkhof, J., Grimaldo, E., Brčić, J., & Lilleng, D. (2022). Bycatch reduction in the deep-water shrimp (*Pandalus borealis*) trawl fishery by increasing codend mesh openness. *Canadian Journal of Fisheries and Aquatic Sciences*, 79(2), 331–341.
URL <https://doi.org/10.1016/j.jnc.2021.126001>
- Jech, J., Horne, J., Chu, D., Demer, D., Francis, D., Gorska, N., Jones, B., Lavery, A., Stanton, T., Macaulay, G., & Reeder, D. (2015). Comparisons among ten models of acoustic backscattering used in aquatic ecosystem research. *The Journal of the Acoustical Society of America*, 138(6), 3742–3764.
URL <https://doi.org/10.1121/1.4937607>
- Kanamori, T., Fujiwara, S., & Takeda, A. (2017). Breakdown point of robust support

- vector machines. *Entropy*, 19, 83.
URL <https://doi.org/10.3390/e19020083>
- Kapoor, S., & Narayanan, A. (2022). Leakage and the reproducibility crisis in ml-based science. *arXiv*. Preprint: not peer reviewed.
URL <https://doi.org/10.48550/arXiv.2207.07048>
- Ke, G., Meng, Q., Finley, T., Wang, T., Chen, W., Ma, W., & Ye, Q. (2017). Lightgbm: A highly efficient gradient boosting decision tree. *Advances in neural information processing systems*, 30.
URL https://proceedings.neurips.cc/paper_files/paper/2017/file/6449f44a102fde848669bdd9eb6b76fa-Paper.pdf
- Kebir, Z., Chambers, C., Frainier, A., Hausner, V., Lennert, A. E., Lento, J., Poste, A., Ravolainen, V., Renner, A. H., Thomas, D. N., et al. (2023). Fifteen research needs for understanding climate change impacts on ecosystems and society in the norwegian high north. *Ambio*, (pp. 1–17).
URL <https://doi.org/10.1007/s13280-023-01882-9>
- Khodabandeloo, B., Agersted, M., Klevjer, T., Macaulay, G., & Melle, W. (2021). Estimating target strength and physical characteristics of gas-bearing mesopelagic fish from wideband in situ echoes using a viscous-elastic scattering model. *The Journal of the Acoustical Society of America*, 149(1), 673–691.
URL <https://doi.org/10.1121/10.0003341>
- Kieser, R., & Mulligan, T. (1984). Analysis of echo counting data: a model. *Canadian*

- Journal of Fisheries and Aquatic Sciences*, 41(3), 451–458.
URL <https://doi.org/10.1139/f84-054>
- Knutsen, T., & Foote, K. G. (1997). Experiences in making acoustic measurements in a mesocosm with calanus finmarchius. *ICES C.M.*, (11), 1–19.
- Knutsen, T., Wiebe, P., Gjørseter, H., Ingvaldsen, R., & Lien, G. (2017). High latitude epipelagic and mesopelagic scattering layers—a reference for future arctic ecosystem change. *Frontiers in Marine Science*, 4, 334.
URL <https://doi.org/10.3389/fmars.2017.00334>
- Komer, B., Bergstra, J., & Eliasmith, C. (2014). Hyperopt-sklearn: automatic hyperparameter configuration for scikit-learn. In *ICML workshop on AutoML*, vol. 9, (p. 50).
URL <https://doi.org/10.25080/Majora-14bd3278-006>
- Korneliussen, R. J. (Ed.) (2018). *Acoustic target classification*, vol. 344.
URL <https://digital.csic.es/bitstream/10261/320155/1/24384.pdf>
- Korneliussen, R. J., & Ona, E. (2003). Synthetic echograms generated from the relative frequency response. *ICES Journal of Marine Science*, 60, 636–640.
URL [https://doi.org/10.1016/S1054-3139\(03\)00035-3](https://doi.org/10.1016/S1054-3139(03)00035-3)
- Kotsiantis, S. B., Zaharakis, I., Pintelas, P., et al. (2007). Supervised machine learning: A review of classification techniques. *Emerging artificial intelligence applications in computer engineering*, 160(1), 3–24.
- Kubilius, R., Bergès, B., & Macaulay, G. J. (2023). Remote acoustic sizing of tethered

- fish using broadband acoustics. *Fisheries Research*, 260, 106585.
URL <https://doi.org/10.1016/j.fishres.2022.106585>
- Kubilius, R., Macaulay, G. J., & Ona, E. (2020). Remote sizing of fish-like targets using broadband acoustics. *Fisheries Research*, 228, 105568.
URL <https://doi.org/10.1016/j.fishres.2022.106585>
- Kögeler, J., Falk-Petersen, S., Kristensen, ., Pettersen, F., & Dalen, J. (1987). Density-and sound speed contrasts in sub-arctic zooplankton. *Polar Biology*, 7(4), 231–235.
URL <https://doi.org/10.1007/bf00287419>
- Kędra, M., Renaud, P., & Andrade, H. (2017). Epibenthic diversity and productivity on a heavily trawled barents sea bank (tromsøflaket). *Oceanologia*, 59(2), 93–101.
URL <https://doi.org/10.1016/j.oceano.2016.12.001>
- Lavery, A., Chu, D., & Moum, J. (2010). Measurements of acoustic scattering from zooplankton and oceanic microstructure using a broadband echosounder. *ICES Journal of Marine Science*, 67(2), 379–394.
URL <https://doi.org/10.1093/icesjms/fsp242>
- Lavery, A., Wiebe, P., Stanton, T., Lawson, G., Benfield, M., & Copley, N. (2007). Determining dominant scatterers of sound in mixed zooplankton populations. *The Journal of the Acoustical Society of America*, 122(6), 3304–3326.
URL <https://doi.org/10.1121/1.2793613>
- Lavery, A. C., Bassett, C., Lawson, G. L., & Jech, J. M. (2017). Exploiting signal processing approaches for broadband echosounders. *ICES Journal of Marine Sci-*

- ence*, 74(8), 2262–2275.
URL <https://doi.org/10.1093/icesjms/fsx155>
- Lawson, G. L., Wiebe, P. H., Ashjian, C. J., Chu, D., & Stanton, T. K. (2006). Improved parametrisation of antarctic krill target strength models. *The Journal of the Acoustical Society of America*, 119, 232–242.
URL <https://doi.org/10.1121/1.2141229>
- Lee, W., Staneva, V., Mayorga, E., Nguyen, K., Satiawan, L., & Majeed, I. (2021). Echopype: Enhancing the interoperability and scalability of ocean sonar data processing. *The Journal of the Acoustical Society of America*, 149(4), A63–A63.
URL <https://doi.org/10.1121/10.0004522>
- Legua, J. A., & Lillo, S. D. (2017). Target strength ex situ of sprattus fuegensis in chilean fjords. In *2017 IEEE/OES Acoustics in Underwater Geosciences Symposium (RIO Acoustics)*, (pp. 1–5).
URL <https://doi.org/10.1109/RIOAcoustics.2017.8349735>
- Link, J. S., Bundy, A., Overholtz, W. J., Shackell, N., Manderson, J., Duplisea, D., Hare, J., Koen-Alonso, M., & Friedland, K. D. (2011). Ecosystem-based fisheries management in the northwest atlantic. *Fish and Fisheries*, 12(2), 152–170.
URL <https://doi.org/10.1111/j.1467-2979.2011.00411.x>
- Liu, L., Chen, C., Lin, C., & Yang, Y. (2005). Elasticity of single-crystal aragonite by brillouin spectroscopy. *Physics and Chemistry of Minerals*, 32(2), 97–102.
URL <https://doi.org/10.1007/s00269-005-0454-y>

Lloyd, S. (1982). Least squares quantisation in pcm. *IEEE Transactions on Information Theory*, 28(2), 129–137.

URL <https://doi.org/10.1109/tit.1982.1056489>

Loranger, S., Jech, J. M., & Lavery, A. C. (2022). Broadband acoustic quantification of mixed biological aggregations at the new england shelf break. *The Journal of the Acoustical Society of America*, 152(4), 2319–2335.

URL <https://doi.org/10.1121/10.0014910>

Love, R. (1975). Predictions of volume scattering strengths from biological trawl data. *The Journal of the Acoustical Society of America*, 57(2), 300–306.

URL <https://doi.org/10.1121/1.380460>

Ludvigsen, M., Berge, J., Geoffroy, M., Cohen, J. C., De La Torre, P. R., Nornes, S. M., Singh, H., Sørensen, A. J., Daase, M., & Johnsen, G. (2018). Use of an autonomous surface vehicle reveals small-scale diel vertical migrations of zooplankton and susceptibility to light pollution under low solar irradiance. *Science Advances*, 4, 1–9.

URL <https://doi.org/10.1126/sciadv.aap9887>

Macaulay, G. J., Peña, H., Fässler, S. M., Pedersen, G., & Ona, E. (2013). Accuracy of the kirchhoff-approximation and kirchhoff-ray-mode fish swimbladder acoustic scattering models. *PloS one*, 8(5), e64055.

URL <https://doi.org/10.1371/journal.pone.0064055>

MacAulay, M. C., Wishner, K. F., & Daly, K. L. (1995). Acoustic scattering from zooplankton and micronekton in relation to a whale feeding site near georges bank

- and cape cod. *Continental Shelf Research*, 15(4-5), 509–537.
URL [https://doi.org/10.1016/0278-4343\(94\)00058-U](https://doi.org/10.1016/0278-4343(94)00058-U)
- MacLennan, D., & Menz, A. (1996). Interpretation of in situ target-strength data. *ICES Journal of Marine Science*, 53(2), 233–236.
URL <https://doi.org/10.1006/jmsc.1996.0027>
- MacLennan, D. N., Fernandes, P. G., & Dalen, J. (2002). A consistent approach to definitions and symbols in fisheries acoustics. *ICES Journal of Marine Science*, 59(2), 365–369.
URL <https://doi.org/10.1006/jmsc.2001.1158>
- Malde, K., Handegard, N. O., Eikvil, L., & Salberg, A.-B. (2020). Machine intelligence and the data-driven future of marine science. *ICES Journal of Marine Science*, 77, 1274–1285.
URL <https://doi.org/10.1093/icesjms/fsz057>
- Martin, L. V., Stanton, T. K., Wiebe, P. H., & Lynch, J. F. (1996). Acoustic classification of zooplankton. *ICES Journal of Marine Science*, 53, 217–224.
URL <https://doi.org/10.1006/jmsc.1996.0025>
- McClatchie, S., Thorne, R. E., Grimes, P., & Hanchet, S. (2000). Ground truth and target identification for fisheries acoustics. *Fisheries Research*, 47(2-3), 173–191.
URL [https://doi.org/10.1016/S0165-7836\(00\)00168-5](https://doi.org/10.1016/S0165-7836(00)00168-5)
- McGehee, D. E., O’Driscoll, R. L., & Traykovski, L. M. (1998). Effects of orientation on acoustic scattering from antarctic krill at 120 khz. *Deep Sea Research Part II*:

- Topical Studies in Oceanography*, 45, 1273–1294.
URL [https://doi.org/10.1016/S0967-0645\(98\)00036-8](https://doi.org/10.1016/S0967-0645(98)00036-8)
- Medwin, H., & Clay, C. S. (1998). *Fundamentals of Acoustical Oceanography*. Boston: Academic Press.
URL <https://doi.org/10.1016/B978-0-12-487570-8.50016-7>
- Monger, B. C., Meir, E., Billings, S., Greene, C. H., & Wiebe, P. H. (1998). Sound scattering by the gelatinous zooplankters *aequorea victoria* and *pleurobrachia bachei*. *Deep Sea Research Part II: Topical Studies in Oceanography*, 45, 1255–1271.
URL [https://doi.org/10.1016/S0967-0645\(98\)00029-0](https://doi.org/10.1016/S0967-0645(98)00029-0)
- Montague, P. R. (1999). Reinforcement learning: an introduction, by sutton, rs and barto, ag. *Trends in cognitive sciences*, 3(9), 360.
URL [https://doi.org/10.1016/S1364-6613\(99\)01331-5](https://doi.org/10.1016/S1364-6613(99)01331-5)
- Morato, T., González-Irusta, J. M., Dominguez-Carrió, C., Wei, C., Davies, A., Sweetman, A. K., Taranto, G. H., Beazley, L., García-Alegre, A., Grehan, A., & Laffargue, P. (2020). Climate-induced changes in the suitable habitat of cold-water corals and commercially important deep-sea fishes in the north atlantic. *Global Change Biology*, 26(4), 2181–2202.
URL <https://doi.org/10.1111/gcb.14996>
- Mordy, C., Cokelet, E., De Robertis, A., Jenkins, R., Kuhn, C., Lawrence-Slavas, N., Berchok, C., Crance, J., Sterling, J., Cross, J., & Stabeno, P. (2017). Advances in ecosystem research: Saildrone surveys of oceanography, fish, and marine mammals

- in the bering sea. *Oceanography*, 30(2), 113–115.
URL <https://doi.org/10.5670/oceanog.2017.230>
- Moriarty, M., Sell, A., Trenkel, V., Lynam, C., Burns, F., Clarke, E., Greenstreet, S., & McGonigle, C. (2018). Resolution of biodiversity and assemblage structure in demersal fisheries surveys: the role of tow duration. *ICES Journal of Marine Science*, 75(5), 1672–1681.
URL <https://doi.org/10.1093/icesjms/fsy050>
- Morley, J. W., Selden, R. L., Latour, R. J., Frölicher, T. L., Seagraves, R. J., & Pinsky, M. L. (2018). Projecting shifts in thermal habitat for 686 species on the north american continental shelf. *PloS one*, 13(5), e0196127.
URL <https://doi.org/10.1371/journal.pone.0196127>
- Nguyen, T. T., & Armitage, G. (2008). A survey of techniques for internet traffic classification using machine learning. *IEEE communications surveys & tutorials*, 10(4), 56–76.
URL <https://doi.org/10.1109/SURV.2008.080406>
- Nielsen, J. R., & Lundgren, B. (1999). Hydroacoustic ex situ target strength measurements on juvenile cod (*gadus morhua* l.). *ICES Journal of Marine Science*, 56(5), 627–639.
URL <https://doi.org/10.1006/jmsc.1999.0515>
- Ohman, M., Davis, R., Sherman, J., Grindley, K., Whitmore, B., Nickels, C., & Ellen, J. (2019). Zooglider: an autonomous vehicle for optical and acoustic sensing

- of zooplankton. *Limnology and Oceanography: Methods*, 17(1), 69–86.
URL <https://doi.org/10.1002/lom3.10301>
- Olsen, E., Aanes, S., Mehl, S., Holst, J., Aglen, A., & Gjørseter, H. (2010). Cod, haddock, saithe, herring, and capelin in the barents sea and adjacent waters: a review of the biological value of the area. *ICES Journal of Marine Science*, 67(1), 87–101.
URL <https://doi.org/10.1093/icesjms/fsp229>
- Ona, E., Godø, O. R., Handegard, N. O., Hjellvik, V., Patel, R., & Pedersen, G. (2007). Silent research vessels are not quiet. *The Journal of the Acoustical Society of America*, 121(4), EL145–EL150.
URL <https://doi.org/10.1121/1.2710741>
- Parker-Stetter, S. L. R., Sullivan, L. G., Warner, P. J., & David, M. (2009). Standard operating procedures for fisheries acoustic surveys in the great lakes.
- Pauly, T., & Penrose, J. D. (1998). Laboratory target strength measurements of free-swimming antarctic krill (*euphausia superba*). *The Journal of the Acoustical Society of America*, 103, 3268–3280.
URL <https://doi.org/10.1121/1.423077>
- Pearcy, W., Greenlaw, C., & Pommeranz, T. (1983). Assessment of euphausiids with five nets and a 120-khz echosounder in fjords of northern norway. *Biological Oceanography*, 2(2-4), 151–177.
URL <https://doi.org/10.1080/00364827.1968.10411128>

Pedersen, G., Falk-Petersen, S., Dunlop, K., Camus, L., Daase, M., Basedow, S., Bandara, K., Tverberg, V., Pederick, J., & Peddie, D. (2019). Autonomous surface vehicles for persistent acoustic monitoring of zooplankton in a highly productive shelf area. In *OCEANS 2019-Marseille*, (pp. 1–7). IEEE.

URL <https://doi.org/10.1109/oceanse.2019.8867089>

Pedregosa, F., Varoquaux, G., Gramfort, A., Michel, V., Thirion, B., Grisel, O., Blondel, M., & et al. (2011). Scikit-learn: Machine learning in python. *The Journal of Machine Learning Research*, *12*, 2825–2830.

URL <https://doi.org/10.5555/1953048.2078195>

Pena, H., & Foote, K. G. (2008). Modelling the target strength of trachurus symmetricus murphyi based on high-resolution swimbladder morphometry using an mri scanner. *ICES Journal of Marine Science*, *65*(9), 1751–1761.

URL <https://doi.org/10.1093/icesjms/fsn190>

Pepin, P., King, J., Holt, C., Gurney-Smith, H., Shackell, N., Hedges, K., & Bundy, A. (2020). *Incorporating Climate, Oceanographic and Ecological Change Considerations Into Population Assessments: A Review of Fisheries and Oceans Canada's Science Review Process*. Canadian Science Advisory Secretariat (CSAS).

Peña, M. (2018). Robust clustering methodology for multifrequency acoustic data: A review of standardisation, initialisation and cluster geometry. *Fisheries Research*, *200*, 49–60.

URL <https://doi.org/10.1016/j.fishres.2017.12.013>

Peña, M. (2019). Mesopelagic fish avoidance from the vessel dynamic positioning

- system. *ICES Journal of Marine Science*, 76(3), 734–742.
URL <https://doi.org/10.1093/icesjms/fsy157>
- Ponçon, Y., Mortier, L., Picheral, M., Fitzek, P., Hayes, D., Abdi, E., Zdroik, J., Beszczynska-Möller, A., Coindat, J., Dunn, M., et al. (2023). Bioglider: an integrated glider solution for enhancing environmental knowledge. In *OCEANS 2023 Gulf Coast conference*.
URL <https://hal.science/hal-04177859>
- Priou, P., Nikolopoulos, A., Flores, H., Gradinger, R., Kunisch, E., Katlein, C., Castellani, G., Linders, T., Berge, J., Fisher, J. A., et al. (2021). Dense mesopelagic sound scattering layer and vertical segregation of pelagic organisms at the arctic-atlantic gateway during the midnight sun. *Progress in Oceanography*, 196, 102611.
URL <https://doi.org/10.1016/j.pocean.2021.102611>
- Proud, R., Cox, M., Le Guen, C., & Brierley, A. (2018). Fine-scale depth structure of pelagic communities throughout the global ocean based on acoustic sound scattering layers. *Marine Ecology Progress Series*, 598, 35–48.
URL <https://doi.org/10.3354/meps12612>
- Proud, R., Cox, M., Wotherspoon, S., & Brierley, A. (2015). A method for identifying sound scattering layers and extracting key characteristics. *Methods in Ecology and Evolution*, 6(10), 1190–1198.
URL <https://doi.org/10.1111/2041-210x.12396>
- Proud, R., Mangeni-Sande, R., Kayanda, R. J., Cox, M. J., Nyamweya, C., Ongore, C., Natugonza, V., Everson, I., Elison, M., Hobbs, L., et al. (2020). Automated

- classification of schools of the silver cyprinid *rastrineobola argentea* in lake victoria acoustic survey data using random forests. *ICES Journal of Marine Science*, 77(4), 1379–1390.
- URL <https://doi.org/10.1093/icesjms/fsaa052>
- Reeder, D. B., Jech, J. M., & Stanton, T. K. (2004). Broadband acoustic backscatter and high-resolution morphology of fish: Measurement and modeling. *The Journal of the Acoustical Society of America*, 116(2), 747–761.
- URL <https://doi.org/10.1121/1.1648318>
- Reiss, C., Cossio, A., Walsh, J., Cutter, G., & Watters, G. (2021). Glider-based estimates of meso-zooplankton biomass density: a fisheries case study on antarctic krill (*euphausia superba*) around the northern antarctic peninsula. *Frontiers in Marine Science*, 8, 256.
- URL <https://doi.org/10.3389/fmars.2021.604043>
- Roa, C., Pedersen, G., Bollinger, M., Taylor, C., & Boswell, K. M. (2022). Taxonomical classification of reef fish with broadband backscattering models and machine learning approaches. *The Journal of the Acoustical Society of America*, 152(2), 1020–1034.
- URL <https://doi.org/10.1121/10.0012192>
- Roberts, P. L., Jaffe, J. S., & Trivedi, M. M. (2011). Multiview, broadband acoustic classification of marine fish: a machine learning framework and comparative analysis. *IEEE Journal of Oceanic Engineering*, 36, 90–.
- URL <https://doi.org/10.1109/JOE.2010.2101235>

Rogers, A. D. (2015). Environmental change in the deep ocean. *Annual Review of Environment and Resources*, 40(1), 1–38.

URL <https://doi.org/10.1146/annurev-environ-102014-021415>

Ross, T., Keister, J. E., & Lara-Lopez, A. (2013). On the use of high-frequency broadband sonar to classify biological scattering layers from a cabled observatory in saanich inlet, british columbia. *Methods in Oceanography*, 5, 19–38.

URL <https://doi.org/10.1016/j.mio.2013.05.001>

Sakinan, S., Lawson, G. L., Wiebe, P. H., Chu, D., & Copley, N. J. (2019). Accounting for seasonal and composition-related variability in acoustic material properties in estimating copepod and krill target strength. *Limnology and Oceanography: Methods*, 17(11), 607–625.

URL <https://doi.org/10.1002/lom3.10336>

Santana Hernández, N. (2019). *A patch of Calanus finmarchicus in the Lofoten-Vesterålen Region. Characteristics and determining factors*. Master's thesis, UiT Norges arktiske universitet.

Scalabrin, C., Marfia, C., & Boucher, J. (2009). How much fish is hidden in the surface and bottom acoustic blind zones? *ICES Journal of Marine Science*, 66(6), 1355–1363.

URL <https://doi.org/10.1093/icesjms/fsp136>

Simmonds, E. J., Armstrong, F., & Copland, P. J. (1996). Species identification using wideband backscatter with neural network and discriminant analysis. *ICES*

Journal of Marine Science, 53, 189–195.

URL <https://doi.org/10.1006/jmsc.1996.0021>

Simmonds, J., & MacLennan, D. (2008). *Fisheries acoustics: theory and practice*. John Wiley & Sons.

URL <https://doi.org/10.1002/9780470995303>

Skaret, G., Johansen, G. O., Johnsen, E., Fall, J., Fiksen, Ø., Englund, G., Fauchald, P., Gjørseter, H., Macaulay, G. J., & Johannesen, E. (2020). Diel vertical movements determine spatial interactions between cod, pelagic fish and krill on an arctic shelf bank. *Marine Ecology Progress Series*, 638, 13–23.

URL <https://doi.org/10.3354/meps13254>

Skern-Mauritzen, M., Ottersen, G., Handegard, N. O., Huse, G., Dingsør, G. E., Stenseth, N. C., & Kjesbu, O. S. (2016). Ecosystem processes are rarely included in tactical fisheries management. *Fish and Fisheries*, 17(1), 165–175.

URL <https://doi.org/10.1111/faf.12111>

Skjoldal, H., Wiebe, P., Postel, L., Knutsen, T., Kaartvedt, S., & Sameoto, D. (2013). Intercomparison of zooplankton (net) sampling systems: Results from the ices/globec sea-going workshop. *Progress in Oceanography*, 108, 1–42.

URL <https://doi.org/10.1016/j.pocean.2012.10.006>

Smith, J. N., Ressler, P. H., & Warren, J. D. (2010). Material properties of euphausiids and other zooplankton from the bering sea. *The Journal of the Acoustical Society of America*, 128(5), 2664–2680.

URL <https://doi.org/10.1121/1.3488673>

- Sobradillo, B., Boyra, G., Martinez, U., Carrera, P., Peña, M., & Irigoien, X. (2019). Target strength and swimbladder morphology of mueller's pearlside (*maurolicus muelleri*). *Scientific Reports*, *9*, 1–14.
URL <https://doi.org/10.1038/s41598-019-53819-6>
- Solvang, H., Haug, T., Knutsen, T., Gjørseter, H., Bogstad, B., Hartvedt, S., Øien, N., & Lindstrøm, U. (2021). Distribution of rorquals and atlantic cod in relation to their prey in the norwegian high arctic. *Polar Biology*, *44*(4), 761–782.
URL <https://doi.org/10.1007/s00300-021-02835-2>
- Soule, M., Barange, M., Solli, H., & Hampton, I. (1997). Performance of a new phase algorithm for discriminating between single and overlapping echoes in a split-beam echosounder. *ICES Journal of Marine Science*, *54*, 934–938.
URL <https://doi.org/10.1006/jmsc.1997.0270>
- Stanton, T., Chu, D., Wiebe, P., Eastwood, R., & Warren, J. (2000). Acoustic scattering by benthic and planktonic shelled animals. *The Journal of the Acoustical Society of America*, *108*(2), 535–550.
URL <https://doi.org/10.1121/1.429584>
- Stanton, T. K., & Chu, D. (2000). Review and recommendations for the modelling of acoustic scattering by fluid-like elongated zooplankton: Euphausiids and copepods. *ICES Journal of Marine Science*, *57*, 793–807.
URL <https://doi.org/10.1006/jmsc.1999.0517>
- Stanton, T. K., Chu, D., & Wiebe, P. H. (1996). Acoustic scattering characteristics

- of several zooplankton groups. *ICES Journal of Marine Science*, 53, 289–295.
URL <https://doi.org/10.1006/jmsc.1996.0037>
- Stanton, T. K., Chu, D., Wiebe, P. H., & Clay, C. S. (1993). Average echoes from randomly oriented random-length finite cylinders: Zooplankton models. *The Journal of the Acoustical Society of America*, 94(6), 3463–3472.
URL <https://doi.org/10.1121/1.407200>
- Stanton, T. K., Chu, D., Wiebe, P. H., Martin, L. V., & Eastwood, R. L. (1998). Sound scattering by several zooplankton groups. i. experimental determination of dominant scattering mechanisms. *The Journal of the Acoustical Society of America*, 103, 225–235.
URL <https://doi.org/10.1121/1.421469>
- Stanton, T. K., Wiebe, P. H., Chu, D., Benfield, M. C., Scanlon, L., Martin, L., & Eastwood, R. L. (1994). On acoustic estimates of zooplankton biomass. *ICES Journal of Marine Science*, 51(4), 505–512.
URL <https://doi.org/10.1006/jmsc.1994.1051>
- Steele, M., Ermold, W., & Zhang, J. (2008). Arctic ocean surface warming trends over the past 100 years. *Geophysical Research Letters*, 35(2).
URL <https://doi.org/10.1029/2007GL031651>
- Stevens, J. R., Jech, J. M., Zydlewski, G. B., & Brady, D. C. (2021). Estimating target strength of estuarine pelagic fish assemblages using fisheries survey data. *The Journal of the Acoustical Society of America*, 150(4), 2553–2565.
URL <https://doi.org/10.1121/10.0006449>

- Stone, M. (1974). Cross-validators choice and assessment of statistical predictions. *Journal of the Royal Statistical Society: Series B (Methodological)*, *36*, 111–133.
URL <https://doi.org/10.1111/j.2517-6161.1974.tb00994.x>
- Stroeve, J. C., Serreze, M. C., Holland, M. M., Kay, J. E., Malanik, J., & Barrett, A. P. (2012). The arctic's rapidly shrinking sea ice cover: a research synthesis. *Climatic change*, *110*, 1005–1027.
URL <https://doi.org/10.1007/s10584-011-0101-1>
- Tam, J. C., Link, J. S., Rossberg, A. G., Rogers, S. I., Levin, P. S., Rochet, M.-J., Bundy, A., Belgrano, A., Libralato, S., Tomczak, M., et al. (2017). Towards ecosystem-based management: identifying operational food-web indicators for marine ecosystems. *ICES Journal of Marine Science*, *74*(7), 2040–2052.
URL <https://doi.org/10.1093/icesjms/fsw230>
- Theodoridis, S., & Koutroumbas, K. (2006). *Pattern recognition*. Elsevier.
- Toresen, R., Gjørseter, H., & de Barros, P. (1998). The acoustic method as used in the abundance estimation of capelin (*mallopus villosus müller*) and herring (*clupea harengus linné*) in the barents sea. *Fisheries Research*, *34*(1), 27–37.
URL [https://doi.org/10.1016/S0165-7836\(97\)00077-5](https://doi.org/10.1016/S0165-7836(97)00077-5)
- Trenkel, V. M., Berger, L., Bourguignon, S., Doray, M., Fablet, R., Massé, J., Mazauric, V., Poncelet, C., Quemener, G., Scalabrin, C., et al. (2009). Overview of recent progress in fisheries acoustics made by ifremer with examples from the bay of biscay. *Aquatic Living Resources*, *22*(4), 433–445.
URL <https://doi.org/10.1051/alr/2009027>

- Trenkel, V. M., Ressler, P. H., Jech, M., Giannoulaki, M., & Taylor, C. (2011). Underwater acoustics for ecosystem-based management: state of the science and proposals for ecosystem indicators. *Marine Ecology Progress Series*, *442*, 285–301.
URL <https://doi.org/10.3354/meps09425>
- Trenkel, V. M., Vaz, S., Albouy, C., Amour, A. B., Duhamel, E., Laffargue, P., Romagnan, J. B., Simon, J., & Lorange, P. (2019). We can reduce the impact of scientific trawling on marine ecosystems. *Marine Ecology Progress Series*, *609*, 277–282.
URL <https://doi.org/10.3354/meps12834>
- Trevorrow, M., Mackas, D., & Benfield, M. (2005). Comparison of multifrequency acoustic and in situ measurements of zooplankton abundances in knight inlet, british columbia. *The Journal of the Acoustical Society of America*, *117*(6), 3574–3588.
URL <https://doi.org/10.1121/1.1920087>
- Trudnowska, E., Gluchowska, M., Beszczynska-Möller, A., Blachowiak-Samolyk, K., & Kwasniewski, S. (2016). Plankton patchiness in the polar front region of the west spitsbergen shelf. *Marine Ecology Progress Series*, *560*, 1–18.
URL <https://doi.org/10.3354/meps11925>
- Urick, R. J. (1983). Principles of underwater sound. *Peninsula Pub.*
- Urmy, S. S., De Robertis, A., & Bassett, C. (2023). A Bayesian inverse approach to identify and quantify organisms from fisheries acoustic data. *ICES Journal of*

Marine Science, (p. fsad102).

URL <https://doi.org/10.1093/icesjms/fsad102>

van Denderen, P. D., van Kooten, T., & Rijnsdorp, A. D. (2013). When does fishing lead to more fish? community consequences of bottom trawl fisheries in demersal food webs. *Proceedings of the Royal Society B: Biological Sciences*, 280(1769), 20131883.

URL <https://doi.org/10.1098/rspb.2013.1883>

Varma, S., & Simon, R. (2006). Bias in error estimation when using cross-validation for model selection. *BMC Bioinformatics*, 7(91), 1–8.

URL <https://doi.org/10.1186/1471-2105-7-91>

Verfuss, U., Aniceto, A., Harris, D., Gillespie, D., Fielding, S., Jiménez, G., Johnston, P., Sinclair, R., Sivertsen, A., Solbø, S., & Storvold, R. (2019). A review of unmanned vehicles for the detection and monitoring of marine fauna. *Marine Pollution Bulletin*, 140, 17–29.

URL <https://doi.org/10.1016/j.marpolbul.2019.01.009>

Wainer, J., & Cawley, G. (2021). Nested cross-validation when selecting classifiers is overzealous for most practical applications. *Expert Systems with Applications*, 182, 115222.

URL <https://doi.org/10.1016/j.eswa.2021.115222>

Walkusz, W., Atchison, S., Hedges, K., & Deslauriers, D. (2020). Assessment of potential impacts of bycatch mortality on the arctic cod (*Boreogadus saida*) populations from the northern (pandalus borealis) and striped (*Pandalus montagui*)

- shrimp fisheries in shrimp fishing areas 1, 2, and 3. Tech. rep., Canadian Science Advisory Secretariat (CSAS).
- Wang, Q., Wekerle, C., Wang, X., Danilov, S., Koldunov, N., Sein, D., Sidorenko, D., von Appen, W.-J., & Jung, T. (2020). Intensification of the atlantic water supply to the arctic ocean through fram strait induced by arctic sea ice decline. *Geophysical Research Letters*, *47*(3), e2019GL086682.
URL <https://doi.org/10.1029/2019GL086682>
- Warren, J. D., Stanton, T. K., Wiebe, P. H., & Seim, H. E. (2003). Inference of biological and physical parameters in an internal wave using multiple-frequency, acoustic-scattering data. *ICES Journal of Marine Science*, *60*(5), 1033–1046.
URL [https://doi.org/10.1016/S1054-3139\(03\)00121-8](https://doi.org/10.1016/S1054-3139(03)00121-8)
- Whitmore, B., Nickels, C., & Ohman, M. (2019). A comparison between zooglider and shipboard net and acoustic mesozooplankton sensing systems. *Journal of Plankton Research*, *41*(4), 521–533.
URL <https://doi.org/10.1093/plankt/fbz033>
- Wiebe, P., Boyd, S., Davis, B., & Cox, J. (1982). Avoidance of towed nets by the euphausiid *nematoscelis megalops* [fish behavior]. *Fishery Bulletin-United States, National Marine Fisheries Service*.
- Wiebe, P. H., Chu, D., Kaartvedt, S., Hundt, A., Melle, W., Ona, E., & Batta-Lona, P. (2010). The acoustic properties of *Salpa thompsoni*. *ICES Journal of Marine Science*, *67*, 583–593.
URL <https://doi.org/10.1093/icesjms/fsp263>

Wilson, C. (2011). The rocky road from research to operations for satellite ocean-colour data in fishery management. *ICES Journal of Marine Science*, 68(4), 677–686.

URL <https://doi.org/10.1093/icesjms/fsq168>

Yassir, A., Andaloussi, S. J., Ouchetto, O., Mamza, K., & Serghini, M. (2023). Acoustic fish species identification using deep learning and machine learning algorithms: A systematic review. *Fisheries Research*, 266, 106790.

URL <https://doi.org/10.1016/j.fishres.2023.106790>

Zhang, J., Zhang, K., Chen, Z., Dong, J., & Qiu, Y. (2021). Hydroacoustic studies on *Katsuwonus pelamis* and juvenile *Thunnus albacares* associated with light fish-aggregating devices in the south china sea. *Fisheries Research*, 233, 105765.

URL <https://doi.org/10.1016/j.fishres.2020.105765>

Zhao, S., Zhang, S., Liu, J., Wang, H., Zhu, J., Li, D., & Zhao, R. (2021). Application of machine learning in intelligent fish aquaculture: A review. *Aquaculture*, 540, 736724.

URL <https://doi.org/10.1016/j.aquaculture.2021.736724>

Appendix A

Supplementary Materials 1

Supplementary Materials for:

**Inverse method applied to autonomous broadband hydroacoustic survey
detects higher densities of zooplankton in near-surface aggregations than
vessel-based net survey**

Muriel Dunn^{1,2*}, Geir Pedersen³, Sünnje L. Basedow⁴, Malin Daase⁴, Stig Falk-Petersen¹, Loïc Bachelot⁵, Lionel Camus¹, and Maxime Geoffroy^{2,4}

¹Akvaplan-niva AS, Fram Centre, Postbox 6606, Stakkevollan, 9296 Tromsø, Norway

² Center for Fisheries Ecosystems Research, Fisheries and Marine Institute of Memorial University of Newfoundland and Labrador, St. John's, NL, A1C 5R3, Canada

³ Institute for Marine Research, 5005 Bergen, Norway

⁴ Department of Arctic and Marine Biology, UiT The Arctic University of Norway, 9019 Tromsø, Norway

⁵ IFREMER, Laboratoire d'Océanographie Physique et Spatiale, 29280 Plouzané, France

*Corresponding author (email: mbd@akvaplan.niva.no)

Table S1: Density values in individuals per m³ from MultiNet tows throughout the study region. Values combined using a weighted average over depth for a single value of density for each stations for each species in the upper 100 m. The species are colour coded by taxonomic group (Copepods in purple; Euphausiids in red; Amphipods in green; Gelatinous in pink; Fish larvae in blue; Pteropods in orange; and Others in white).

Collection/Net type	MPS180	MPS180	MPS180	MPS180	MPS	MPS	MPS	MPS	MPS180							
Date	21.06.2018	21.06.2019	21.06.2020	21.06.2018	22.06.2018	22.06.2018	22.06.2018	22.06.2018	22.06.2018	22.06.2018	22.06.2018	22.06.2018	22.06.2018	22.06.2018	22.06.2018	22.06.2018
Area/Station name	7	7	7	7	8	8	8	8	8	9	9	9	9	10	10	10
Layer [m]	5-0	10-5	10-30	30-100	100-30	30-10	10-5	5-0	100-30	30-10	10-5	5-0	100-30	30-10	10-5	5-0
Calanus finmarchicus AM					0.95	5.00			0.63	5.00			1.48	0.57	7.62	6.66
C. finmarchicus AF	64.00	19.20	38.40	117.03	33.33	45.00	64.00	12.00	5.71	115.00	28.57	22.22	2.29	205.71	300.00	
C. finmarchicus CV	1280.00	524.80	3046.40	431.54	375.24	1160.00	1708.00	796.00	148.57	770.00	777.14	711.11	51.43	6811.43	6200.00	
C. finmarchicus CIV	102.40	22.40	38.40	138.97	20.95	70.00	68.00	8.00	49.52	25.00	22.86	35.55	6.29	114.29	100.00	
C. finmarchicus CIII		3.20	12.80	14.63	5.71	1.25			7.62	1.67		1.48	0.19	7.62		
C. finmarchicus CII			0.00	7.31	3.81	1.25	4.00	4.00	1.90	1.67		1.48	0.19			
C. finmarchicus CI					1.90		12.00		0.63	1.67		1.48	0.57	3.81		
C. hyperboreus CV						2.50	4.00		0.63	5.00		8.89	0.19	7.62	6.66	
C. hyperboreus CIV					0.95	1.25			3.81	5.71		8.89	0.57	7.62		
C. hyperboreus CIII																
Microcalanus spp.	230.40	28.80	25.60	343.77	32.38	5.00	32.00	8.00	17.14	10.00	11.43	48.89	32.00	22.86	6.66	
Pseudocalanus spp. AM	76.80	6.40	0.00	131.66	0.95				0.63				0.19			
Pseudocalanus spp. AF					7.62	1.25	2.00		11.43	1.67			2.29	7.62	6.66	
Pseudocalanus spp. CV					24.76	15.00	16.00		3.81	5.00	1.90	4.44	2.29	7.62	6.66	
Pseudocalanus spp. CIV					26.67				5.71	5.00		4.40	4.57	22.86	6.66	
Pseudocalanus spp. CI-CIII					20.95	1.25	4.00		1.90	10.00		4.44	0.19	68.57	6.66	
Metridia longa AM																
M. longa AF	38.40	6.40		36.57					0.63	1.67	5.71				6.66	
M. longa CV	25.60			58.51	0.95				0.63	5.00	1.90	4.44	0.19		6.66	
M. longa CIV				36.57					1.90	5.00		1.48	0.57			
M. longa CIII					1.90											
M. longa CII					3.81											
M. longa CI		3.20			3.81											
Paraeuchaeta norvegica AF																
Paraeuchaeta spp. CV														0.06		0.80
Paraeuchaeta spp. CIV														0.19		
Paraeuchaeta spp. CIII									0.63					0.19		
Paraeuchaeta spp. CII									0.63							
Paraeuchaeta spp. CI																
Acartia spp.																
Chiridius obtusifrons	12.80															
Heterorhabdus norvegicus	12.80															
Metridia lucens AM					2.86	3.33			1.90	1.67	1.90	8.89	1.14		6.66	
Metridia lucens AF					5.71	3.33	4.00		3.81			4.44	14.86	7.62	6.66	
M. lucens CI-CV					25.71	3.33	8.00	4.00	7.62	1.67		1.48	10.29		6.66	
Anomalocera patersoni												0.20				
Scaphocalanus magnus		3.20														
Scolecithricella minor									0.63							
Temora longicornis																
Microsetella norvegica												1.9				
Harpacticoida indet.								8.0								
Oithona atlantica	12.80				60.95	65.00	16.00	4.00	15.24	1.67	5.71	8.89	25.71		6.66	
Oithona similis	1049.60	185.60	345.60	1367.77	1603.81	1465.00	1072.00	316.00	647.62	460.00	771.43	680.00	195.24	388.57	300.00	
Oncaea spp.																
Triconia (=Oncaea) borealis		9.60		21.94	3.81	2.50			3.81	1.67		4.44	3.43	3.81	6.66	
Copepoda nauplii		19.20		7.31	1.90	5.00	16.00	12.00	7.62	1.67	11.43	4.44	1.14	7.62	40.00	
Ostracoda										1.67						
Cirripedia nauplii						10.00	112.00	28.00		5.00	1.90					

Collection/Net type	MPS180	MPS180	MPS180	MPS180	MPS	MPS	MPS	MPS	MPS180							
Date	21.06.2018	21.06.2019	21.06.2020	21.06.2018	22.06.2018	22.06.2018	22.06.2018	22.06.2018	22.06.2018	22.06.2018	22.06.2018	22.06.2018	22.06.2018	22.06.2018	22.06.2018	
Area/Station name	7	7	7	7	8	8	8	8	9	9	9	9	10	10	10	
Layer [m]	5-0	10-5	10-30	30-100	100-30	30-10	10-5	5-0	100-30	30-10	10-5	5-0	100-30	30-10	10-5	
Cirripedia cypris																
Cirripedia Facetotecta nauplii																
Themisto abyssorum			12.80		0.74		1.60		0.75	2.87	0.00	0.80	0.06	4.61	6.66	
Themisto libellula									0.06							
Themisto spp. <1mm																
Isopoda Bopyridae									0.63	1.67			0.19	7.62	6.66	
Isopoda indet.																
Thysanoessa inermis					0.6	0.4										
Thysanoessa longicaudata																
Thysanoessa raschii					1.5	0.2										
Euphausiacea nauplii					1.9											
Euphausiacea calyptopis					0.5					1.67			0.19			
Euphausiacea furcilia	25.60		51.20	21.94	1.43	2.20	1.60		7.66	6.07	5.71	0.80	1.71	9.22	6.66	
Eupagurus zoea																
Eupagurus megalopa																
Decapoda indet. larvae					1.26	1.20	0.80		0.29	1.40		2.40	0.17	1.80	0.80	
Aglantha digitale	51.20	32.00			2.86	5.00	28.00	28.00		5.00	29.37	8.89	0.19	7.62	6.66	
Hydrozoa medusae indet.																
Hydrozoa larvae																
Dimophyes arctica																
Ctenophora larvae																
Nemertea pilidium																
Clione limacina veliger						2.50										
Limacina helicina veliger					0.95	15.00	32.00	20.00		1.67						
Limacina retroversa	25.60		102.40	7.31	3.33	1.25	68.00	9.60	13.33	25.00	5.71	4.44	1.14	22.86	20.00	
Gastropoda veliger									0.63	1.67	5.71	4.44	0.57			
Bivalvia veliger					0.95	2.50	32.00	4.00	0.63	5.00	1.90			7.62		
Polychaeta larvae																
Polychaeta larvae mitraria																
Polychaeta secondary larvae									5.71					3.81		
Echinodermata larvae		12.80		7.31							1.90		0.57			
Bryozoa larvae					1.90		24.00	8.00	1.90	10.00		4.44		7.62	20.00	
Eukrohnia hamata	12.80			21.94	0.34	0.20			1.20		0.80	0.80	0.91	4.01	2.40	
Sagitta elegans				0.00	0.17	0.60			0.34	5.00			0.69			
Fritillaria borealis	25.60			0.00							1.90					
Oikopleura spp.				7.31	2.86	6.67	4.00	0.00	11.49	1.67	1.90	8.89	5.14	22.86		
Appendicularia larvae																
Pisces larvae					0.06	0.40		0.80		0.80		0.80		0.20		
Paracalanus spp.														3.81		

Collection/Net type	MPS180	WP2	WP2	WP2	MPS	MPS	MPS									
Date	22.06.2018	23.06.2018	23.06.2018	23.06.2018	23.06.2018	23.06.2018	23.06.2018	23.06.2018	23.06.2018	23.06.2018	24.06.2018	24.06.2018	24.06.2018	24.06.2018	24.06.2018	24.06.2018
Area/Station name	10	11	11	11	11	12	12	12	12	12	13	13	13	14	14	14
Layer [m]	5-0	100-30	30-10	10-5	5-0	100-30	30-10	10-5	5-0	100-30	30-10	10-0	100-30	30-10	30-10	10-5
Calanus finmarchicus AM	6.66	1.90	16.00			8.00	1.43	1.11	3.34	5.28	11.43					1.90
C. finmarchicus AF	240.00	38.10	96.00	20.00	40.00	43.57	30.00	90.00	144.00	74.29	68.57	230.00	11.43	76.00	208.00	
C. finmarchicus CV	5973.34	339.05	4464.00	672.00	1440.00	21.43	366.67	2310.00	3408.00	491.43	4068.57	3445.00	76.19	680.00	2320.00	
C. finmarchicus CIV	120.00	13.33	64.00	28.00	24.00	7.86	13.33	60.00	48.00	17.14	51.43	35.00	43.81	32.00	104.00	
C. finmarchicus CIII					2.66	1.43	13.33	10.00	16.00	2.86		4.00	11.43	6.00	8.00	
C. finmarchicus CII	6.66					2.14	6.67	3.34	16.00	3.81			2.86	4.00	8.00	
C. finmarchicus CI	6.66						3.33	3.34	16.00	0.95			1.90	4.00	8.00	
C. hyperboreus CV																
C. hyperboreus CIV		0.63				0.71	3.33		5.34	0.29				0.11		
C. hyperboreus CIII	20.00	3.81	2.67	8.00	2.66	1.90	1.11			0.57				0.11		
Microcalanus spp.	20.00	43.81	5.33	28.00	48.00	15.24	3.33	50.00	16.00	240.00			17.14	12.00	4.00	
Pseudocalanus spp. AM						0.24										
Pseudocalanus spp. AF	6.66	0.63			2.66	3.81	3.33		5.34	8.57		0.80	1.90		4.00	
Pseudocalanus spp. CV	6.66	11.43	5.33		2.66	45.71	23.33	3.34	32.00	91.43		0.80	30.48	32.00	16.00	
Pseudocalanus spp. CIV	20.00	7.62			16.00	32.38	20.00	10.00	32.00	34.29			13.33			
Pseudocalanus spp. CI-CIII		1.90			2.66	17.14	23.33	3.34	16.00	45.71			15.24	12.00		
Metridia longa AM				1.34												
M. longa AF	6.66				2.66											
M. longa CV	6.66	0.63		1.34	2.66			3.34								
M. longa CIV	6.66	0.63	2.67							5.71						
M. longa CIII										5.71						
M. longa CII										2.86				1.90		
M. longa CI										2.86				3.81		
Paraeuchaeta norvegica AF																4.00
Paraeuchaeta spp. CV		0.40				0.06										
Paraeuchaeta spp. CIV		0.63				0.24		10.00								
Paraeuchaeta spp. CIII						0.71			5.34							
Paraeuchaeta spp. CII						0.24										
Paraeuchaeta spp. CI																
Acartia spp.								3.34								8.00
Chiridius obtusifrons																
Heterorhabdus norvegicus																
Metridia lucens AM	6.66					2.86	1.11			2.86				1.90		
Metridia lucens AF	20.00	1.90	2.67		2.66	7.14	3.33	3.34	5.34	2.86				1.90		
M. lucens CI-CV	20.00	3.81		4.00	16.00	12.86	1.11		16.00	24.76				6.67	0.40	
Anomalocera patersoni																
Scaphocalanus magnus																
Scolecithricella minor	20.00	0.63														
Temora longicornis																
Microsetella norvegica																
Harpacticoida indet.										5.34						
Oithona atlantica	6.66	11.43	5.33		16.00	34.29	33.33	3.34	16.00	68.57				76.19	4.00	
Oithona similis	220.00	451.43	32.00	492.00	480.00	394.29	1390.00	490.00	1056.00	2202.86	200.00	12.00	1676.19	488.00	224.00	
Oncaea spp.						2.66			3.34							
Triconia (=Oncaea) borealis	6.66	0.63			2.66	3.81	1.11		5.34	22.86				5.71	4.00	
Copepoda nauplii	20.00	1.90		4.00	2.66	13.33	23.33	30.00	64.00	17.14			2.00	1.90	4.00	4.00
Ostracoda		0.63		1.34		0.24										
Cirripedia nauplii													6.00			56.00

Collection/Net type	MPS180	WP2	WP2	WP2	MPS	MPS	MPS									
Date	22.06.2018	23.06.2018	23.06.2018	23.06.2018	23.06.2018	23.06.2018	23.06.2018	23.06.2018	23.06.2018	23.06.2018	24.06.2018	24.06.2018	24.06.2018	24.06.2018	24.06.2018	24.06.2018
Area/Station name	10	11	11	11	11	12	12	12	12	12	13	13	13	14	14	14
Layer [m]	5-0	100-30	30-10	10-5	5-0	100-30	30-10	10-5	5-0	100-30	30-10	10-0	100-30	30-10	10-5	
<i>Cirripedia cypris</i>													0.23			
<i>Cirripedia Facetotecta nauplii</i>						0.69	3.33									
<i>Themisto abyssorum</i>	9.86	1.38	0.40	1.34	3.46	3.37	1.11	3.34	0.00	0.51	2.40	0.00	0.57	1.40	0.80	
<i>Themisto libellula</i>																
<i>Themisto</i> spp. <1mm																
Isopoda Bopyridae		1.90			8.00	0.24	1.11									
Isopoda indet.						0.24										
<i>Thysanoessa inermis</i>			0.20								0.57					
<i>Thysanoessa longicaudata</i>						0.17					0.11					
<i>Thysanoessa raschii</i>						0.40							0.51	0.80		
Euphausiacea nauplii																
Euphausiacea calyptopis		0.63				0.24		3.34			0.95			0.48		
Euphausiacea furcilia	9.06	7.07	11.33	1.34	5.06	4.84	20.40	20.80	6.94	18.10	20.00	2.00	7.62	16.00	2.40	
Eupagurus zoea											0.40	0.40	0.80	0.46	0.80	
Eupagurus megalopa												0.40				
Decapoda indet. larvae	1.60	0.46	0.40			0.06	0.40		2.40		5.40	2.40				
<i>Aglantha digitale</i>	40.00	11.60	16.20	76.00	129.60	7.96	30.40	30.80	80.00	9.31	80.00		0.11	33.33	16.00	
Hydrozoa medusae indet.																
Hydrozoa larvae				1.34												
Dimophyes arctica																
Ctenophora larvae																
Nemertea pilidium					2.66											
<i>Clione limacina veliger</i>						0.24					0.11					
<i>Limacina helicina veliger</i>													2.00	1.90	4.00	4.00
<i>Limacina retroversa</i>	20.00	13.33	80.00	1.34	56.00	7.62	83.33	100.00	224.00	2.571428571	1840.00	6.00	4.76	26.80	29.60	
Gastropoda veliger											2.9					
Bivalvia veliger		0.63					1.11		5.34	8.6			3.81	4.00		
Polychaeta larvae	6.66									2.9			0.95			
Polychaeta larvae mitraria				4.00												
Polychaeta secondary larvae	6.66	1.90		1.34	16.00		6.67	10.00	5.34							
Echinodermata larvae							3.33									
Bryozoa larvae	6.66	0.63	5.33	4.00	2.66	0.71			5.34	2.9		2.00	0.95			
<i>Eukrohnia hamata</i>	1.60	3.90	0.20		1.60	3.26	0.80	0.80	3.20	0.628571429			3.50	0.20	0.80	
<i>Sagitta elegans</i>		0.46	5.33	4.00	2.66	1.11	2.11		7.74	1.885714286			1.83	1.00		
<i>Fritillaria borealis</i>																
<i>Oikopleura</i> spp.	6.66	19.05	32.00	16.00	73.60	34.40	16.67	3.34	6.14	24.76190476				11.43		
Appendicularia larvae																
Pisces larvae	0.80	0.06			0.80		0.20						0.40			
<i>Paracalanus</i> spp.	20.00	1.90		1.34							5.71					

Collection/Net type	MPS	MPS180	MPS180	MPS180	MPS180	MPS						
Date	24.06.2018	24.06.2018	24.06.2018	24.06.2018	25.06.2018	25.06.2018	25.06.2018	25.06.2018	25.06.2018	25.06.2018	25.06.2018	25.06.2018
Area/Station name	14	15	15	15	16	16	16	16	17	17	17	17
Layer [m]	5-0	100-30	30-10	10-5	5-0	100-30	30-5	5-0	100-30	30-10	10-5	5-0
Calanus finmarchicus AM		3.43	1.67	2.22	1.34	0.48		5.33	0.86	1.00	5.33	4.00
C. finmarchicus AF	232.00	12.57	135.00	186.66	64.00	44.76	16.00	88.00	0.57	15.00	8.00	4.00
C. finmarchicus CV	3224.00	88.00	645.00	1086.66	348.00	493.33	1411.20	2208.00	1.71	144.00	136.00	112.00
C. finmarchicus CIV	152.00	5.71	25.00	33.34	16.00	3.81	64.00	122.67	1.14	21.00	5.33	16.00
C. finmarchicus CIII	8.00	2.29	5.00	6.66	1.34	1.90	6.40	26.67		1.00	2.67	4.00
C. finmarchicus CII	8.00	1.14	5.00	6.66	1.34		9.60	5.33		2.00	5.33	8.00
C. finmarchicus CI	16.00	1.14	10.00	6.66	1.34		16.00	5.33	0.19	1.00	2.67	20.00
C. hyperboreus CV												
C. hyperboreus CIV	2.67	1.14	1.67	6.66				0.80			0.80	
C. hyperboreus CIII		0.38		2.22		0.95		1.60				
Microcalanus spp.		53.33	1.67	6.66	68.00			64.00	35.43	24.00	74.67	176.00
Pseudocalanus spp. AM			1.67						1.14			
Pseudocalanus spp. AF	1.60	5.71	1.67	2.22	4.00	0.95	3.20		4.00	4.00		4.00
Pseudocalanus spp. CV	8.00	5.71	25.00	13.34	12.00	5.71	12.80	24.00	2.86	22.00	8.00	4.00
Pseudocalanus spp. CIV		6.86	5.00	2.22	4.00	1.90	6.40		4.00	16.00	2.67	8.00
Pseudocalanus spp. CI-CIII		2.29	5.00	2.22	8.00			48.00	1.43	12.00	10.67	8.00
Metridia longa AM												
M. longa AF						0.48			0.29		5.33	0.80
M. longa CV	5.33	1.14	1.67	2.22		3.33		1.60	0.86		5.33	0.80
M. longa CIV					1.34						5.33	
M. longa CIII	5.33							1.60	0.19	2.00		2.67
M. longa CII				2.22						2.00		
M. longa CI									0.29	2.00		2.67
Paraeuchaeta norvegica AF												
Paraeuchaeta spp. CV						0.06		0.80				
Paraeuchaeta spp. CIV		0.38			1.34	1.43			0.11			
Paraeuchaeta spp. CIII		0.38		2.22		1.43		0.80	0.17	0.20		
Paraeuchaeta spp. CII						0.95			0.23			
Paraeuchaeta spp. CI						0.48						
Acartia spp.			1.67									
Chiridius obtusifrons												
Heterorhabdus norvegicus						0.19		0.80				
Metridia lucens AM	5.33	0.38	1.67	2.22	1.34				0.57	1.00		12.00
Metridia lucens AF	1.60	17.14	5.00	6.66	4.00	3.33		0.80	7.43	4.00	2.67	8.00
M. lucens CI-CV	10.67	28.57	10.00	2.22	8.00	0.48			5.43	9.00	2.67	16.00
Anomalocera patersoni												
Scaphocalanus magnus												
Scolecithricella minor						0.95						4.00
Temora longicornis			1.67									
Microsetella norvegica												
Harpacticoida indet.												
Oithona atlantica	32.00	12.57	1.67	6.66	32.00	17.14			21.14	22.00	21.33	3.20
Oithona similis	544.00	384.76	505.00	326.66	872.00	272.38	419.20	464.00	133.71	796.00	597.33	656.00
Oncaea spp.		0.38										
Triconia (=Oncaea) borealis	8.00	3.43	1.67	6.66	12.00	1.90		32.00	4.00			16.00
Copepoda nauplii		4.57	25.00	33.34	104.00	1.90	201.60	544.00		14.00	101.33	72.00
Ostracoda		0.76				0.95		17.60				
Cirripedia nauplii	80.00		1.67								2.67	2.67

Legend
Copepods
Euphausiids
Amphipods
Gelatinous
Fish larvae
Pteropods
Other

Collection/Net type	MPS	MPS180	MPS180	MPS180	MPS180	MPS						
Date	24.06.2018	24.06.2018	24.06.2018	24.06.2018	25.06.2018	25.06.2018	25.06.2018	25.06.2018	25.06.2018	25.06.2018	25.06.2018	25.06.2018
Area/Station name	14	15	15	15	16	16	16	16	17	17	17	17
Layer [m]	5-0	100-30	30-10	10-5	5-0	100-30	30-5	5-0	100-30	30-10	10-5	5-0
Cirripedia cypris												
Cirripedia Facetotecta nauplii		0.4			1.3							
Themisto abyssorum		0.84	1.87		2.14		0.32	0.80				
Themisto libellula												
Themisto spp. <1mm						0.17						
Isopoda Bopyridae		0.38										
Isopoda indet.												
Thysanoessa inermis		0.06							0.11			
Thysanoessa longicaudata		0.06										
Thysanoessa raschii		0.46										
Euphausiacea nauplii			1.67							2.00	2.67	2.67
Euphausiacea calyptopis		1.14	5.00		1.34		1.07		0.23			3.20
Euphausiacea furcilia	2.40	11.71	2.46	0.00	4.80	0.97	3.20	0.80	0.29	2.20	1.60	0.00
Eupagurus zoea												
Eupagurus megalopa			0.20									
Decapoda indet. larvae		0.17	0.20	0.80		0.06						
Aglantha digitale	75.47	5.71	20.20	33.34	44.00	0.34	2.45	2.40	1.66	3.20	61.33	96.00
Hydrozoa medusae indet.				2.22	4.00							
Hydrozoa larvae												
Dimophyes arctica								0.80				
Ctenophora larvae										0.14		2.00
Nemertea pilidium				2.22								
Clione limacina veliger												2.67
Limacina helicina veliger	32.00					0.48	6.40	8.00		4.00	2.67	4.00
Limacina retroversa	36.00	10.29	180.00	73.34	40.00	12.63	7.47	0.00	0.00	0.80	0.80	1.60
Gastropoda veliger						1.34					2.67	
Bivalvia veliger	8.00	1.14	1.67	13.34	4.00					1.00		2.67
Polychaeta larvae		0.38			1.34					1.00		8.00
Polychaeta larvae mitraria												
Polychaeta secondary larvae			5.00		4.00							
Echinodermata larvae		0.38			4.00							
Bryozoa larvae	40.00		5.00		8.00					12.00		24.00
Eukrohnia hamata	0.80	4.32	1.87		1.60	6.34	3.52	7.20	0.46	0.20		0.80
Sagitta elegans	0.00	0.23			4.00	0.11				0.40		0.00
Fritillaria borealis					4.00				3.43	4.00	10.67	
Oikopleura spp.		13.94	20.00	26.66	32.00	0.48	3.20		1.14	19.00	32.00	24.00
Appendicularia larvae												
Pisces larvae												
Paracalanus spp.		1.14			4.00							

Table S2: Density values in individuals per m³ from Tucker Trawl tows throughout the study region. Values extrapolated from subsample counts to total sample and divided by opening area (1m²), tow speed (1.03 m/s) and tow time (900 s). The species are colour coded by taxonomic group (Copepods in purple; Euphausiids in red; Amphipods in green; Gelatinous in pink; Fish larvae in blue; Pteropods in orange and Others in white).

Stations	7	8	9	10	11	12	13	14	15	16	17	
Target depth (m)	25	30	40	30	30	30	30	30	30	20	20	
Calanus spp.	52.332	9.735	19.469	42.598	28.306	8.837	28.168	4.798	5.316	11.599	1.381	Legend
Thyssanoessa inermis	8.975	1.864	1.726	3.314	5.523	2.209	4.142	1.691	1.726	4.453	2.813	Copepods
Themisto abyssorum	1.381	1.381	1.588	1.036	3.452	1.105	1.795	0.552	2.002	0.587	0.311	Euphausiids
Limacina retroversa	10.770	16.017	0.759	2.209	8.837	6.559	2.693	2.002	1.519	3.866	0.483	Amphipods
Munida rugosa	1.795	2.900	1.795	1.657	1.795	0.759	1.381	1.761	0.863	0.104	0.155	Gelatinous
Chaetognata (Eukrohnia ?)	0.138					0.069				0.242	0.173	Fish larvae
Aglantha digitale	0.138								0.242	0.173	0.035	Pteropods
Mertensia ovum					0.276			0.035				Others
Gadidae juveniles	1.933	0.069	0.207	0.000	0.138	0.138	0.138	0.069	0.104	0.173	0.069	
Capelin juveniles		0.069	0.069	0.069	0.138	0.069	0.276					
Thyssanoessa longicaudata				0.069								
Calianassa (tyrrhena ?)		0.138	0.069	0.138				0.069				
Megalopa larvae		0.069						0.138			0.017	
Brachyuria larvae		0.069						0.035				
Isopoda sp.	0.276											
Copepod paraeuchatea sp.	2.624											
Total	80.362	32.311	25.683	51.090	48.466	19.745	38.593	11.150	11.771	21.195	5.437	

Table S3: Relative density of each taxonomic group at each station of MultiNet samples from Table S1.

Taxonomic group	Station 7	Station 8	Station 9	Station 10	Station 11	Station 12	Station 13	Station 14	Station 15	Station 16	Station 17
Copepods	0.97	0.99	0.96	0.99	0.95	0.92	0.89	0.97	0.90	0.98	0.94
Euphausiid larvae	0.01	0.00	0.01	0.00	0.00	0.01	0.00	0.00	0.01	0.00	0.00
Amphipods	0.00	0.00	0.00	0.00	0.00	0.00	0.00	0.00	0.00	0.00	0.00
Gelatinous	0.01	0.00	0.01	0.01	0.03	0.04	0.01	0.01	0.03	0.01	0.04
Fish larvae	0.00	0.00	0.00	0.00	0.00	0.00	0.00	0.00	0.00	0.00	0.00
Pteropods	0.01	0.01	0.02	0.00	0.02	0.03	0.09	0.01	0.05	0.01	0.00
Other	0.00	0.00	0.01	0.00	0.00	0.00	0.00	0.00	0.00	0.00	0.01

Table S4: Relative density of each taxonomic groups at each station of Tucker Trawl samples from Table S2.

Taxonomic group	Station 7	Station 8	Station 9	Station 10	Station 11	Station 12	Station 13	Station 14	Station 15	Station 16	Station 17
Copepods	0.65	0.30	0.76	0.83	0.58	0.45	0.73	0.43	0.45	0.55	0.25
Euphausiid larvae	0.11	0.06	0.07	0.07	0.11	0.11	0.11	0.15	0.15	0.21	0.52
Amphipods	0.02	0.04	0.06	0.02	0.07	0.06	0.05	0.05	0.17	0.03	0.06
Gelatinous	0.00	0.00	0.00	0.00	0.01	0.00	0.00	0.00	0.02	0.02	0.04
Fish larvae	0.02	0.00	0.01	0.00	0.01	0.01	0.01	0.01	0.01	0.01	0.01
Pteropods	0.13	0.50	0.03	0.04	0.18	0.33	0.07	0.18	0.13	0.18	0.09
Other	0.06	0.10	0.07	0.04	0.04	0.04	0.04	0.18	0.07	0.00	0.03

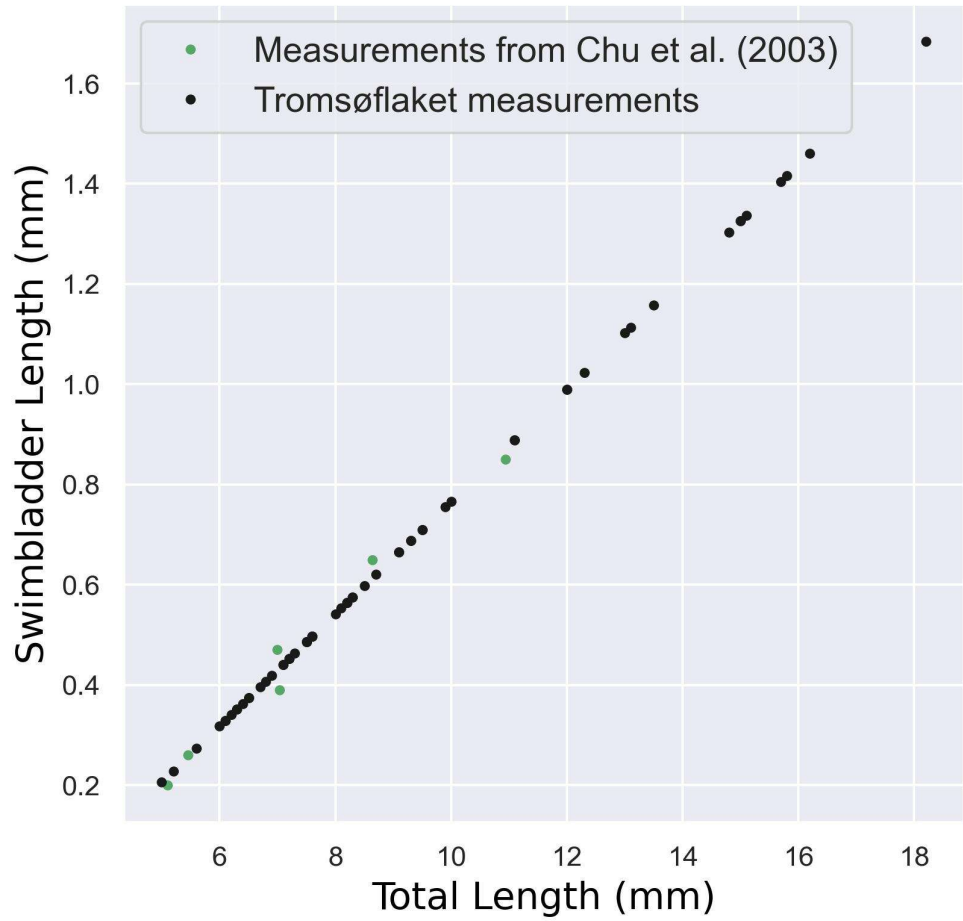


Figure S1: Fish total length to swimbladder length for the range of total fish length measurements from Tromsøflaket with Tucker trawl samples. The literature values used to determine the linear regression are in green and the Tucker trawl measurements are in black.

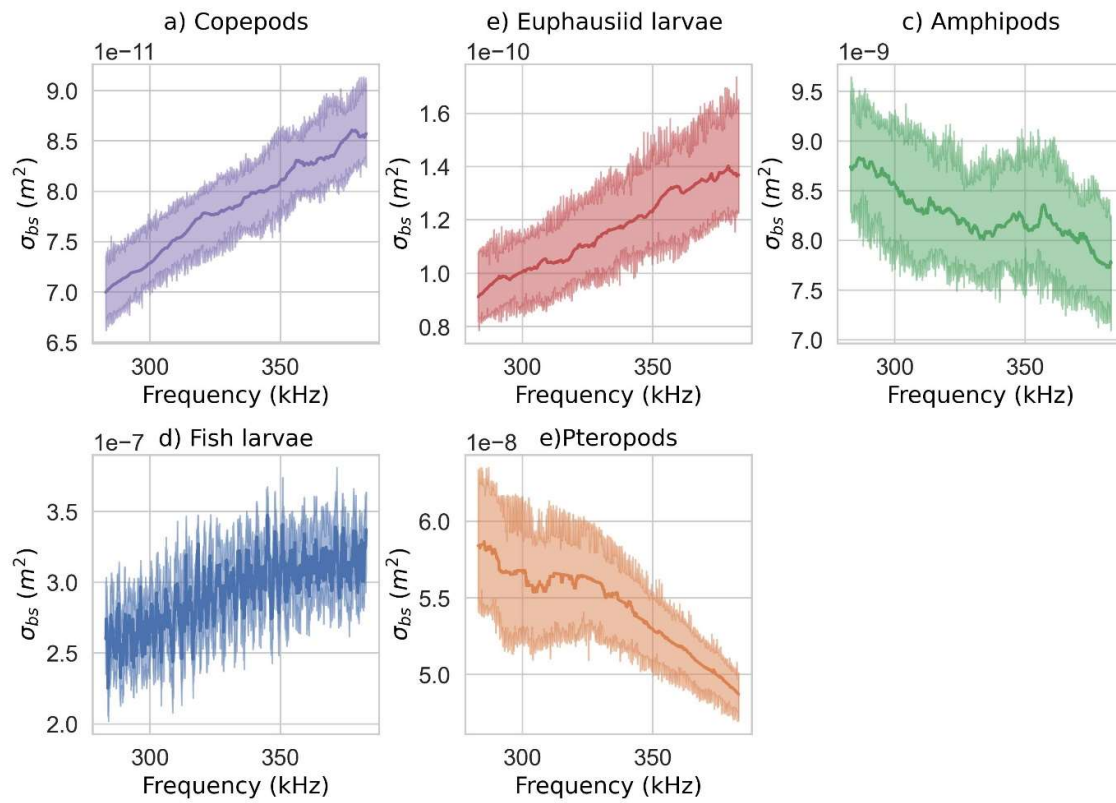


Figure S2: Theoretical cross-sectional backscatter for each taxonomic group (a-e) summarized for 1000 model simulations. The solid line represents the median and the shaded region represents the 5th and 95th percentiles. Note the different scales of each panel.

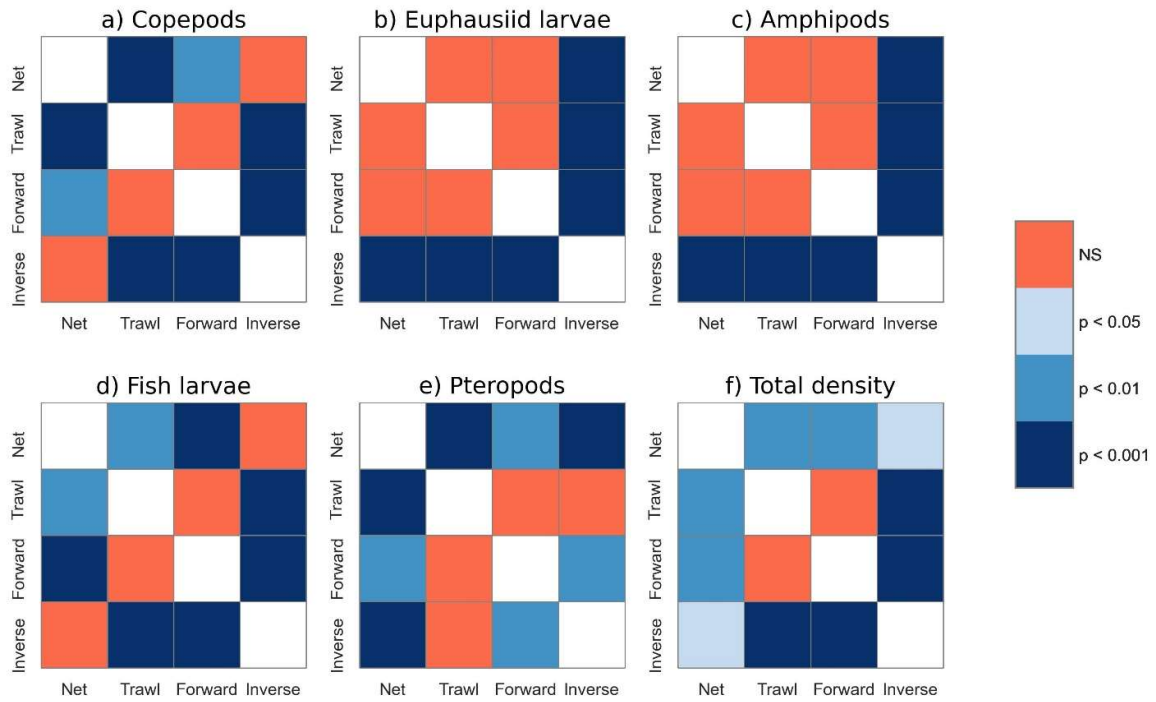


Figure S3: Sign plots to denote the statistical significance between density estimates for each taxonomic group (a-e) and total density (f) of the four measurement methods. Net represents MultiNet estimates, and Trawl is Tucker Trawl estimates. The acoustic survey density estimates are Forward for the forward method and Inverse for the inverse method.

Appendix B

Supplementary Materials 2

Supplementary Information for:

Model-informed classification of broadband acoustic backscatter from zooplankton in an *in situ* mesocosm

Muriel Dunn^{1,2*}, Chelsey McGowan-Yallop^{3*}, Geir Pedersen⁴, Stig Falk-Petersen⁵, Malin Daase⁶, Kim Last³, Tom J. Langbehn⁷, Sophie Fielding⁸, Andrew S. Brierley⁹, Finlo Cottier^{3,6}, Sünnje L. Basedow⁶, Lionel Camus¹ & Maxime Geoffroy^{2,6}.

¹Akvaplan-niva AS, Fram Centre, Postbox 6606, Stakkevollan, 9296 Tromsø, Norway

²Centre for Fisheries Ecosystems Research, Fisheries and Marine Institute of Memorial University of Newfoundland, St. John's A1C 5R3, Canada

³Scottish Association for Marine Science, Oban, Argyll PA37 1QA, UK

⁴Institute for Marine Research, 5005 Bergen, Norway

⁵Independent scientist, 9012 Tromsø

⁶Department of Arctic and Marine Biology, UiT The Arctic University of Norway, 9036 Tromsø, Norway

⁷Department of Biological Sciences, University of Bergen, 5020 Bergen, Norway

⁸British Antarctic Survey, Natural Environment Research Council, High Cross, Cambridge CB30ET, United Kingdom

⁹Pelagic Ecology Research Group, School of Biology, Scottish Oceans Institute, Gatty Marine Laboratory, University of St Andrews, St Andrews, KY16 8LB, United Kingdom

* These authors contributed equally: Muriel Dunn and Chelsey McGowan-Yallop

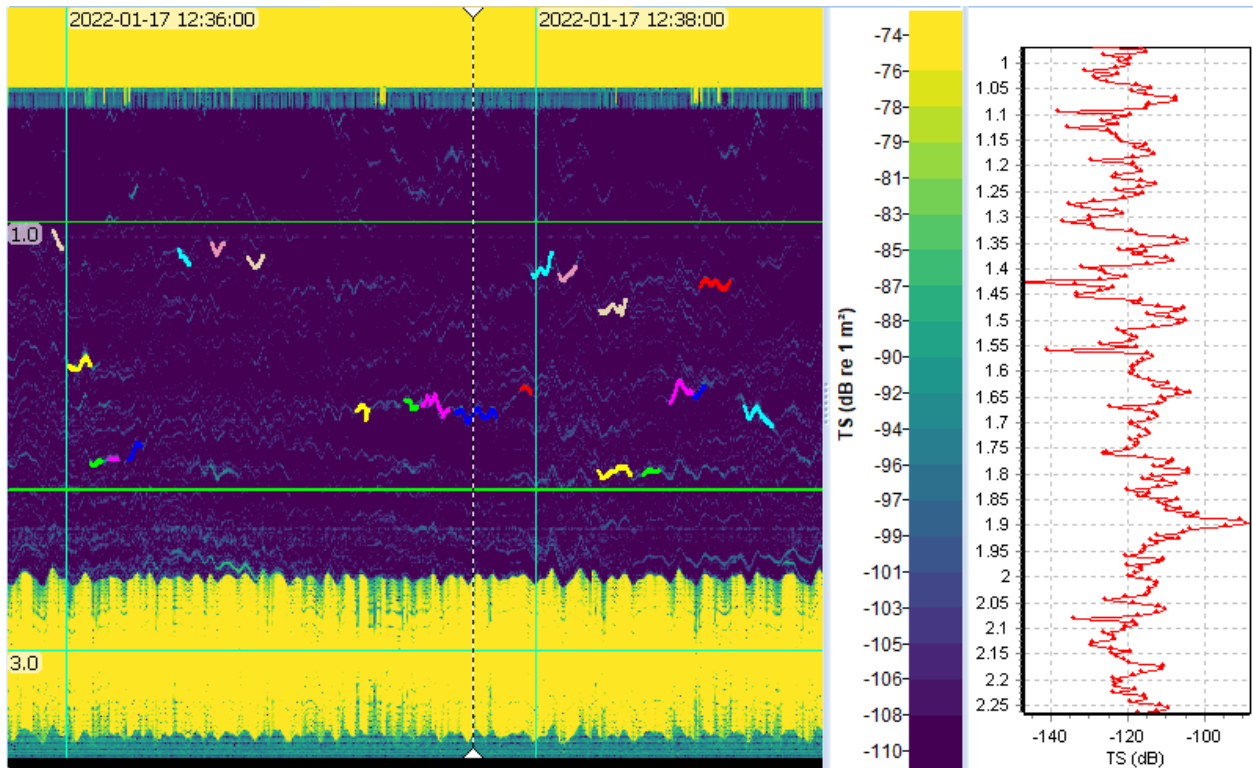


Figure S1. Left: Pulse compressed target strength echogram excerpt of 3.5 minutes from the total 3 hours of data collected during the AZKABAN mesocosm experiment. The bottom of the net is at 3 m. The tracks were identified from single target detections and are highlighted as bright coloured tracks superimposed on the echogram. The analysis domain for the experiment was bounded by the green horizontal lines at 1 m and 2.25 m to minimize interference from near-field and net bottom. Image was exported directly from Echoview using the "Export to Image" option. *Right:* Graphed ping at the dotted vertical line in the left panel. The graphed ping is bounded by the analysis domain limits (1 m and 2.25 m). Note the stronger signal at 1.9 meters shows the dark blue track that coincides with the dotted vertical line.

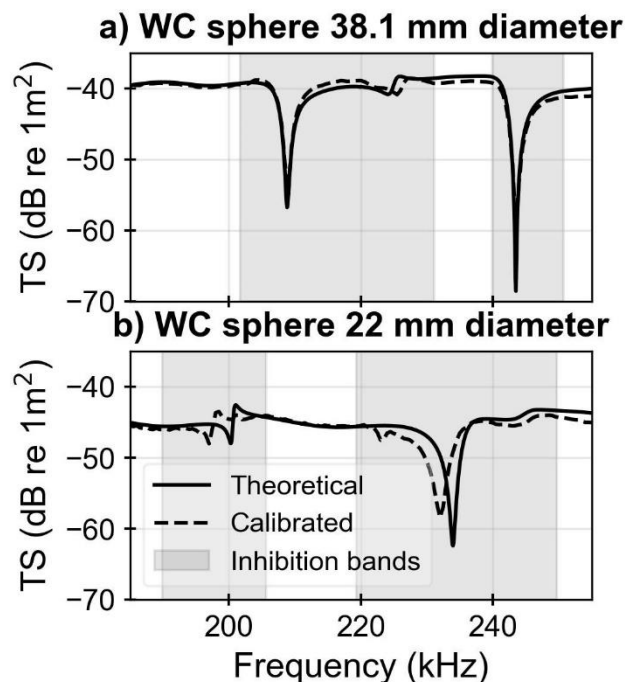


Figure S2. Theoretical target strength spectra (solid line) and calibrated target strength spectra (dashed line) for the a) 38.1 mm diameter tungsten carbide (WC) sphere and b) 22 mm diameter tungsten carbide (WC) sphere. The inhibition bands for each sphere are indicated by the grey area and were not used for to calculate the final calibration parameters.

The calibration results from the 38.1 mm sphere were preferred over the 22 mm when both spheres had available calibrations values because of the lower root mean square values (~ 0.2), a measure of error, and a higher signal-to-noise ratio. We observed a lateral shift in the nulls between 220 - 240 kHz and between 195- 205 kHz with the 22 mm sphere which had a spark-eroded suspension point (Supplementary Information Figure S1b). Large inhibition bands were used to reduce the effect of the spark-eroded suspension point (Renfree *et al.*, 2020).

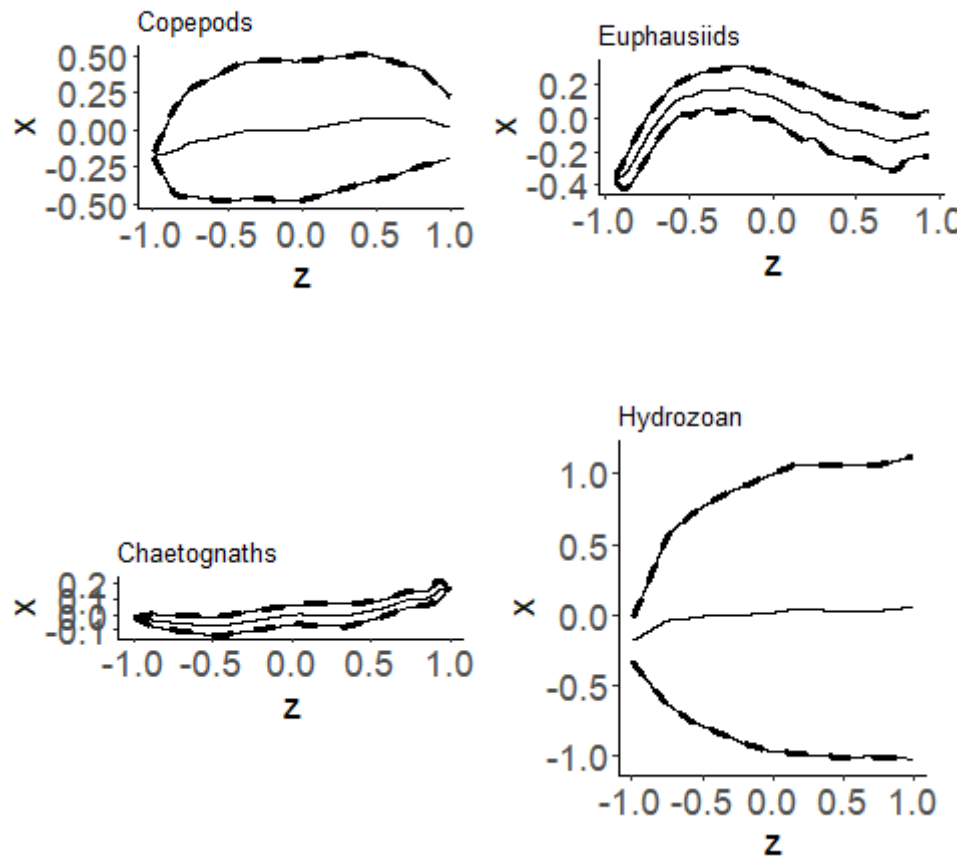


Figure S3: Shape files for each species scattering model ensembles. The shapes are selected as a representative and the best picture of an individual from each species.

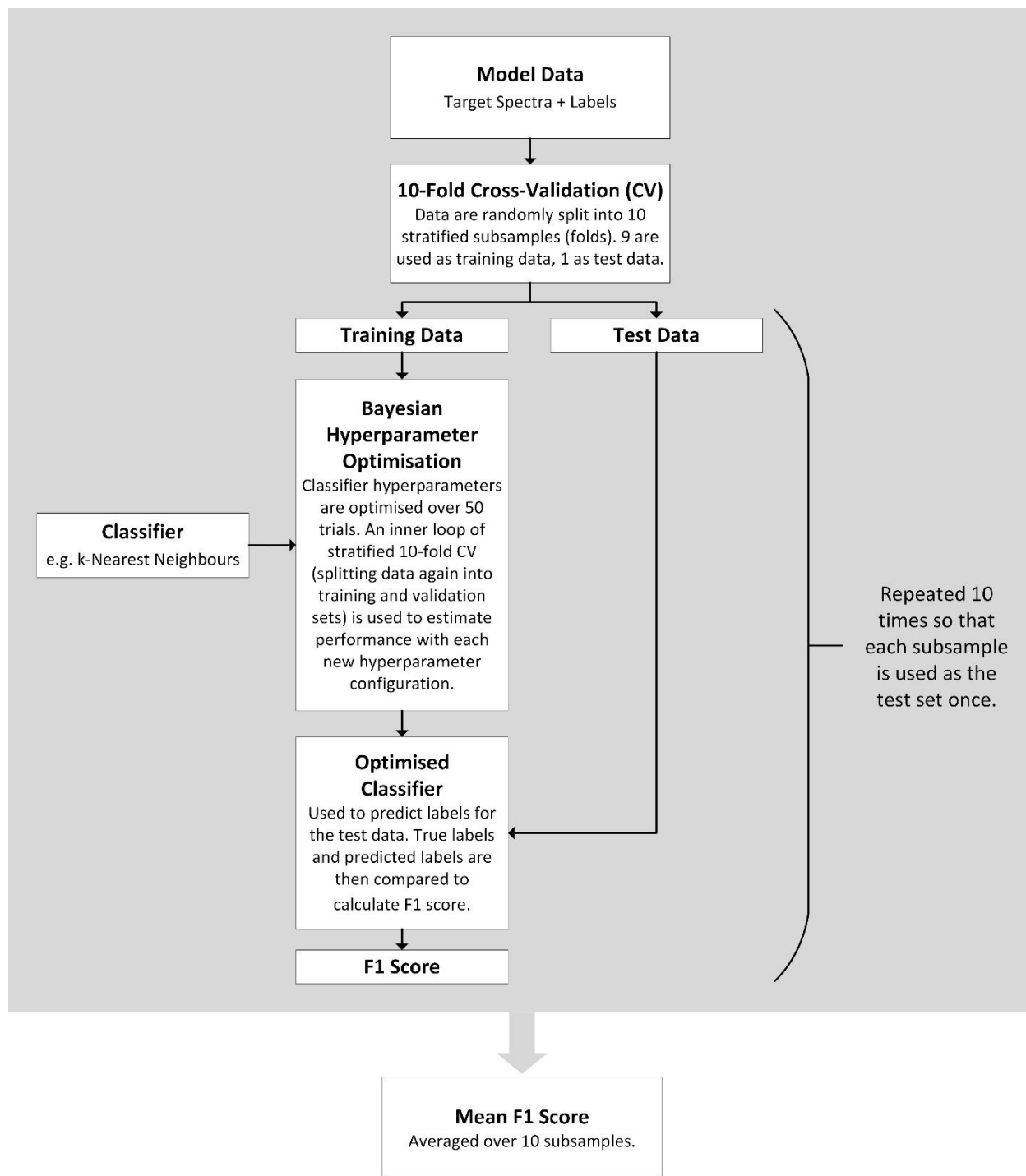


Figure S4: Nested cross-validation procedure used to estimate performance for a classifier trained on the entire labelled modelled dataset. The 'Model Data' block includes the target spectra results calculated by the scattering models for each taxonomic group, the labels are the associated taxonomic group parameterised for the scattering model result. F1 score is used as the evaluation metric.

Table S1: Single Target Detection - wideband algorithm parameters for target analysis (target detection) and for target removal in noise level analysis (noise level).

Parameter	Target detection	Noise level
Compensated TS Threshold (dB re 1m ²)	-120.0	-120.0
Pulse Length Determination Level (dB re 1W)	6.0	5.0
Min. Normalised Pulse Length	0.5	0.05
Max. Normalised Pulse Length	1.5	1.5
Min. Target Separation (m)	0.5	0.001
Max. Beam Compensation (dB re 1m ²)	39.0	18.0
Max SD of Minor-Axis Angle (deg)	0.6	0.5
Max SD of Major-Axis Angle (deg)	0.6	0.5

We used the pulse length determination level parameter to threshold the signal strength of the broadband targets relative to the background noise. The pulse length determination level is the value below the peak value at which pulse length is measured (Soule *et al.*, 1996). Here, the pulse length determination level parameter provided some noise filtering by ensuring that accepted peaks have a prominence of at least 6 dB re 1W (Table 2). If the noise level were within 6 dB re 1W of the peak value, the normalised pulse length should exceed the thresholds typically used in single target detection, and the peak would be rejected. A maximum two-way beam compensation of 6 dB re 1m² was used to restrict all targets to the 3 dB re 1m² beam angle. A minimum target separation of 0.4 m was used to reduce the likelihood of incorporating multiple targets into each target spectra. We further filtered the detected targets to be within the 4 degrees off-axis angle and 6 dB re 1m² beam compensation.

Table S2: Target tracking algorithm parameters.

	Major axis (degree)	Minor axis (degree)	Range (m)	TS (dB re 1m ²)	Ping gap
Track detection					
Alpha	0.7	0.7	0.5		
Beta	0.5	0.5	0.3		
Target gates					
Exclusion distance (m)	0.15	0.15	0.1		

Missed ping expansion	0	0	0		
Weights	30	30	60	60	0
Track acceptance					
Minimum number of single targets in a track	4				
Minimum number of pings in track	4 pings				
Maximum gap between single targets	2 pings				

Table S3. Confusion matrix averaged over all folds in the outer stratified 10-fold cross-validation for kNN (mean \pm standard deviation) for normalized modelled target spectra.

	Predicted species			
Species	Chaetognaths	Copepods	Euphausiids	Hydrozoans
Chaetognaths	56.6 \pm 5.0	8.9 \pm 1.4	13.1 \pm 2.5	22.3 \pm 2.9
Copepods	2.7 \pm 1.2	93.3 \pm 3.1	3.8 \pm 2.4	0.2 \pm 0.4
Euphausiids	11.8 \pm 3.6	12.5 \pm 3.7	69.2 \pm 4.1	6.5 \pm 1.7
Hydrozoans	23.7 \pm 5.2	1.7 \pm 1.3	11.0 \pm 3.3	63.6 \pm 5.2

Table S4. Confusion matrix averaged over all folds in the outer stratified 10-fold cross-validation for LightGBM (mean \pm standard deviation) for normalized modelled target spectra.

	Predicted species			
Species	Chaetognaths	Copepods	Euphausiids	Hydrozoans
Chaetognaths	53.2 \pm 4.9	6.8 \pm 1.5	13.4 \pm 3.7	26.6 \pm 4.3
Copepods	2.6 \pm 1.4	90.8 \pm 2.7	5.2 \pm 2.0	1.4 \pm 1.1
Euphausiids	9.1 \pm 2.3	8.9 \pm 2.6	72.2 \pm 3.8	9.8 \pm 2.2
Hydrozoans	18.9 \pm 5.6	1.6 \pm 1.1	10.4 \pm 2.2	69.1 \pm 5.3

Table S5. Confusion matrix averaged over all folds in the outer stratified 10-fold cross-validation for SVM (mean \pm standard deviation) for normalized modelled target spectra.

	Predicted species			
Species	Chaetognaths	Copepods	Euphausiids	Hydrozoans
Chaetognaths	36.8 ± 3.9	20.5 ± 3.1	19.0 ± 4.9	23.7 ± 2.5
Copepods	0.9 ± 1.2	79.7 ± 3.0	16.5 ± 2.5	2.9 ± 1.4
Euphausiids	4.0 ± 2.1	18.4 ± 4.9	70.2 ± 4.1	7.4 ± 2.6
Hydrozoans	24.7 ± 4.7	5.8 ± 2.9	14.7 ± 2.6	54.8 ± 5.6

Table S6. Classifier F1 scores estimated through nested cross-validation for kNN (mean ± standard deviation) for 5 different continuous frequency bandwidths.

	70 kHz (45 - 90 kHz)	120 kHz (90 - 170 kHz)	200 kHz (185 - 255 kHz)	333 kHz (283 - 383 kHz)	Full (45-383 kHz)
Class-weighted	0.78 ± 0.02	0.86 ± 0.01	0.70 ± 0.02	0.64 ± 0.02	0.92 ± 0.02
Chaetognaths	0.60 ± 0.03	0.76 ± 0.03	0.58 ± 0.04	0.59 ± 0.03	0.88 ± 0.02
Copepods	0.93 ± 0.01	0.90 ± 0.02	0.87 ± 0.02	0.82 ± 0.03	0.95 ± 0.01
Euphausiids	0.76 ± 0.03	0.85 ± 0.02	0.70 ± 0.03	0.57 ± 0.03	0.89 ± 0.03
Hydrozoa	0.81 ± 0.01	0.92 ± 0.02	0.66 ± 0.04	0.57 ± 0.04	0.96 ± 0.01

Table S7. Classifier F1 scores estimated through nested cross-validation for kNN (mean ± standard deviation) for normalized scattering models with copepod material properties from Antarctica.

	Predicted species			
Species	Chaetognaths	Copepods	Euphausiids	Hydrozoans
Chaetognaths	57.0 ± 6.7	10.0 ± 2.6	13.8 ± 4.4	19.1 ± 4.8
Copepods	3.7 ± 2.5	91.3 ± 2.8	4.7 ± 1.7	0.3 ± 0.6
Euphausiids	10.7 ± 3.1	13.3 ± 5.3	68.9 ± 6.2	7.1 ± 2.0
Hydrozoans	24.5 ± 3.6	2.8 ± 1.5	11.1 ± 3.1	61.6 ± 4.2

Code S1. Optimised kNN model as determined by Bayesian hyperparameter optimisation using HyperOpt-Sklearn 1.0.3.

```
KNeighborsClassifier(algorithm='kd_tree', leaf_size=36, metric='l2', n_jobs=-1,
                    n_neighbors=1, p=1.6822439326937353, weights='distance')
```

Code S2. Optimised LightGBM model as determined by Bayesian hyperparameter optimisation using HyperOpt-Sklearn 1.0.3.

```
LGBMClassifier(boosting_type='goss', colsample_bytree=0.5097647467361791,
               learning_rate=0.012631457372918417, max_delta_step=0,
               max_depth=7, min_child_weight=1, n_estimators=3400,
               num_leaves=46, objective='binary',
               reg_alpha=0.0002621872624005705, reg_lambda=1.8302350814675785,
               scale_pos_weight=1, seed=0, subsample=0.810277827141478)
```

Code S3. Optimised SVM model as determined by Bayesian hyperparameter optimisation using HyperOpt-Sklearn 1.0.3.

```
SVC(C=3.003839970561586, coef0=0.4612291525680026,
    decision_function_shape='ovo', degree=1, random_state=3, shrinking=False,
    tol=5.715337840164192e-05)
```

Code S4. Optimised kNN model as determined by Bayesian hyperparameter optimisation using HyperOpt-Sklearn 1.0.3. trained with copepod parametrised with Antarctic waters material properties

```
KNeighborsClassifier(leaf_size=22, n_jobs=-1, n_neighbors=4,
                    p=2.6840910661386785, weights='distance')
```

References.

Renfree, J.S., Andersen, L.N., Macaulay, G., Sessions, T.S., Demer, D.A. 2020. Effects of sphere suspension on echosounder calibrations. *ICES Journal of Marine Science*, 77: 2945-2953.

Appendix C

Ethics approval for AFKABAN experiments

Forskning- og innovasjonsstasjonen Kraknes (FISK)
Framsenteret, Postboks 6606 Langnes
9296 Tromsø

Fakturaref: AZKABAN-Fish2023
Vår ref: 22/231325
Dato: 24.01.2023
Org.nr: 937375158

Att. Jenny Jensen

Statens tilsyn for planter, fisk, dyr og næringsmidler



VEDTAK OM BRUK AV FORSØKSDYR - FOTS ID 29801

Virksomhetsnummer 160: Forskning- og innovasjonsstasjonen Kraknes (FISK)

Behandlet av Mattilsynet, 24.01.2023.

Saken gjelder

Søknaden gjelder en endring av et allerede godkjent forsøk. Formålet med forsøket er å forsøke å estimere fiskebestander ved bruk av autonome fartøyer med ekkolodd, altså undervannsdroner og "glidere" som ikke trenger lys.

Ved bruk av ekkolodd til bestandsestimering av fisk er det i dag vanlig at man bruker fartøyer som har lys om bord. Lyset må være der fordi folk må kunne se når de arbeider og ellers beveger seg på fartøyet. Mest sannsynlig tiltrekker eller skremmer lyset fisk, og dersom fisken svømmer nærmere eller lengre bort fra båten, og siden ekkoloddet ser "rett ned" i vannsøylen, kommer dette til å påvirke hvor mye fisk ekkoloddet registrerer. Det godkjente forsøket skal forsøke å finne mer skånsomme metoder for å gjøre bestandsestimater.

Underveis i forsøket er det fanget mye dypvannsreke (*Pandalus borealis*) sammen med forsøksfiskene. Arten er av kommersiell interesse og er også en viktig del av økosystemene i nordlige havområder (byttedyr), og søker mener at den oppståtte situasjonen er en gylden mulighet for å studere også denne arten med ekkolodd. Det ønskes derfor å utvide forsøket med 200 dypvannsreker. Prosedyrer for rekeene blir som for de øvrige artene i forsøket.

Dokumenter i saken:

1. Endringssøknad med FOTS-id 29801 datert 23/01-23.

Vedtak

Mattilsynet, region Sør og Vest, avdeling nasjonale oppgaver, godkjenner bruken av forsøksdyr ihht endringssøknad jfr. forskrift 18.juni 2015 om bruk av dyr i forsøk § 6.

Begrunnelse

Søknaden inneholder tilstrekkelige opplysninger til at Mattilsynet kan fatte vedtak.

Mattilsynet vurderer at formålet med endringen av forsøket er tilstrekkelig beskrevet i søknaden og tilleggsinformasjonen slik at kravene i forsøksdyrforskriften § 10 (formål med forsøket), § 11 (metoder, teststrategier og endepunkter) og § 9 (erstatning, reduksjon og forbedring) er oppfylt. Mattilsynet vurderer det slik at dyr ikke utsettes for unødvendige belastninger, jf. forsøksdyrforskriften § 1.

Vi minner om kravet om årsrapportering, jf. forsøksdyrforskriften § 36. Manglende rapportering vil kunne medføre at vi ikke behandler nye søknader.

Søker vil bli innkrevd gebyr på 1700 NOK (+ 100 NOK i administrasjonsgebyr) for behandling av søknad om godkjenning av endring av dyreforsøk, jf. forskrift av 13.2.2004 nr. 406 om betaling av gebyrer for særskilte ytelser fra Mattilsynet jf. § 5.

Vedtak kan påklages til Mattilsynet, jfr. lov 10 feb 1967 om behandlingsmåten i forvaltningssaker (forvaltningsloven) § 28. Klagefristen er 3 uker fra mottak av dette brev, jfr. forvaltningsloven § 29. Klagen stiles til Mattilsynet, Hovedkontoret, men sendes via avdeling

nasjonale oppgaver.

Med hilsen

Ole Aamodt
avdelingssjef

Med hilsen

Dag Atle Tuft
seniorrådgiver

Kopi:
personell med særskilt kontrollansvar
postmottak@mattilsynet.no

Appendix D

Supplementary Materials 3

Supplementary Information for:

Classification of three coinciding species (Atlantic cod, polar cod, and northern shrimp) using broadband hydroacoustics

Muriel Dunn^{1,2}, Geir Pedersen³, Malin Daase^{4,5}, Jørgen Berge⁴, Emily Venables⁴, Sünnje Linnéa Basedow⁴, Stig Falk-Petersen⁶, Jenny Jensen¹, Tom J. Langbehn⁷, Lionel Camus¹ & Maxime Geoffroy^{2,4}

¹Akvaplan-niva AS, Fram Centre, Postbox 6606, Stakkevollan, 9296 Tromsø, Norway

²Centre for Fisheries Ecosystems Research, Fisheries and Marine Institute of Memorial University of Newfoundland, St. John's A1C 5R3, Canada

³Institute for Marine Research, 5005 Bergen, Norway

⁴Department of Arctic and Marine Biology, UiT The Arctic University of Norway, 9036 Tromsø, Norway

⁵Department of Arctic Biology, The University Centre in Svalbard, 9171 Longyearbyen, Norway

⁶Independent scientist, 9012 Tromsø

⁷Department of Biological Sciences, University of Bergen, 5020 Bergen, Norway

January 10th, 2024

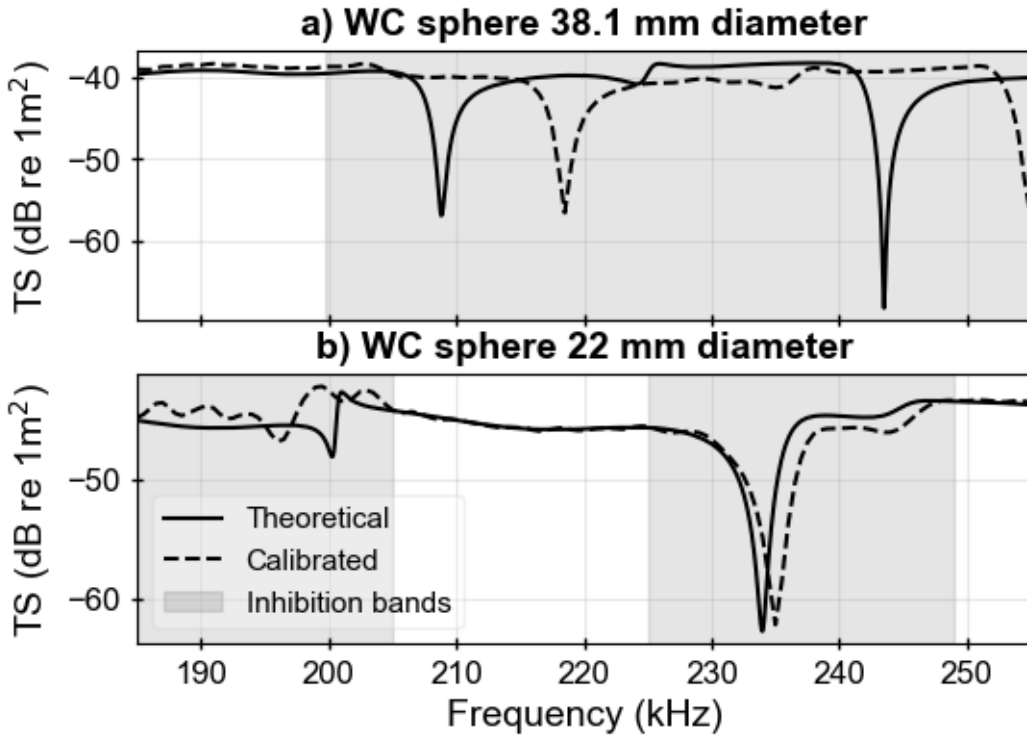


Figure S1: Theoretical target spectra for a) 38.1 mm and b) 22 mm tungsten carbide calibration spheres (black line) for the 185-255 kHz frequency bandwidth. Averaged measured target strength with calibration parameters applied for each sphere (dotted line). The calibration parameters applied to the measured target strength measurements were linearly interpolated over the inhibition band (shaded regions) because of the non-flat theoretical target spectra in these regions.

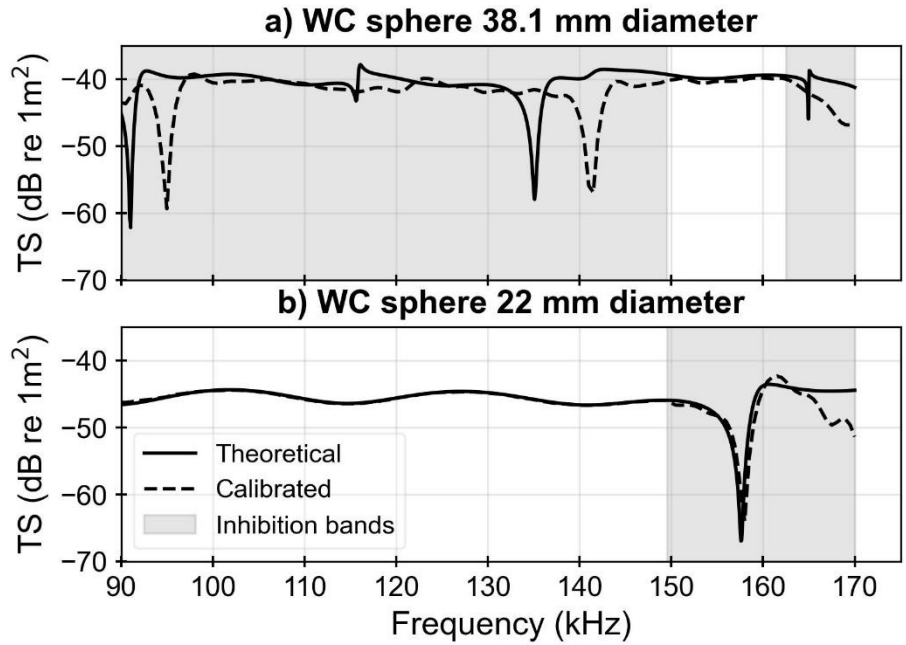
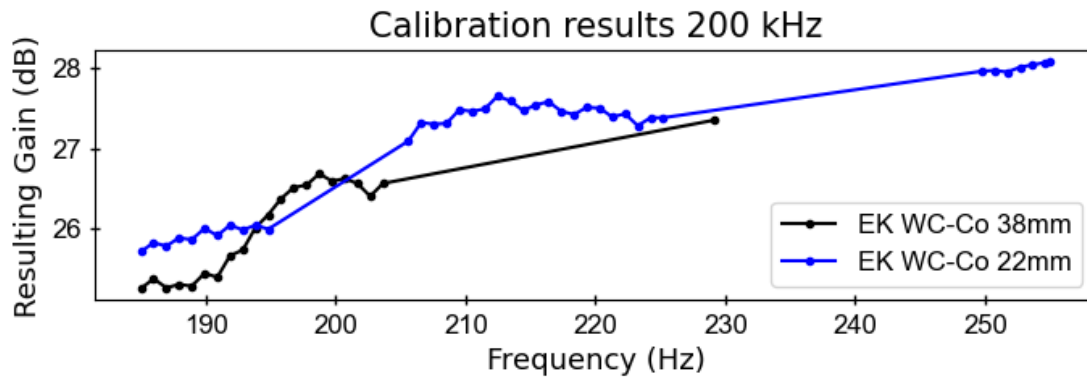


Figure S2: Theoretical target spectra for a) 38.1 mm and b) 22 mm tungsten carbide calibration spheres (black line) for the 90-170 kHz frequency bandwidth. Averaged measured target strength with calibration parameters applied for each sphere (dotted line). The calibration parameters applied to the measured target strength measurements were linearly interpolated over the inhibition band (shaded regions) because of the non-flat theoretical target spectra in these regions.

A)



B)

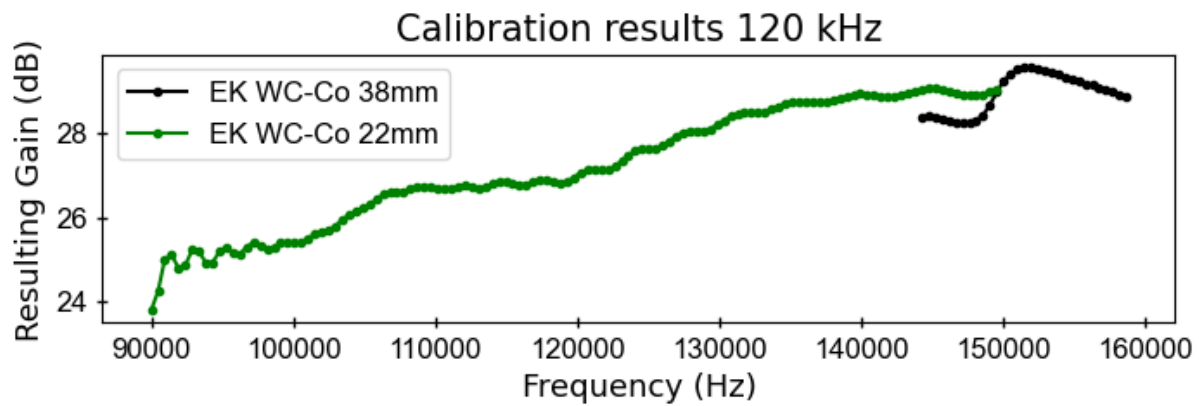


Figure S3: The resulting gain from calibrations for A) the 200 kHz transducer and B) the 120 kHz transducer. Both transducers were calibrated using two spheres of different diameters (38.1 mm and 22 mm). The gain values are not available across the entire bandwidths because of the inhibition bands determined by the nulls in the target spectra of each sphere. Where gain values from both spheres were available generally the 22 mm results were used because of the better-quality measurements (except for <205 kHz for the 200 kHz transducer).